Volume 35 June, 1957 Number 1

UNIVERSITY OF MICHIGAN
JUN 13 1957
ENGINEERING LIBRARY

Engin. Library

INST
UNIVERSITY OF MICHIGAN
GENERAL LIBRARY
ANN ARBOR MICH U S A
8X DEC 57

The Canadian Journal of Chemical Engineering

formerly

CANADIAN JOURNAL OF TECHNOLOGY

CONTENTS

Effect of Gas Thermal Conductivity on Local Heat Transfer in a Fluidized Bed.	*A. Jacob and G. L. Osberg*	5
Counter Diffusion of Ions in Water.	*E. R. Gilliland, R. F. Baddour and D. J. Goldstein*	10
The Effect of Sonic Energy on Mass Transfer in Solid-Gas Contacting Operations.	*J. W. Hodgins, T. W. Hoffman and D. C. Pei*	18
Studies on Flocculants for Settling, Thickening and Filtration in the Sherritt Gordon Process.	*D. J. I. Evans, W. Kunda and P. Chiang*	25
The Decomposition, Oxidation, Ignition and Detonation of Fuel Vapors and Gases. Part 31—The Effect of Flow Configuration in an Annular Reactor of Vycor Glass on the Oxidation of Pentane.	*R. O. King, S. Sandler and R. Strom*	33
Flooding Phenomena in Packed Gas Absorption Columns.	*G. W. Minard and M. D. Winning*	39

Published by

THE CHEMICAL INSTITUTE OF CANADA

OTTAWA CANADA

The Canadian Journal of Chemical Engineering

formerly

Canadian Journal of Technology

VOLUME 35 | JUNE, 1957 | NUMBER 1

EDITOR:

W. M. CAMPBELL

Chemistry and Metallurgy Division, Atomic Energy of Canada Limited, Chalk River, Ont.

Managing Editor: GARNET T. PAGE

Assistant Editor: R. N. CALLAGHAN

Editorial Assistant:
R. G. WATSON

Circulation Manager:
M. M. HOLDEN

EDITORIAL BOARD:

Chairman
J. R. DONALD, Montreal, Que.

A. CHOLETTE, Quebec, Que.
W. H. GAUVIN, Montreal, Que.
G. W. GOVIER, Edmonton, Alta.
E. B. LUSBY, Toronto, Ont.
R. R. McLAUGHLIN, Toronto, Ont.
E. R. ROWZEE, Sarnia, Ont.
H. R. L. STREIGHT, Montreal, Que.
LÉO MARION, Ottawa, Ont.
G. A. LEDINGHAM, Saskatoon, Sask.
GLEN GAY, Ottawa, Ont.

EX-OFFICIO:

C. B. PURVES, Montreal, Que.
E. A. CROCKETT, Sarnia, Ont.
H. P. GODARD, Kingston, Ont.
A. I. JOHNSON, Toronto, Ont.

Manuscripts for publication should be submitted to the Editor: Dr. W. M. Campbell, Chemistry and Metallurgy Division, Atomic Energy of Canada Limited, Chalk River, Ontario. (Instruction to authors are on inside back cover)

Proofs, correspondence concerning proofs, and orders for reprints should be sent to: The Chemical Institute of Canada, 18 Rideau Street, Ottawa 2, Ont.

Subscriptions, renewals, requests for single or back numbers and all remittances should be sent to: The Chemical Institute of Canada, 18 Rideau Street, Ottawa 2, Ont.

C.J.Ch.E. is published by The Chemical Institute of Canada every two months. Subscription rate is $3.00 per year and .75c per single copy; U.S. and U.K.—$3.50; and Foreign—$4.00 per year.

Unless it is specifically stated to the contrary, the Institute assumes no responsibility for the statements and opinions expressed in *The Canadian Journal of Chemical Engineering*. Views expressed in the editorials do not necessarily represent the official position of the Institute.

Editorial Offices: Dr. W. M. Campbell, Chemistry and Metallurgy Division, Atomic Energy of Canada Limited, Chalk River, Ont.

Production and circulation offices: 18 Rideau Street, Ottawa 2, Ont.

Change of Address: Advise the Circulation Department, The Chemical Institute of Canada, 18 Rideau Street, Ottawa 2, Ont. in advance of any change of address, providing old as well as new address. Enclose address label if possible.

UNIVERSITY OF MICHIGAN LIBRARIES

"The Canadian Journal of Chemical Engineering"

formerly "The Canadian Journal of Technology"

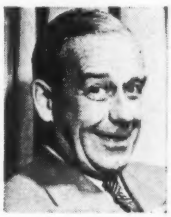

The National Research Council of Canada and The Chemical Institute of Canada have entered into an agreement whereby the N.R.C. publication "The Canadian Journal of Technology" was transferred to the Institute in 1957.

Commencing with this issue, the journal will be published by the Institute in a new format. The name of the journal has been changed to "The Canadian Journal of Chemical Engineering", and it will be adapted to the interests of Canadian chemical engineers, carrying both research and review papers.

This new journal will provide a Canadian medium for the publication of progress in chemical engineering and allied technical fields in this country, and, with the full support of members of the profession, will be a valuable contribution to the advancement of this field of science in our country.

E. W. Steacie

Clifford Purves

A NEW ENDEAVOUR

H. P. Godard

Director of Publicity and Publications

THIS conversion and renaming of the long established Canadian Journal of Technology is designed to provide additional service to the chemical engineering members of The Chemical Institute of Canada, and to provide a national publication forum for the increasing amount of chemical engineering research and development being done in this county. It recognizes the growth of the chemical engineering profession in Canada and the increasing proportion of chemical engineers in the Institute. A glance at the registration figures for chemists and chemical engineers now in our universities makes it clear that this step is being taken none too soon.

The Institute has always had a basic policy of serving the chemical engineer as well as the chemist. The Chemical Engineering Division is one of the largest and most active of the eleven subject divisions in the Institute. It has held annual divisional meetings since 1951 and participated strongly in the annual conventions of the Institute. It met jointly with the A.I.Ch.E. in Toronto in 1953 and is planning another joint meeting in Montreal in 1958.

Local chemical engineering groups are active within the Institute in Edmonton, Montreal, Saguenay and Vancouver. Chemical engineering student groups are active at the University of Alberta and the University of Toronto.

"Chemistry in Canada" has been the news journal of the Institute and will continue to report the general news of interest to Canadian chemical engineers. *The Canadian Journal of Chemcial Engineering* will be strictly technical. Its policy is described on the following page by editor W. M. Campbell.

Credit for the idea and timing that have led to this new venture goes to past president Roger Gaudry (1955-1956) who pushed the idea so energetically and enthusiastically that in short order the idea has become a reality.

Along with this new service to chemical engineers, the "Canadian Journal of Chemistry" or the "Canadian Journal of Biochemistry and Physiology" is being made available to chemists without charge so that at long last all members receive both a news journal and a technical journal as part of the services rendered by the Institute.

The time is ripe, the immediate outlook for papers is good, now it depends on you--the readers. Let's all help whenever possible. Tuum Est!

EDITORIAL

W. M. CAMPBELL, Editor.

The First Issue

EDITORIALS will not be a regular feature of *The Canadian Journal of Chemical Engineering* but will appear only on special occasions. The first issue is undoubtedly a special occasion. I would like here to review the policies which have been laid down for the journal and to ask for help and suggestions from the readers, writers and reviewers.

C.J.Ch.E. will be published every two months by The Chemical Institute of Canada. It is a continuation of the "Canadian Journal of Technology" formerly published by the National Research Council, Ottawa, and it will maintain the high technical standard of this former journal. The essential difference, however, is that C.J.Ch.E. will be devoted entirely to chemical engineering and closely related subjects. For example, applied chemistry is a closely related subject if it is slanted towards chemical engineering. The dividing line here is somewhat indefinite but it should become clearer after the first few issues have been published.

The basic aim of C.J.Ch.E. is to provide a service to all chemical engineers in the country. With this objective before them the editorial board has recommended that each issue should have some research and some non-research papers with a yearly average of about 60% research and 40% non-research. The non-research papers will deal with subjects such as recent developments in unit operations, flow sheets and descriptions of new Canadian processes, waste treatment and pollution problems, equipment experiences, economics, operations research, and technical notes. Papers of general interest to chemists as well as to chemical engineers will be published by *Chemistry In Canada* as in the past.

Publication is essential for the research man, so we do not anticipate any problem in getting research papers, provided the technical standard of the journal is high. But publication is less essential for the non-research man—the plant engineer, the design engineer, etc.—and yet he is interested in finding out what his colleagues in other plants are doing. In turn he must be prepared to write about the things he has learned and the place to do this is in C.J.Ch.E. Thus, this is an appeal to all chemical engineers, whether engaged in teaching, research, plant operations or design, to contribute to the journal and, what is just as important, to write and tell me what kind of articles we should publish. The more specific these suggestions are the more help they will be.

There is another group of men who are essential to the success of the journal—the reviewers. We expect to publish about 50 papers per year and since each paper is reviewed by two men we will need about 100 reviews per year. Quite a number of men have volunteered to help and over 30 have already reviewed papers. These reviews have been well done and I would like to thank all these men for the time spent on studying the papers and for the helpful suggestions which they made. But we do not want to overwork these men, so I am appealing for more volunteers, particularly those who are familiar with recent developments in unit operations. Just drop me a line giving the field with which you are most familiar.

We have an excellent start on this new endeavour —many good papers have been submitted and many more have been promised. The success of the journal will depend on three groups, the authors, reviewers and readers. It is only with the continued help of the first two groups and the expected help of the third group that the C.J.Ch.E. will become the success that it now promises to be.

Effect of Gas Thermal Conductivity on Local Heat Transfer in a Fluidized Bed[1]

A. JACOB[2] and G. L. OSBERG[3]

Bed-wall heat transfer measurements in fluidized beds, as well as experiments with various heater probes, indicate that the smaller the heat transferring surface the larger the heat transfer coefficient. Furthermore, temperature gradients in fluidized beds are very small, except near the hot surface. It is, therefore generally believed that particle-particle heat transfer coefficients in the bulk of the bed are very large, probably because of the transient character of the heat transfer mechanism. To shed more light on this mechanism the authors measured heat transfer coefficients in fluidized beds of glass beads with a horizontal hot wire probe. The diameter of the wire (0.0052 in.) was of the same order of magnitude as the particle diameters (0.0115, 0.00602, 0.00242, 0.00122 in.). Eight gases with thermal conductivities ranging from 0.0048 to 0.097 btu(ft.) (hr.) (°F.) at 32°F. have been investigated. A heat transfer mechanism based on transient heat flow is proposed. The experimental data were correlated by the formula

$$h = h_o (1 - \epsilon)(1 - e^{-pk_f})$$

Where h is the observed heat transfer coefficient
h_o,p, are empirical constants
ϵ void fraction
k_f the thermal conductivity of the gas

Introduction

A characteristic feature of a fluidized bed in contact with a hot surface, e.g. the column wall, is the absence of temperature gradients in the bulk of the bed. Such gradients exist, however, near the hot surface. Hence, it is there that most of the resistance to heat transfer occurs.

To account for the high thermal resistance near the hot surface Leva and Grummer (1), Dow and Jakob (2) and Wicke (3) use the concept of a laminar gas film at the heater surface which controls the heat transfer by steady-state conduction. The thickness of this film is decreased by the scouring action of the moving particles giving rise to higher heat transfer coefficients in fluidized beds than in still beds or empty tubes. According to van Heerden and co-workers (4) a laminar film of the particle-fluid suspension which is formed between heater wall and fluidized bed constitutes the heat controlling element in the case of large heater surfaces. Beyond this film the high eddy conductivity of the bed results in a sharp decrease of the thermal resistance. The same authors were able to show that the heat transfer coefficients depend on the size of the heat transfer surface, high coefficients being obtained with small surfaces. Experiments with small heater probes performed by Mickley and Fairbanks (5) and Osberg (6) confirm this observation. Van Heerden and coworkers postulate therefore an unsteady-state heat transfer mechanism which is dominant at the "entrance" section of a heater, where particles at bed temperature touch the hot surface. Here, the full temperature difference between wall and bed gives rise to high local heat transfer coefficients, a thin gas film acting as conductive medium. When moving along the wall temperature equilibrium between particles and wall will be established so that the steady-state conduction through the laminar film of the particle-fluid suspension becomes more important.

A mechanism based on purely transient heat transfer is proposed by Mickley and Fairbanks (5), namely unsteady-state heat diffusion into packets of the solid-fluid suspension which are in rapid exchange at the heater wall.

This paper is based on experiments which have been undertaken to shed more light on the mechanism of heat transfer in a fluidized bed. The authors take the view that in most cases heat transfer in fluidized beds is made up of both steady-state and unsteady-state processes. This should show up in the heat transfer correlations through the presence of two additive terms. The relative importance of the latter depends on the experimental conditions, e.g. the size and shape of the heat transfer surface, its position in the bed and the bed dynamics. It is obvious that the smaller the heater surface the larger the contribution by the unsteady-state process. Thus, by making the

1 *Manuscript received February 2, 1957.*
Contribution from Division of Applied Chemistry, National Research Council, Ottawa, Ont.
2 *National Research Council of Canada Postdoctorate Fellow, 1955-56; now with Ciba Limited, Switzerland.*
3 *Head, Chemical Engineering Section, Applied Chemistry Division, N.R.C., Ottawa, Ont.*

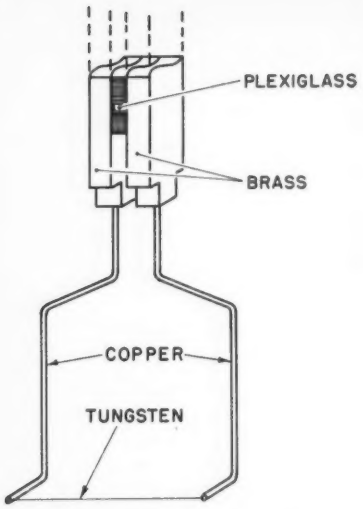

Figure 1—Hot wire probe.

heater very small, e.g. by using a hot wire probe as in the present case, the stationary term can be neglected. This results in a simplified correlation formula as only transient heat transfer has to be considered.

Experimental

The hot wire probe is shown in Figure 1. A tungsten wire 1.79 in. long and with a diameter of 0.0052 in. served as a filament. Tungsten was chosen because its mechanical properties are superior to those of platinum. The ends of the No. 10 gauge copper support wires were slotted and the tungsten wire attached by pinching and silver soldering. The two copper wires were hard soldered to two parallel brass rods, 0.5 x 0.25 in., 5 ft. long, separated by a strip of plexiglass, 0.125 in. thick. Two heavy stranded copper wires connected the brass rods to the bridge circuit shown in Figure 2. The hot wire probe formed one arm of the bridge. The current through the hot wire could be varied from about 0.5 to 5 amperes by means of two variable resistors.

The temperature-resistance relationship of the probe was found by calibration. To that purpose the probe was immersed in a mineral oil bath with stirrer and the total resistance of filament and leads measured at various oil temperatures by means of the bridge. From these values the resistance of the leads, found by short-circuiting the tungsten wire, was deducted.

A 3-in. Pyrex tube fitted with a stainless steel porous plate served as a fluidizing column. Spherical Scotchlite glass beads were used as a solid (Table 1). The particle diameter D_p given in Table 1 is the arithmetical mean of 100 particle diameters measured with a microscope. 2.86 lb. of solid were used for each run. Table 2 shows some of the properties of the eight fluidizing gases.

In a preliminary experiment heat transfer coefficients from the wire to the bed were measured with the probe at various distances above the porous plate. The vertical heat transfer profile so obtained showed a flat maximum at about half the height of the fluidized bed. Therefore, the hot wire was held for all experiments in a horizontal position at a distance of 4.7 in. from the bottom of the column.

To obtain a reading at a certain gas flow rate the bridge was set to a resistance corresponding to the desired wire temperature and the current through the wire adjusted to balance the bridge. For every gas-solid combination the flow rates were chosen to cover the whole range from still bed to vigorously bubbling bed. Furthermore, current readings were taken at different wire temperatures t_w, normally 112°F. and 212°F. For gases of high thermal conductivity, however, the maximum current carrying capacity of the bridge limited t_w to 167°F. Bed height, bed temperature and the pressure drop through 0.5 ft. of the bed were recorded, too. Every run was repeated once.

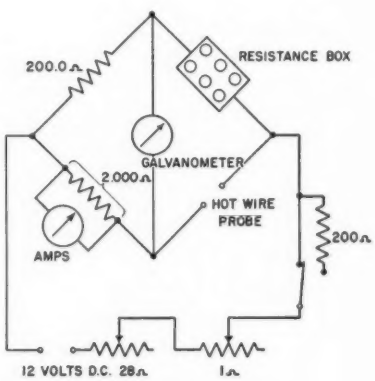

Figure 2—Bridge circuit.

Calculation of the Heat Transfer Coefficients

The power dissipated by the hot wire amounts to

$$Ji^2R_{t_w} \qquad (1)$$

which would lead to a heat transfer coefficient of

$$h^1 = \frac{Ji^2R_{t_w}}{\pi D_w l\,(t_w - t_b)}$$

However, not all the heat is given off to the bed at the surface of the hot wire. There is a heat loss by conduction through the tungsten wire to the copper leads, which are assumed to be at bed temperature.

It can be shown that the relative error amounts to

$$\frac{h^1 - h}{h^1} = \frac{R_{t_b}}{R_{t_w}} \times \frac{2}{\beta l} \qquad (2)$$

where

$$\beta^2 = \frac{4h}{k_w D_w} \qquad (3)$$

In Figure 3 heat transfer coefficients obtained with particles of a diameter $D_p = 11.5 \times 10^{-3}$ in. are plotted versus G/G_{mf}. The results for four gases are shown only. The similarity between the curves suggests the use of the maximum of every curve as a reference state to compare the thermal properties of the various solid-fluid combinations. h_{max} - values as well as the corresponding reduced mass velocities are found in Table 3.

TABLE 1
PROPERTIES OF GLASS BEADS*

Manufacturer's No.	Sieve Limits	D_p 10^{-3} ins.	ρ_s lbs./(ft.^{3})	ρ_b lbs./(ft.^{3})
118		1.22	154	93.0
	− 150 + 200	2.42	152	94.9
	− 80 + 100	6.02	152	93.0
109		11.5	156	94.3

* 3 m "Superbrite" glass beads manufactured by Minnesota Mining and Manufacturing Co. Ltd., 900 Fauquier Ave., St. Paul 6, Minn.

Heat Transfer Mechanism

The solids flow pattern in a fluidized bed is such that the particles can be assumed to move essentially in a direction perpendicular to the axis of a horizontal wire submerged in the center of the bed. In the model proposed here heat transfer from the hot wire to the fluidized bed is effected by the transient heating of particles touching the wire for a short time or passing it very closely. After having left the wire the particles give off their heat to other particles and the fluidizing gas. Obviously, the time between two successive contacts of one particle with the wire is large compared with the relaxation time of the particle-gas system. Consequently, particles arriving at the wire are at bed temperature.

The following assumptions have been made:

1. Heat transfer from the wire to the particles occurs only by conduction through a gas film, solid-solid heat exchange being negligible.
2. Thermal contact between one particle and the wire is established during a certain time τ, which is the residence time of the particle in the vicinity of the wire. τ is the average value and applies to all particles of a particular fluidized bed.
3. Heat transfer by forced convection to the fluidizing gas is neglected.
4. No temperature gradient is established within the particle during the heat-up period.
5. No temperature gradient exists in the filament in a direction perpendicular to the wire axis.

The heat flowing across the fluid space between a single particle and the heated wire in time dt is

$$k_f/b \,.A.\,(t_w - t_p) \qquad (4)$$

Heat accumulated by the particle in time dt is

$$C_{part.} \,.\, dt_p/_{dt} \qquad (5)$$

Equating (4) and (5) and rearranging

$$dt_p/_{dt} = \frac{k_f \,.A.}{bC_{part.}} \,.\, (t_w - t_p) \qquad (6)$$

Let $\alpha = k_f A/bC_{part.}$. From an integration over the average residence time τ, and the subtraction of $(t_w - t_b)$ from each side,

$$t_p - t_b = (t_w - t_b)\,(1 - e^{-\alpha\tau}) \qquad (7)$$

During the residence time τ, the heat quantity received by one particle is

$$q = C_{part.}\,(t_p - t_b) = C_{part.}\,(t_w - t_b)\,(1 - e^{-\alpha\tau}) \qquad (8)$$

TABLE 2

PROPERTIES OF GASES

Gas	k_f at 32°F. Btu/(ft.)(hr.)(deg. F.)	Temperature coefficient of k_f $(deg.\ F.)^{-1}$	Prandtl No. $\frac{C_p\mu}{k_f}$	Ref.
H_2	0.101	0.00155	0.718	(7)
He	0.0849	0.00117	0.638	(7)
81.0% H_2 19.0% N_2	0.0719	0.00155	0.444	(7) (8)
78.9% H_2 21.1% N_2	0.0633	0.00155	0.477	(7) (8)
37.6% H_2 62.4% N_2	0.0294	0.00158	0.519	(7) (8)
33.3% H_2 67.7% N_2	0.0272	0.00158	0.526	(7) (8)
Air	0.0141	0.00161	0.705	(7)
CO_2	0.00849	0.00261	0.809	(7)
Freon-12	0.00479	0.00372	0.732	(9)

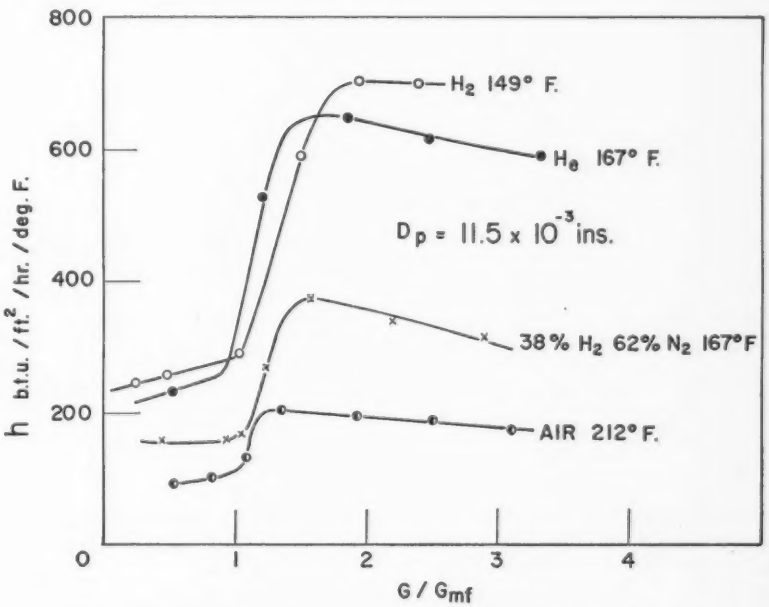

Figure 3—Heat transfer coefficients vs reduced mass velocity.

If n is the number of particles touching unit wire surface in unit time, the expression for heat transfer coefficient can be written

$$h = \frac{n \,.\, q}{t_w - t_b} = n\, C_{part.} \left(1 - e^{\frac{-Ak_f\tau}{bC_{part.}}}\right) \qquad (9)$$

Since n is proportional to the numbers of particles per unit volume, it is also proportional to $(1 - \epsilon)$, when a particular size group has been chosen. Substituting,

$$n.\ C_{part.} = h_o\,(1 - \epsilon) \qquad (10)$$

and

$$p = \frac{\tau A}{bC_{part.}} \qquad (11)$$

equation (9) now reads

$$h = h_o\,(1 - \epsilon)\,(1 - e^{-pk_f}) \qquad (12)$$

h_o and p are experimental constants,

TABLE 3
CALCULATED AND EXPERIMENTAL h_{max} — VALUES

D_p 10^{-3} ins.	Gas	t_w deg. F.	t_f deg. F.	$G/G_{mf_{exp.}}$	$1-\epsilon$	h_{max}, exp. Btu/(ft.²) (hr.) (deg. F.)	h_{max}, calc. Btu/(ft.²) (hr.) (deg. F.)	Deviation %
1.22	H_2	149	61	118[1]	0.481	1,260	1,261	+0.1
	He	167	69	248[1]	0.406	1,065	1,048	−1.6
	81.0 H_2 19.0 N_2	167	67	230[1]	0.437	1,115	1,109	−0.5
	78.9 H_2 21.1 N_2	167	66	216[1]	0.440	1,050	1,092	+4.0
	33.3 H_2 66.7 N_2	167	60	258[1]	0.422	740	765	+3.4
	Air	212	72	188[1]	0.415	513	508	−1.0
	CO_2	212	69	80[1]	0.425	375	375	0.0
	Freon-12	167	53	145[1]	0.429	275	240	−12.7
2.42	H_2	149	59	5	0.517	1,050	1,057	+0.7
	He	167	67	81[1]	0.469	990	937	−5.4
	81.0 H_2 19.0 N_2	167	66	8	0.496	960	966	+0.6
	78.9 H_2 21.1 N_2	167	65	5	0.502	950	947	−0.3
	33.3 H_2 66.7 N_2	167	58	5	0.512	595	660	+10.9
	Air	212	70	4.5	0.513	395	432	+9.4
	CO_2	212	68	7	0.474	305	285	−6.6
	Freon-12	212	66	4	0.510	217	201	−7.4
6.02	H_2	149	58	1.9	0.534	865	839	−3.0
	He	167	67	1.9	0.549	810	830	+2.5
	81.0 H_2 19.0 N_2	167	64	1.9	0.537	840	784	−6.7
	78.9 H_2 21.1 N_2	167	63	1.9	0.549	775	769	−0.8
	33.3 H_2 66.7 N_2	167	57	–	0.545	480	494	+2.9
	Air	212	69	1.5	0.559	290	320	+10.3
	CO_2	212	70	1.7	0.558	230	228	−0.9
	Freon-12	212	66	1.7	0.546	150	145	−3.3
11.5	H_2	149	56	1.95	0.525	705	716	+1.6
	He	167	64	1.6	0.518	645	661	+2.5
	81.0 H_2 19.0 N_2	167	63	1.6	0.542	650	656	+0.9
	78.9 H_2 21.1 N_2	167	61	1.7	0.525	630	598	−5.1
	37.6 H_2 62.4 N_2	167	57	–	0.517	375	368	−1.9
	Air	212	68	1.25	0.537	210	218	+3.8
	CO_2	212	68	1.3	0.535	147	152	+3.4
	Freon-12	212	65	1.15	0.543	102	97.7	−4.2

[1] G_{mf} calculated according to Graf E., Thesis. Zurich (1955).

their values depending on experimental conditions. Using h_{max} values defined earlier, a set of constants has been computed for each specified particle size. These sets have been calculated from the experimental results by the method of least squares; and are given in Table 4. h_{max} values calculated with these constants are compared with experimentally determined h_{max} values in Table 3.

The temperature t_f at which the thermal conductivity k_f of a gas was taken, was chosen to be the arithmetical mean between the wire temperature t_w and a mean particle temperature t_p

TABLE 4
SUMMARY OF EMPIRICAL CONSTANTS IN FORMULA (12)

D_p 10^{-3} ins.	h_o btu/(ft.²) (hr.) (deg. F.)	p (ft.) (hr.) (deg. F.)/Btu
1.22	2,660	36
2.42	2,110	30
6.02	1,660	25
11.5	1,550	18

$$t_f = \frac{t_w + t_p}{2} = t_w - \frac{t_w - t_b}{2pk_f}(1 - e^{-pk_f}) \qquad (13)$$

To calculate t_f from equation (13) an approximate value of p was determined by taking k_f at the mean temperature between wire and bed.

In Figure 4 experimental h_{max}–values have been plotted against the gas thermal conductivity. The curves were calculated from equation (12) using the values for h_o and p given in Table 4.

Discussion

The fact that heat transfer coefficients from a hot wire to a fluidized bed can be reasonably well predicted for eight different fluidizing gases with the use of only two experimental constants is strong support for the mechanism proposed here. So far, the two constants h_o and p have to be determined by experiment. Further experimental work has to be done to arrive at correlations for h_o and p with variables like G, D_p, D_w and the physical properties of gas and solid, as well as the dimensions of the column.

A more general correlation involving the constants h_o and p, should yield useful information about the dynamics of a fluidized bed. h_o has the dimension of a heat transfer coefficient. The product $h_o\ (1-\epsilon)$ actually represents the inherent heat transfer potential of a fluidized bed in contact with a hot wire. Because of the finite values of gas thermal conductivities only a fraction of this potential can be utilized, this fraction being represented by the factor $(1-e^{-pk_f})$. According to equation (10) $h_o\ (1-\epsilon)$ is closely related to the solids mass flow past the wire:

$$n\ m_{part.} = \frac{h_o\ (1-\epsilon)}{c_s} = n \times \frac{\pi}{6} \cdot D_p^3\ \rho_s \qquad (14)$$

The dimension of $\frac{h_o\ (1-\epsilon)}{c_s}$ is that of

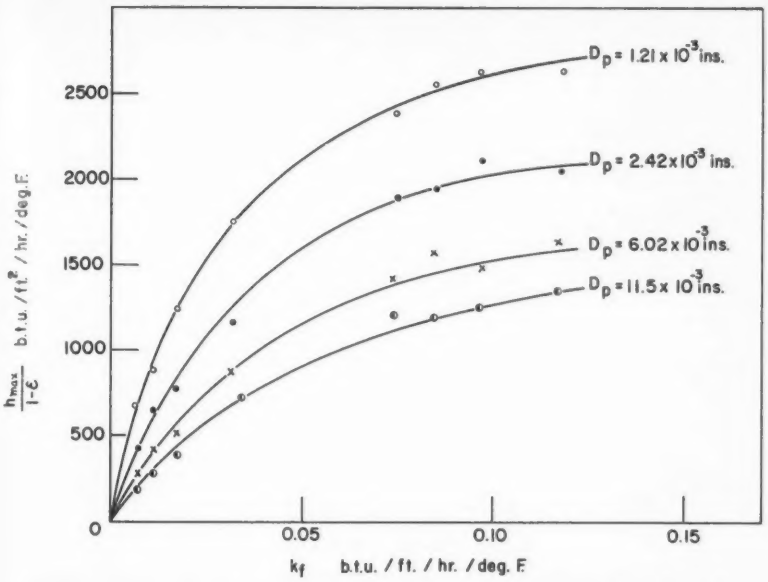

Figure 4—Maximum heat transfer coefficients vs gas thermal conductivity.

a mass velocity, $ML^{-2}t^{-1}$. There is not necessarily a simple relationship between this mass velocity and the solids motion of the bed, because of the possible interference to flow of particles by the hot wire itself. But since the solids mass velocity is related to the linear particle velocity it should be possible to measure particle velocities with a suitable hot wire probe.

Nomenclature

A	Area of heat path
b	Length of heat path
$C_{part.}$	Heat capacity of one particle
c_s	Heat capacity of solid
D_p	Particle diameter
D_w	Wire diameter
G	Superficial mass velocity of fluid
G_{mf}	Superficial mass velocity at incipient fluidization
h	Heat transfer coefficient
i	Electric current through wire probe
J	Thermal equivalent of electrical energy
k_f	Thermal conductivity of fluid
k_w	Thermal conductivity of wire material (tungsten)
l	Length of hot wire
$m_{part.}$	Mass of one particle
n	Number of particles per unit time, touching unit wire surface
R_{tb}	Resistance of wire at bed temperature
R_{tw}	Resistance of hot wire
t_b	Bed temperature
t_f	Temperature at which thermal conductivity of fluids were taken
t_p	Particle temperature
t_w	Wire temperature
t	Time
ϵ	Void fraction
μ	Viscosity of fluid
ρ_b	Bulk density of solid
ρ_s	Density of solid
τ	Residence time

References

(1) Leva, M., and Grummer, M., Chem. Eng. Progr. *48*, 307 (1952).
(2) Dow, W. M., and Jakob, M., Chem. Eng. Progr. *47*, 637 (1951).
(3) Wicke, E., Chem. Ing. Tech. *23*, 405 (1951).
(4) van Heerden, C., Nobel, A. P. P., and van Krevelen, D. W., Ind. Eng. Chem. *45*, 1237 (1953).
(5) Mickley, H. S., and Fairbanks, D. F., A.I.Ch.E. Journal *1*, 374 (1955).
(6) Osberg, G. L., Ind. Eng. Chem. *43*, 1871 (1951).
(7) Dickins, B. G., Proc. Roy. Soc. (London). *A143*, 517 (1934).
(8) Brunot, A. W., Trans. Am. Soc. Mech. Engrs. *62*, 613 (1940).
(9) McAdams, W. H., Heat Transmission, McGraw-Hill (1954).

* * *

Counter Diffusion of Ions in Water[1]

E. R. GILLILAND[2], *R. F. BADDOUR*[3], *and D. J. GOLDSTEIN*[4]

In most ion diffusion processes, more than one ion has a concentration gradient. Differences in ionic mobilities result in the buildup of a potential gradient by the diffusion process itself. Thus, for ionic diffusion problems, the flux must be expressed as the sum of two terms, one involving concentration gradient and the other involving the electric field. Such an expression has long been known to apply to salt diffusion. It is shown here that the same expression is applicable to the simultaneous diffusion of two ions of the same charge in opposite directions, whether or not the third, common ion is mobile.

The general equations for the simultaneous diffusion of many ions are set up. These equations are integrated for the case of diffusion in diaphragm cells. The results of this integration agree well with experimental data obtained for the counter diffusion of hydrogen ion with ammonium, calcium, and lanthanum ions, all in tenth normal chloride solutions.

It is concluded that rates of counter diffusion of simple ions in dilute water solutions can be estimated quite well from the ionic equivalent conductances alone.

By counter diffusion is meant the diffusion of two ions of the same charge in opposite direction. This problem occurs in many cases of mass transfer where diffusion of ionic species is involved. Counter diffusion is involved in correlating liquid side resistance to the rate of ion exchange (1). Sherwood and Wei (2) have recently used the methods discussed here to investigate the rate of neutralization of HCl by NaOH in a diaphragm cell.

These two cases will be discussed later, with the wider aspects of the problem, when a specific case has first been dealt with. This specific case is counter diffusion in diaphragm cells and the theoretical prediction of the experimental results.

Experimental Equipment

Experiments were made in diaphragm cells. A cell is pictured in Figure 1. It is a device for obtaining two well stirred reservoirs separated by a completely stationary water layer. The two reservoirs are filled with different solutions and interchange between the reservoirs takes place by diffusion through the stationary layer separating them. The concentration of the various species in each reservoir is determined as a function of time. The diffusion zone is held stationary by making it a water filled, porous, glass diaphragm. It is the repeated experience of many investigators that diffusion coefficients determined in a diaphragm cell are the same as diffusion coefficients determined by other methods (3).

Procedure. (1) The lower reservoir, the one with the stop-cock, was rinsed with the desired solution, and then the reservoir and diaphragm were filled with this solution. (2) The upper reservoir was rinsed with a different solution and some 50 cc. put into the reservoir. (3) The cell was left for 45 min. to establish concentration gradients through the diaphragm. (4) The upper solution was poured off and a volume of fresh solution equal to the volume of the lower compartment was pipetted into the upper reservoir. The time was noted as the start of the run. The material balance at the end of the run always showed that there was no noticeable change in the concentrations in the lower reservoir during the preliminary run. (5) The cell was put in a water bath at 25°C. and rotated about its longitudinal axis with this axis at about 7° to the vertical. This caused the glass sinker and float to roll around the diaphragm and stir the reservoirs. (6) At the end of the run the reservoir solutions were drawn off and analyzed.

Systems Studied. The counter diffusion of H^+ with NH_4^+, H^+ with Ca^{++}, and H^+ with La^{+++} was studied. The anion was always Cl^- and the initial total normality was 0.1. Table 1 gives a list of the solutions initially put into each reservoir.

These systems were selected because they represent a good range of valency. Also, all the ions except La^{+++} could be readily determined chemically. H^+ is the fastest moving ion, and these systems have a large difference between the ionic self diffusion coefficients of the counter diffusing ions. It was therefore thought that a significant movement of Cl^- might occur.

The total normality of 0.1 is large enough to make chemical analysis simple and small enough so that infinite dilution values of diffusivities might be applicable. The initial normality difference between the reservoirs of 0.04 was large enough to prevent errors caused by differencing two large numbers, and small enough so that some idea of the effect of the ratio of concentrations of the counter diffusing ions might be obtained. The initial normality difference of 0.1 is the worst case from the point of view of the approximations in the theoretical treatment.

Chemical Analysis. The primary standards were prepared by dissolving known weights of silver nitrate or sodium chloride in known volumes of water. The standards were titrated against each other. Reagent grade chemicals, without further purifica-

1 *Manuscript received February 21, 1957.*
Contribution from the Chemical Engineering Department, Massachusetts Institute of Technology, Cambridge, Mass.
2 *Professor of Chemical Engineering, Massachusetts Institute of Technology.*
3 *Assistant Professor of Chemical Engineering, Massachusetts Institute of Technology.*
4 *Chemical Engineer, Canadian Industries Limited, Central Research Laboratory, McMasterville, Que.*

tion, were used. Stock solutions of exactly 0.1N HCl, NH_4Cl, $CaCl_2$ and $LaCl_3$ were prepared. The various initial reservoir solutions were made by mixing appropriate volumes of these stock solutions.

Hydrogen ion was determined by titrating with ammonium hydroxide or sodium hydroxide to an end point with bromophenol blue. Ammonium ion was determined by adding 5 cc. of neutral 37% formaldehyde to the neutral solution and determining the liberated hydrogen ion by titrating with sodium hydroxide to an end point with phenophthalein. Calcium ion was titrated with ethylene diamine tetraacetic acid disodium salt containing a little magnesium ion to an end point with Eriochrome black T in the presence of an ammonium hydroxide-ammonium chloride buffer. Lanthanum ion was not determined.

Accuracy. The question of whether transfer through the diaphragm occurs by other means than diffusion has been fully discussed [3, 4, 5]. It is not thought to have happened in these experiments. The water bath was controlled at 25± 0.2°C. A change of 0.2°C. will not change the ionic diffusion coefficients by more than 1%. Also this temperature change will not cause a significant volume of solution to be pumped from the lower, closed reservoir into the diaphragm. Many of the runs of less than three days were made three times and the results are reproducible. The accuracy is probably limited by the chemical analysis, and it is estimated that the concentrations were determined to within 0.0005 N.

Calibration of Diaphragm Cells. If a Fick type equation

$$N = -\mathcal{D}\,\delta c/\delta x \qquad (1)$$

is integrated for a diaphragm cell with the coefficient assumed constant, the result is [3]

$$\ln(\Delta c_f/\Delta c_b) = -\beta\mathcal{D}t \qquad (2)$$

where β is the cell constant given by

$$\beta = \frac{A}{l}\left(\frac{1}{V'} + \frac{1}{V''}\right) \qquad (3)$$

The method of integration is similar to the one used later with the more complex differential equation for counter diffusion. β was determined by allowing 0.1N KCl to diffuse into initially pure water until the reservoir concentrations were about 0.088 N and 0.012N (48 hours). A value of $\mathcal{D}$, the integral salt diffusion coefficient of potassium chloride, of

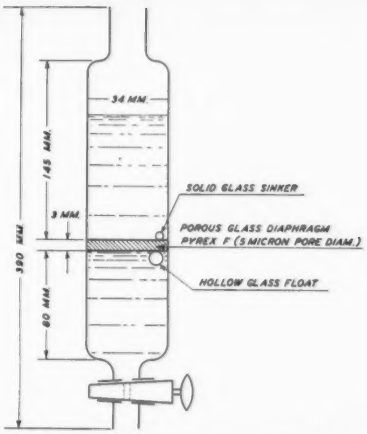

Figure 1—Glass diaphragm diffusion cell. (Material is pyrex; all dimensions are approximate).

1.87 x 10^{-5}cm²/sec (as recommended by Stokes [5]) was used to compute β.

Two cells were used in this series of experiments. They were calibrated repeatedly over the course of nine months. The cell constants determined from these calibrations did not vary over this period. Values of β for the two cells were 0.0844 ± .008 and 0.0842 ± .008 (the error figures are average deviations of 6 different calibrations, each calibration being the average of three runs). A value of β of 0.0843 was used in all the calculations.

Experimental Results

The experimental results are presented graphically in Figures 2 to 17. The legends for the graphs are lengthy and have been listed in Table 1 instead of on the graphs. The difference in reservoir concentrations for each ion is plotted against the time. The results show some interesting features. The plots for the counter diffusing ions are nearly straight lines on a semi-logarithmic scale. As equations (1) and (2) show, this means that a constant coefficient can be assigned to each ion satisfactorily. However, the curves are not quite straight, being slightly concave upwards, showing that the apparent coefficient decreases as time increases, i.e., as Δc decreases. The La^{+++} points were computed by assuming electroneutrality in each reservoir since La^{+++} was not determined chemically.

The chloride ion, which is referred to as the *common ion*, has zero concentration gradient at zero time, and must have zero concentration gradient at equilibrium at infinite time. Thus the concentration difference should pass through a maximum. This is the case, and the peak value of Δc is quite large, in some cases more than 25% of the initial Δc for the counter diffusing ions.

Theoretical Treatment of the Simultaneous Diffusion of Many Ions

The basic theory is well established [3, 5]. It will be mentioned here because the underlying assumptions need emphasizing. First, a clear distinction must be made between the practical coefficient, $\mathcal{D}$*, and the ionic self diffusion coefficient at zero concentration, D. The practical coefficient is in general a function of the mobilities, concentrations and concentration gradients of all the ions present. Its usefulness depends on how constant it is. It is demonstrably useful for the experiments done here, and the method of calculating it will be discussed. D is a property of the individual ion. It is computed from the ionic equivalent conductance, λ, by the relationship

$$D = \frac{RT\lambda}{F^2 z} \qquad (4)$$

D is related to the ionic electrical mobility, u, by the equation

$$D = \frac{RTu}{Fz} \qquad (5)$$

It should be noted that a table of ionic equivalent conductances at infinite dilution is the only information needed for the calculations in this work. However, activity data are helpful, especially if a higher total normality is used (the experimental total normality was 0.1).

Since all ions do not move at the same rate under the same concentration gradients, most diffusion experiments result in a separation of ions, and an electric potential is set up by the diffusion process itself. Thus, in the general case, the equation $N = -D\delta c/\delta x$ is not correct; an extra term involving the potential gradient must be added. The most useful way of expressing ionic flux in free diffusion is, therefore, to write.

$$N_i = E\,u_i c_i - D_i\,\delta c_i/\delta x \qquad (6)$$

for ions of the i type. The quantities λ, u, z, have been taken positive for cations and negative for anions. Equation (4) shows that with this convention, D is always positive. This convention means that equation (6) applies to cations or anions.

Now, although a separation of ions occurs, it is very small. If n equiva-

*The use of two different symbols, $\mathcal{D}$ and D, is not usual, and has been adopted here for clarity.

lents of a cation are placed r centimeters away from n equivalents of an anion in water, the potential gradient between them is about 1.1 x 10^{15} n/r^2 volts/cm. Thus only a very small separation of ions is needed to produce a large potential gradient, and, in making a material balance it is a very good approximation to assume electro-neutrality and write

$$\Sigma c_i(+) = \Sigma c_i(-) \quad (7)$$

where Σ means summed for all the ions, cations or anions, present. Differentiating,

$$\Sigma G_i(+) = \Sigma G_i(-) \quad (8)$$

where G has been used as an abbreviation for $\delta c/\delta x$. To preserve electroneutrality it is necessary to put

$$\Sigma N_i(+) = \Sigma N_i(-) \quad (9)$$

Combining equation (6) with equation (9) to eliminate E, and with equation (5) to eliminate u, gives

$$N_i = -D_i G_i + D_i z_i c_i \frac{\Sigma D_i G_i(+) - \Sigma D_i G_i(-)}{\Sigma D_i z_i c_i(+) - \Sigma D_i z_i c_i(-)} \quad (10)$$

Vinograd and McBain [6] derived equation (10) and have successfully used it to predict the simultaneous diffusion of two salts. Sherwood and Wei [2] have used it to predict the rate of neutralization of HCl by NaOH and of acetic acid by NaOH.

Integration of the Diffusion Equations for Counter Diffusion in a Diaphragm Cell

In the simplest case of counter diffusion, which includes the experiments described here, *three ions are involved*. Let suffixes 1 and 2 refer to counter diffusing cations, and suffix 3 refer to the common anion. Equations (7) and (8) can be used to eliminate c_3 and G_3 from equations (10) to give

$$N_1 = f G_1 + g G_2 \quad (11a)$$

$$N_2 = h G_1 + k G_2 \quad (11b)$$

where

$$f = \frac{D_1 D_3 (z_3 - z_1)c_1 - D_1 (D_2 z_2 - D_3 z_3)c_2}{(D_1 z_1 - D_3 z_3)c_1 + (D_2 z_2 - D_3 z_3)c_2} \quad (12a)$$

$$g = \frac{D_1 (D_2 - D_3) z_1 c_1}{(D_1 z_1 - D_3 z_3)c_1 + (D_2 z_2 - D_3 z_3)c_2} \quad (12b)$$

$$h = \frac{D_2 (D_1 - D_3) z_2 c_2}{(D_1 z_1 - D_3 z_3)c_1 + (D_2 z_2 - D_3 z_3)c_2} \quad (12c)$$

$$k = \frac{D_2 D_3 (z_3 - z_2)c_2 - D_2 (D_1 z_1 - D_3 z_3)c_1}{(D_1 z_1 - D_3 z_3)c_1 + (D_2 z_2 - D_3 z_3)c_2} \quad (12d)$$

Now two further approximations will be made. The *concentration gradients will be taken as linear*, i.e., the substitutions

$$G_1 = \Delta c_1/l, \quad G_2 = \Delta c_2/l \quad (13)$$

will be made, and the quantities, *f, g, h, k, will be taken as constants* during the integration. f, g, h, k, will be evaluated at *average values of* c_1 *and* c_2. These values were the arithmetic average of the reservoir concentrations. Because the reservoirs have equal volume the arithmetic average concentration is also the concentration everywhere at infinite time.

At the boundaries of the diaphragm, the concentration, c, must equal the reservoir concentrations, c′, c″. Also, in the reservoirs

$$AN/V' = \delta c'/\delta t \text{ and } AN/V'' = -\delta c''/\delta t \quad (14)$$

so that

$$\delta (c' - c'')/\delta t = \delta \Delta c/\delta t = (A/V' + A/V'')N \quad (15)$$

Combining the boundary condition (15) with equations (11) and the approximations (13), gives

$$\delta \Delta c_1/\delta t = \beta(f \Delta c_1 + g \Delta c_2) \quad (16a)$$

$$\delta \Delta c_2/\delta t = \beta(h \Delta c_1 + k \Delta c_2) \quad (16b)$$

The integration of equations (16) for the initial condition

$$\Delta c_1 = -\Delta c_2 = \Delta_o \text{ at } t = 0 \quad (17)$$

gives the result

$$\Delta c_1 = A_1 e^{\beta m_1 t} + B_1 e^{\beta m_2 t} \quad (18a)$$

$$\Delta c_2 = A_2 e^{\beta m_1 t} + B_2 e^{\beta m_2 t} \quad (18b)$$

where m_1, m_2 are the roots of the quadratic equation

$$m^2 - (f+k)m + kf - gh = 0 \quad (19)$$

and

$$A_1/\Delta_o = (m_2 - f + g)/(m_2 - m_1), \quad B_1/\Delta_o = (m_1 - f + g)/(m_1 - m_2) \quad (20)$$

$$A_2 = (m_1 - f) A_1/g, \quad B_2 = (m_2 - f) B_1/g \quad (21)$$

When these equations are applied to special cases, the results are reasonable. If c_1/c_2 is allowed to tend to zero, it is found that ion 1 (which is present in trace quantities) moves with its self diffusion coefficient. The special case $D_3 = 0$ (which is referred to as the case of immobile common ion), and the case $D_1 = D_2$ which gives the same result, will be discussed later.

If $D_2 = D_3$, it is found that the coefficients A_2 and B_2 are indeterminate, being zero over zero. In fact, the solution of the equations is a little different. Equations (18) to (20) apply, but equation (21) does not apply and must be replaced by equation (22),

$$A_2'/\Delta_o = h/(f-k), \quad B_2/\Delta_o = (k - f - h)/(f - k) \quad (22)$$

This case is important because the self diffusion coefficients of NH_4^+ and Cl^- are so close that equations (22) had to be used and not equations (21) in calculating the H^+–NH_4^+–Cl^- system.

The Calculated Curves. In making the calculations, the following values of the self diffusion coefficients were used: $H^+ = 9.311 \times 10^{-5}$, $NH_4 = 1.954 \times 10^{-5}$, $Ca^{++} = 0.7919 \times 10^{-5}$, $La^{+++} = 0.6166 \times 10^{-5}$, $Cl^- = 2.032 \times 10^{-5}$, cm^2/sec. These were computed from values of the ionic equivalent conductance from Conway's "Electrochemical Data". It must be remembered that z_3 is negative. The experimental points for the common ion are less accurate than those for the counter diffusing ions, as the measured concentrations are differenced to four significant figures instead of three.

Equations (18) to (22) were used to compute *the solid lines in the graphs*, Figures 2 to 17. The agreement between theory and experiment is quite satisfactory, particularly considering the approximations involved. For example, for the experiments plotted in Figure 6, at zero time, c_1/c_2 was zero at one surface of the diaphragm and infinite at the other surface, and yet a satisfactory prediction of the experimental results was obtained by taking c_1/c_2 equal to one throughout the diaphragm for all time. The reason why such extreme variations in concentration can be ignored is not fully understood, but must be tied up with the fact that the diaphragm is very small and very little material accumulates in it. For the mathematically simpler case of immobile common ion, the assumption that no material accumulates in the diaphragm makes it possible to demonstrate that the variations of concentration can be ignored (see below).

The solid lines plotted in Figures 2, 3, 4, 5 were calculated by taking $C_{H^+}/C_{NH_4^+} = 0.25, 0.667, 1.5, 4$, respectively. The agreement between theory and experiment improves in this order. Part of the reason for this is that the quantities f, g, h, k, change less rapidly with $C_{H^+}/C_{NH_4^+}$ when $C_{H^+}/C_{NH_4^+}$ is large. The same trend is noticeable for the Ca^{++}–H^+ results.

Vinograd and McBain have successfully used the same approximations as here to predict the simultaneous diffusion of two salts (three ions moving in the same direction). However, counter diffusion experiments test the usefulness of the approximations more than salt diffusion experi-

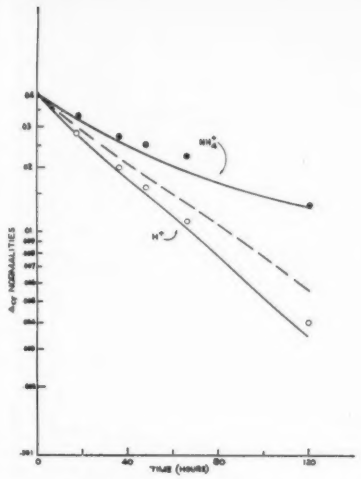

Figure 2 — see Table 1

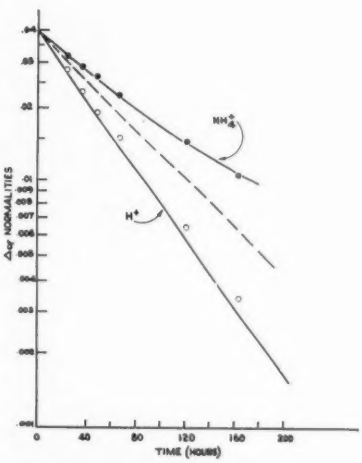

Figure 3 — see Table 1

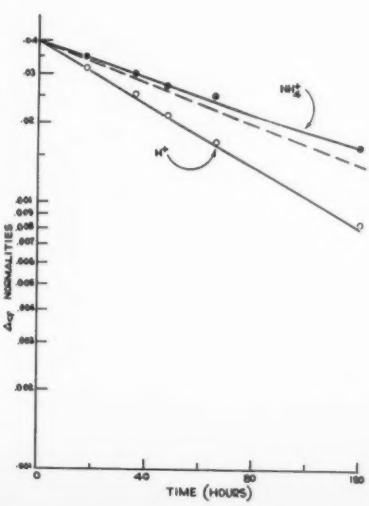

Figure 4 — see Table 1

TABLE 1
SYSTEMS STUDIED AND LEGENDS FOR THE GRAPHS, FIGURES 2 TO 17

Initial Solution Normalities		Results Presented in Figure Number
Reservoir 1	Reservoir 2	
HCl 0, NH_4Cl 0.10	HCl 0.04, NH_4Cl 0.06	2, and 15 curve 1
HCl 0.02, NH_4Cl 0.08	HCl 0.06, NH_4Cl 0.04	3, and 15 curve 2
HCl 0.04, NH_4Cl 0.06	HCl 0.08, NH_4Cl 0.02	4, and 15 curve 3
HCl 0.06, NH_4Cl 0.04	HCl 0.10, NH_4Cl 0	5, and 15 curve 4
HCl 0.1	NH_4Cl 0.1	6 and 16
HCl 0, $CaCl_2$ 0.10	HCl 0.04, $CaCl_2$ 0.06	7, and 17 curve 1
HCl 0.02, $CaCl_2$ 0.08	HCl 0.06, $CaCl_2$ 0.04	8, and 17 curve 2
HCl 0.04, $CaCl_2$ 0.06	HCl 0.08, $CaCl_2$ 0.02	9, and 17 curve 3
HCl 0.06, $CaCl_2$ 0.04	HCl 0.10, CaCl 0	10, and 17 curve 4
HCl 0, $LaCl_3$ 0.10	HCl 0.04, $LaCl_3$ 0.06	11
HCl 0.02, $LaCl_3$ 0.08	HCl 0.06, $LaCl_3$ 0.04	12
HCl 0.04, $LaCl_3$ 0.06	HCl 0.08, $LaCl_3$ 0.02	13
HCl 0.06, $LaCl_3$ 0.04	HCl 0.10, $LaCl_3$ 0	14

LEGENDS FOR THE GRAPHS

Figures 2–14: Counter Diffusing ions

Experimental points, ○ = H^+, ● = NH_4^+, Ca^{++} or La^{+++}

Calculated lines

_____ _____ with immobile common ion

_____ with mobile common ion

– – – – – – – – – – – – with mobile common ion and activity correction

Figures 15–17: Common ion

Experimental points for Cl^-; calculated lines

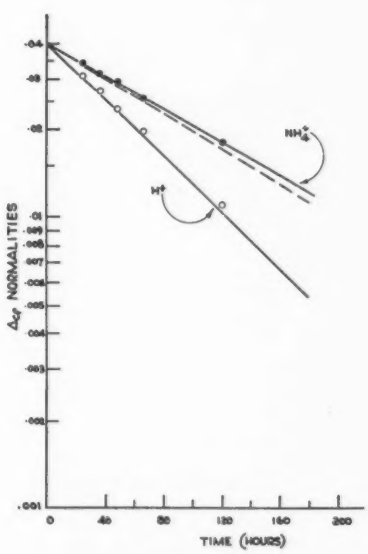

Figure 5 — see Table 1

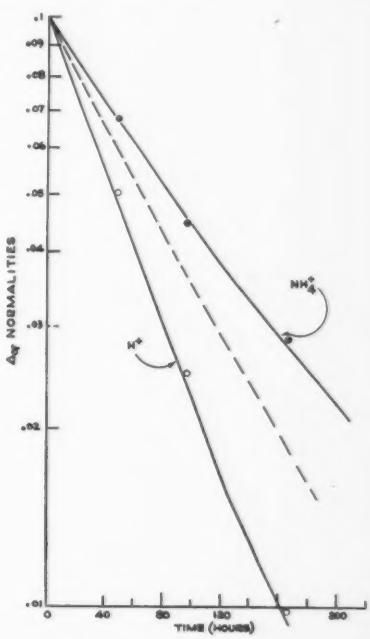

Figure 6 — see Table 1

ments because the ratios of the ionic concentrations vary much more in counter diffusion experiments.

The Effect of Finite Concentration. The values of the ionic self diffusion coefficients, used to compute the solid lines of the graphs, were themselves computed from values of the ionic equivalent conductance at *zero concentration* by using equation (4). In fact, zero concentration has been assumed throughout this treatment. The basic flux equation (6) has no terms for inter-

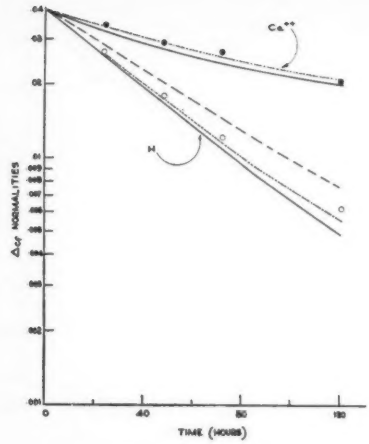

Figure 7 — see Table 1

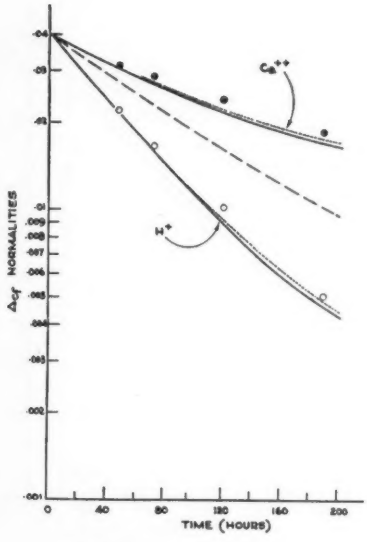

Figure 8 — see Table 1

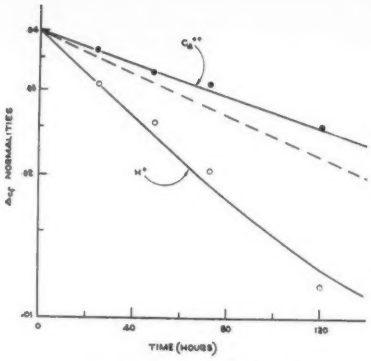

Figure 9 — see Table 1

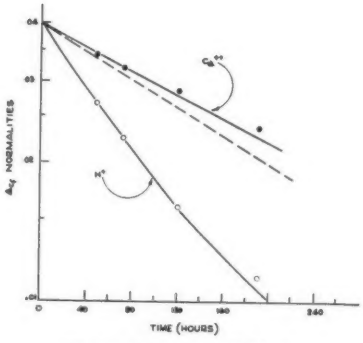

Figure 10 — see Table 1

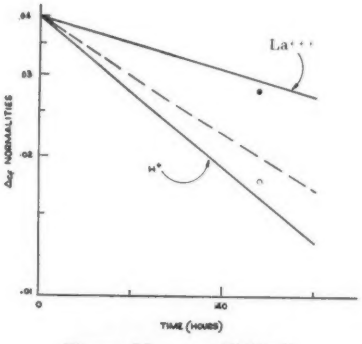

Figure 11 — see Table 1

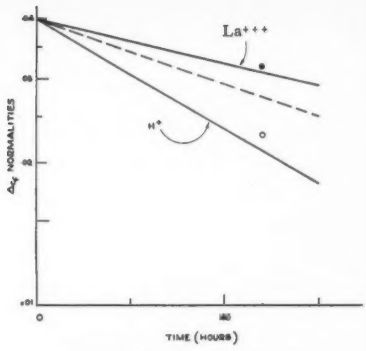

Figure 12 — see Table 1

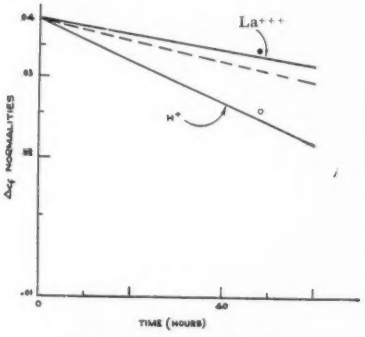

Figure 13 — see Table 1

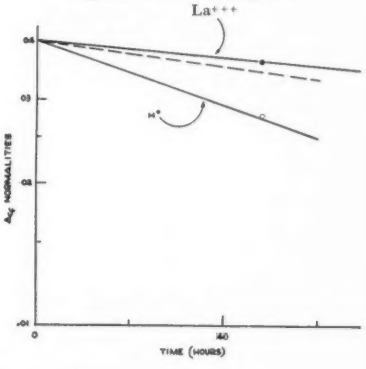

Figure 14 — see Table 1

action between the ions (other than the general field term) which would be needed at finite concentrations.

Hartley [7] points out that the chemical potential gradient is the driving force for a diffusion process. In the flux equation (6), the concentration gradient term should have involved activities and not concentrations. This means that one way to correct for finite concentration is to multiply every self diffusion coefficient used by the correction term $(1 - \delta \ln \gamma / \delta \ln c)$. Here γ is the ionic activity coefficient, and, for the counter diffusing ions the variation of γ with c in solutions of constant normality is needed. To get a rough picture of this correction, the simplest method was used. It was assumed, after Lewis and Randall, that the activity coefficients were functions of

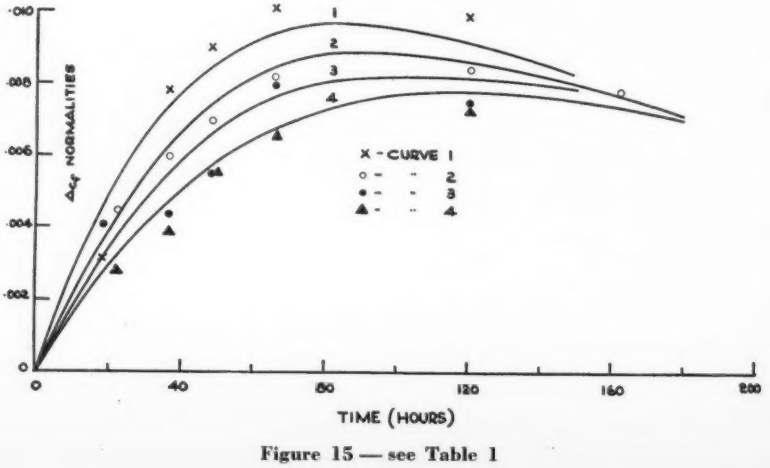

Figure 15 — see Table 1

the ionic strength only. This results in no correction for the $H^+ - NH_4^+ - Cl^-$ system because the ionic strength is independent of $C_H^+/C_{NH_4}^+$. For two sets of the $H^+ - Ca^{++} - Cl^-$ system, the correction was appreciable. The corrected curves are plotted as dotted lines in Figures 7 and 8. The dotted lines describe the experiments better than the solid lines. In Figure 9 and 10 the correction is negligible. Corrections for the $H^+ - La^{+++} - Cl^-$ system would be similar to those for the $H^+ - Ca^{++} - Cl^-$ system, only larger. However, the activity coefficient of La^{+++} is so different from one that it is doubtful if the Lewis and Randall limiting rule can be applied and the corrections were not made.

The integration of equations (11) is specific for the geometry of the diaphragm cells. It is worth while considering some other approaches to this problem, which could be used for other problems. The success of the approximations used in integrating suggests that the same approximations could be used in other methods of solution.

Ionic Practical Counter Diffusion Coefficients with Mobile Common Ion

Following the method of Vinograd and McBain, practical coefficients can be defined for the two counter diffusing ions by the equations.

$$N_1 = -\mathcal{D}_1 G_1, \quad N_2 = -\mathcal{D}_2 G_2 \qquad (23)$$

Equations (11) and (13) show that the practical coefficients are given by

$$\mathcal{D}_1 = f + (g\Delta c_2/\Delta c_1) \qquad (24a)$$

$$\mathcal{D}_2 = k + (h\Delta c_1/\Delta c_2) \qquad (24b)$$

In Table 2, under the heading mobile common ion, some values of $\mathcal{D}_1$ and $\mathcal{D}_2$ are given for two of the systems studied. These values were computed by taking the value of $\Delta c_1/\Delta c_2$ at the very beginning of the experiment, at zero time; i.e., $\Delta c_1/\Delta c_2 = -1$. Also, as before, f, g, h, k were computed by using average values of c_1 and c_2. If these coefficients were to be used in the cell equation, (2), to find the curve of Δc against time, the curves for the counter diffusing ions would coincide with the solid lines in Figures 2 to 14 at zero time and be straight lines having the same slope that the solid lines have at zero time. Because the experimental lines are remarkably straight, *the constant practical coefficients are very useful*, and certainly their use is simpler than using the integrated equations, (18) to (22). For short experiments, this approach to predicting the curves is probably the best.

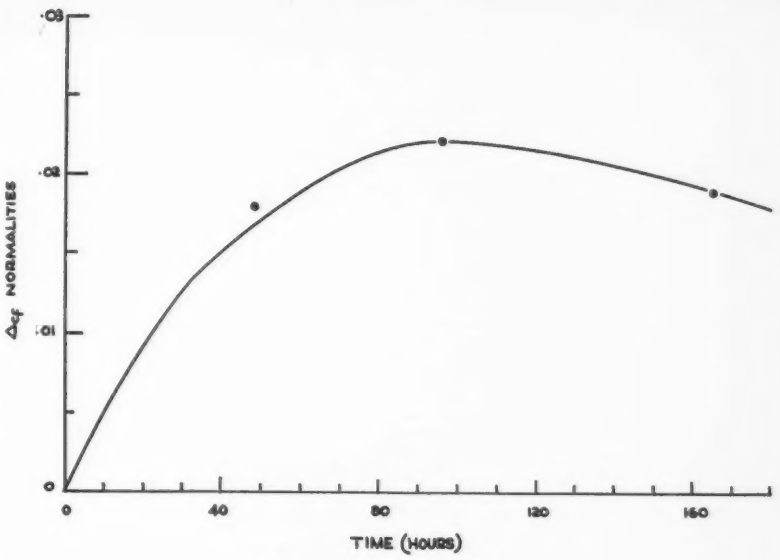

Figure 16 — see Table 1

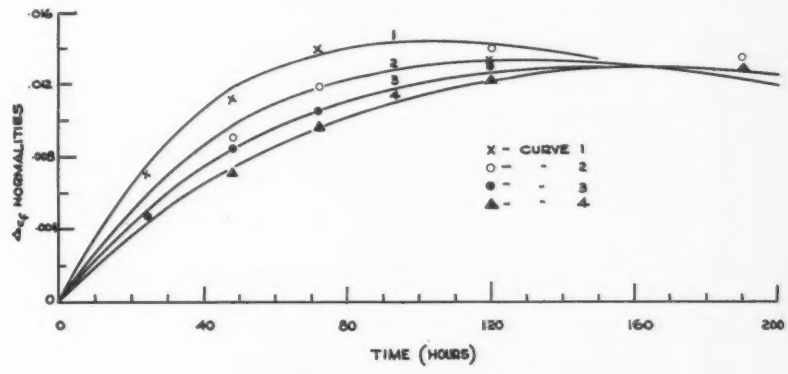

Figure 17 — see Table 1

Counter Diffusion Coefficient with Immobile Common Ion

If an experiment is imagined in which the Cl^- ion is replaced by an immobile ion, then only two ions are moving and the equations are mathematically much simplified and are interesting to study. This system is of some practical importance for correlating rate coefficients in ion exchange [1]. In this case there are two exchanging, counter diffusing ions, but the common ion of the solution is excluded from the resin, and it is probably best to assume it to be immobile.

The two counter diffusing ions have equal and opposite initial concentration gradients and must therefore have the same diffusion coefficient if electroneutrality is to be preserved. If, in equations (12), D_3 is put equal to zero, (or if D_1 is put equal to D_2, for in this case no electric potential can be set up by the diffusion process and the common ion should not move), the single counter diffusion coefficient is found to be given by

$$1/\mathcal{D}_{12} = \frac{z_1c_1/(z_1c_1+z_2c_2)}{D_2} + \frac{z_2c_2/(z_1c_1+z_2c_2)}{D_1} \qquad (25)$$

The same result can be obtained more directly by writing equation (10) for ion 1 and eliminating c_2 and G_2 by using the electroneutrality conditions (7) and (8).

The dashed lines in Figure 2 to 14 have been computed from equation (25) together with the cell equation (2). The lines are slightly curved because the dependence of $\mathcal{D}_{12}$ on c_1/c_2 has been taken into account as discussed below. It will be seen that the mobility of the common ion al-

TABLE 2
CALCULATED PRACTICAL DIFFUSION COEFFICIENTS
The Initial Reservoir Solutions were 0.1N in Cl^-
The Cations Being H^+ and Either NH_4^+, Ca^{++} or La^{+++}

Initial Reservoir Normalities of H^+		Calculated Practical Diffusion Coefficients, $cm^2/sec \times 10^5$									
		Mobile Common Ion (eqn. 24)				Immobile Common Ion					
Reservoir 1	Reservoir 2	H^+	NH_4^+	H^+	Ca^{++}	$NH_4^+ - H^+$		$Ca^{++} - H^+$		$La^{+++} - H^+$	
						t = 0	t = ∞	t = 0	t = ∞	t = 0	t = ∞
0	0.04	6.80	4.08	6.24	2.89	5.68	5.30	4.73	4.24	4.91	4.46
0.02	0.06	5.36	3.20	4.61	2.00	3.83	3.71	2.65	2.52	2.76	2.59
0.04	0.08	4.42	2.64	3.54	1.44	2.90	2.85	1.71	1.65	1.70	1.63
0.06	0.10	3.76	2.25	2.84	1.05	2.34	2.32	1.17	1.14	1.06	1.03
0	0.10	4.84	2.90	4.00	1.69	3.86	3.23	2.76	2.03	2.81	2.06

ways increases the apparent coefficient of the faster of the counter diffusing ions, and decreases the apparent coefficient of the slower. This must be because the faster ion takes some of the common ion with it. The fact that equation (25) is obtained from the integrated equations which fit the experimental results, coupled with the fact that the experimental results always lie to either side of the curve calculated from equation (25) suggests that this equation would be correct if a truly immobile common ion had been used.

It was mentioned that this case is simple, mathematically, because only two ions are involved, and that some allowance for the variation of $\mathcal{D}$ with c can be made for this case. The method used is Stokes' [5]. The assumption of a linear concentration gradient is still made, and the additional (most reasonable) assumption that the diaphragm is too small for any material to accumulate in it, is made. With these assumptions, Fick's equation can be integrated for the geometry of a cell, taking into account that c_1/c_2 and therefore $\mathcal{D}_{12}$ vary both with position in the diaphragm, and with time.

Stokes' treatment is as follows. If no material accumulates in the diaphragm, the flux must be constant through the diaphragm. That is, $\mathcal{D}\delta c/\delta x$ is independent of x, and a coefficient $\mathcal{D}'$ may be defined by the equation

$$\mathcal{D}'\Delta c/l = \mathcal{D}\delta c/\delta x \qquad (26)$$

$\mathcal{D}'$ is a function of time, and therefor of Δc, but is independent of x.

Now suppose that Fick's equation, (1), is to be applied to a diaphragm cell, but $\mathcal{D}$ is a differential coefficient, a function of c. The substitution $\delta c/\delta x = \Delta c/l$ can be made if $\mathcal{D}'$ is used instead of $\mathcal{D}$. When this is done and the boundary condition (15) is used, the cell differential equation is obtained

$$\delta\Delta c/\delta t = -\beta'\mathcal{D}'\Delta c \qquad (27)$$

The integration of this equation for constant $\mathcal{D}'$ gives an equation like (2). However, $\mathcal{D}'$ in fact varies with time, and so an integral coefficient, $\bar{\mathcal{D}}$, will be *defined* by the equation

$$\ln(\Delta c_f/\Delta c_b) = -\beta'\bar{\mathcal{D}}t \qquad (28)$$

and $\bar{\mathcal{D}}$ will be related to D'. To arrive at $\bar{\mathcal{D}}$, $\mathcal{D}'$ is first found. From equation (26)

$$\mathcal{D}' = (1/\Delta c)\int_{c''}^{c'} \mathcal{D}dc \qquad (29a)$$

Then from equations (28) and (27)

$$\bar{\mathcal{D}} = \ln(\Delta c_f/\Delta c_b)\Big/\int_{c_b}^{c_f} (d\Delta c/\mathcal{D}'\Delta c) \qquad (29b)$$

In the counter diffusion case, the differential coefficient $\mathcal{D}$, from equation (25), can be rewritten

$$\mathcal{D} = \frac{D_1D_2(z_1c_1+z_2c_2)}{z_1c_1D_1+z_2c_2D_2} \qquad (30)$$

It is best at this point to introduce two new symbols.

(i) Only two ions (which have the same charge) are moving and electroneutrality insists that $c_1 + c_2$ be a constant everywhere.

$$\text{Let } a = c_1 + c_2 \qquad (31)$$

(ii) It is assumed that no material accumulates in the diaphragm. In this case, material conservation says that the *mass* of ion i in the two reservoirs is constant. Since, in all the work here, *the two reservoirs have equal volume*, *the concentration* of ion i in the two reservoirs may be put equal to a constant.

$$\text{Let } 2b_1 = c_1' + c_1'' \qquad (32a)$$

$$2b_2 = c_2' + c_2'' \qquad (32b)$$

b_1, b_2 are the average concentrations of the ions. Because the two reservoirs have equal volume, b_1, b_2 are also the concentrations of the ions which prevail everywhere after an infinitely long experiment.

Since equation (31) holds in the reservoirs as well as in the diaphragm,

$$b_1 + b_2 = a \qquad (33)$$

Using equation (31), $\mathcal{D}$ can be expressed as a function of c_1 only.

$$\mathcal{D} = \frac{D_1D_2[(z_1-z_2)c_1 + z_2a]}{(z_1D_2-z_2D_1)c_1 + z_2D_2a}$$

Then from equation (29a)

$$\mathcal{D}' = \frac{D_1D_2(z_1-z_2)}{z_1D_1-z_2D_2} + \frac{az_1z_2D_1D_2(D_1-D_2)}{\Delta_1(z_1D_1-z_2D_2)^2}\ln\frac{(z_1D_1-z_2D_2)c_1' + z_2D_2a}{(z_1D_1-z_2D_2)c_1'' + z_2D_2a}$$

where Δ has been written for c' -c".

Since $c_1' = b_1 + \Delta_1/2$ and $c_1'' = b_1 - \Delta_1/2$, the log term in $\mathcal{D}'$ can be written

$$\ln\frac{[2z_2D_2a/(z_1D_1-z_2D_2)] + 2b_1 + \Delta_1}{[2z_2D_2a/(z_1D_1-z_2D_2)] + 2b_1 - \Delta_1}$$

Define

$$Q = 2z_2D_2a/(z_1D_1 - z_2D_2) + 2b_1 \quad (34a)$$

$$P = az_1z_2D_1D_2\,(D_1 - D_2)/(z_1D_1 - z_2D_2)^2 \quad (34b)$$

$$S = D_1D_2\,(z_1 - z_2)/(z_1D_1 - z_2D_2) \quad (34c)$$

Then

$$\mathcal{D}' = S + (P/\Delta)\,1n\,(Q + \Delta)/(Q - \Delta) \quad (35)$$

Incidentally, when $z_1 = z_2$, $S = 0$, and in fact z disappears from the equations and the algebra becomes very much simpler.

In general, $\overline{\mathcal{D}}$ must be found from $\mathcal{D}'$ by graphical integration of equation (29b). However, the two extreme limits of $\overline{\mathcal{D}}$ when $a = 0$ and when $t = \infty$, can be evaluated by taking limits.

1. $t \to 0$, $\Delta_f \to \Delta_b$.

$$\overline{\mathcal{D}} = S + (P/\Delta_b)\,1n\,(Q + \Delta_b)/(Q - \Delta_b) \quad (36)$$

2. When $t \to \infty$, $\Delta_f \to 0$.

$$\overline{\mathcal{D}} = S + 2P/Q \quad (37)$$

If, in equation (37), the definitions of S, P, Q are substituted from equations (34), and a is eliminated by equation (33), it is found that

$$1/\overline{\mathcal{D}} = \frac{z_1b_1/(z_1b_1 + z_2b_2)}{D_2} + \frac{z_2b_2/(z_1b_1 + z_2b_2)}{D_1} \quad (38)$$

This is like equation (25), and shows that the integral coefficient for an infinitely long experiment is the same as the differential coefficient computed at the values assumed by the concentrations everywhere at infinite time.

3. It can be shown that the integral coefficient always lies between the values given by equations (36) and (37).

Table 2 shows some values of counter diffusion coefficients with immobile common ion for the three cation pairs used in the experiments. In calculating the dashed lines on the graphs, $\overline{\mathcal{D}}$ was assumed to be a linear function of Δc between its values at $\Delta c = \Delta c_b$, $(t = 0)$ and $\Delta c = 0$, $(t = \infty)$. A few graphical integrations of equation (29b) show that this is true to within about 15%.

The notable feature of these results is that $\overline{\mathcal{D}}$ varies little with time. When this work was being done, it was the discovery that $\overline{\mathcal{D}}$, in this case, varied so little with time, that encouraged the use of constant values of concentration when integrating the equations for a mobile common ion.

Conclusions

The experimental results show that the electric potential set up by the counter diffusion process can cause the common ion to build up a considerable concentration gradient when it had no concentration gradient initially. The plots of concentration difference against time on a semilogarithmic scale are nearly straight lines for the counter diffusing ions. This means that a single practical coefficient can be assigned to each of these ions to get a satisfactory prediction of the experiments.

The agreement between theory and experiment is most satisfactory. It is not thought that this agreement is specific to the sysems studied. Any similarly simple system would work. By a simple system is meant simple ions in dilute solution. No allowance has been made for complex ion formation, or partial ionization, although the success of Sherwood and Wei in predicting the counter diffusion of acetic acid and sodium hydroxide suggests that partial ionization can be allowed for. The activity corrections made were of the simplest sort and would be inadequate for more concentrated solutions than those used.

It has proved possible to predict counter diffusion results using only a table of ionic equivalent conductances at infinite dilution. The method used is already known to work for salt diffusion, but counter diffusion is a greater test of the approximations in the theory.

Nomenclature

a	total cation concentration of each reservoir. In the case of immobile common ion, $a = c_1' + c_2' = c_1'' + c_2'' = c_1 + c_2$.
A	effective cross section of the diaphragm, cm²
A_1,A_2	coefficients used in the mobile common ion equation (18)
2b	total ion concentration in the cell. Because the diaphragm has negligible volume, $2b_1 = c_1' + c_1''$, $2b_2 = c_2' + c_2''$.
B_1,B_2	coefficients used in the mobile common ion equation (18)
c	concentration, equiv./cc. If the numerical value is followed by N, the units are normalities, equiv./litre.
c',c''	concentration in the two reservoirs
D	ionic self-diffusion coefficient, at zero concentration, cm²/sec.
$\mathcal{D}$	practical diffusion coefficient, cm²/sec.
$\overline{\mathcal{D}}$	integral practical diffusion coefficient
$\mathcal{D}'$	coefficient averaged through the diaphragm
E	potential gradient, volts/cm.
f,g,h,k	quantities defined by equations (12)
F	The Faraday, 96,488 coulomb/equiv.
G	abbreviation for $\delta c/\delta x$
l	effective diaphragm thickness, cm.
m_1,m_2	exponential indices used in equations (18)
N	flux, equiv./(cm²) (sec.)
P,Q,S	quantities defined by equations (34) and used for the case of immobile common ion
R	The gas constant, 8.314 joules/(gm−ion) (°K)
T	temperature, °K.
t	time, secs.
u	ionic electrical mobility, cm²/(sec)(volt). Positive for cations, negative for anions.
V',V''	reservoir volumes, cm³.
x	distance through the diaphragm along the diffusion path, cm.
z	ion valency, equiv./gm−ion. Positive for cations, negative for anions.
β	cell constant $= \frac{A}{l}\left(\frac{1}{V'} + \frac{1}{V''}\right)$ cm⁻²
$\Delta,\Delta c$	$= c' - c''$
λ	ionic equivalent conductance, cm²/(equiv)(ohm). Positive for cations, negative for anions.

Suffixes

b	beginning, at time zero.
f	final, at time t.
i	refers to ions of the i type.
1,2	counter diffusing cations.
3	common anion.

References

(1) Gilliland and Baddour, Ind. Eng. Chem. *45*, 330 (1953).
(2) Sherwood and Wei, A.I.Ch.E. Jour. *1*, 522 (1955).
(3) Gordon, Anals N.Y. Acad. Science *46*, 285 (1945).
(4) Nielson, Adamson and Cobble, J. Am. Chem. Soc. *74*, 446 (1952).
(5) Stokes, J. Am. Chem. Soc. *72*, 763, 2243 (1950).
(6) Vinograd and McBain, J. Am. Chem. Soc. *63*, 2008 (1941).
(7) Hartley, Phil. Mag. *12*, 473 (1931).

Acknowledgments

This work was done while D. J. Goldstein was the holder of the Arthur D. Little Fellowship, and he is most grateful to the Arthur D. Little Company for this aid.

* * *

NOTE: This article is based on a paper presented at the C.I.C. Chemical Engineering Division's Conference, Kingston, March, 1957.

The Effect of Sonic Energy on Mass Transfer in Solid-Gas Contacting Operations[1]

J. W. HODGINS[2], *T. W. HOFFMAN*[3], *and D. C. PEI*[4]

The addition of sonic vibrational energy to the gas in solid-gas contacting equipment causes a significant increase in the rate of transfer of material between these two phases. The amount by which the mass transfer rate is raised is a function of the gas flowrate, with greatest effects for low flowrates through fixed beds.

Mass transfer results are presented for the evaporation of naphthalene from the surface of coated glass beads into a stream of air passing through them with the conditions varying from fixed bed to a fully fluidized bed. Experiments with a single naphthalene sphere are described, and mention is made of a hot-wire microphone developed for the purpose of measuring the sound.

Sound intensities up to 160 decibels were used at frequencies up to 12,000 cycles per second. Largest effects were observed at resonance with low frequencies (100-700 cycles per second), and the minimum effective intensity was 120 decibels. Maximum improvement of the mass transfer rate was about 120% for beds of spheres, and about 220% for the single sphere. This difference in enhancement effect is attributed to the acoustic properties of the cavity, and some elementary aspects of a cavity design are discussed.

Introduction

In furnaces where powdered fuel is being burned, dramatic increases in combustion rate and efficiency have been reported (1) under the condition wherein sonic resonance is established in the combustion chamber. The improvement in combustion is attributed to the "scrubbing" off the gas film at particle surface and chamber wall, allowing ingress of fresh air to the fuel and enhanced heat transfer. The burning of powdered fuel is analogous to the situation in equipment for contacting gas with a fluidized solid. In this case, however, there are distinct limits imposed by the system to the amount of turbulence which can be introduced by mechanical means, and the condition of sonic resonance will probably never be reached by alteration of the flowrate, because slugging or extreme elutriation will intervene. It seemed reasonable to assume that sonic energy might decrease surface film resistance to mass transfer, however, if the sound were added to the gas from an external source, rather than producing it by the passage of gas. For an input power of 1 watt per sq. cm. cross sectional area, at a frequency of 256 cycles per second (middle C), air particles will vibrate with an amplitude of 5 mm.—a distance larger than the diameter of most fluidized particles. Since significant gas movement could be obtained in this way, it was decided to extend the examination of sonic effects to fixed, as well as fluidized beds.

Gas-solid contacting is used for many purposes—for example, catalytic reactions such as cracking of gas oil, roasting, drying, and adsorption of gases and vapours. In many of these operations the slow step is due to the resistance offered to the transfer of material between gas and solid, by the film at the interface. The thickness of this film is a function (among other things) of the degree of turbulence at the interface. Accordingly one test of the efficacy of sonic energy input to gas-solid contacting equipment, is to measure the rate of transfer of material from the surface of the solid into the gas stream in the absence and in the presence of sound. In order that the characteristics of the bed of solids remained substantially unchanged during the experiments, it was decided to coat solid particles (glass beads) with a material (naphthalene) which could be evaporated into an air stream. This ensured that the size distribution, surface area, density, voidage and sound absorption characteristics remained constant over the experimental period. Accordingly, this paper will deal with the improvement of the rate of transfer of naphthalene from the surface of glass spheres into an air stream, by means of the application of sonic vibrational energy to the air.

The effect of sound energy upon the fluidizing property of normally non-fluent beds of solids has already been described by Morse (2), who found that low frequency (50-500 cycles per second) high intensity (greater than 110 decibels) sonic energy will cause certain fine particles to fluidize under conditions where they are normally non-fluent. No effect was observed on coarse, free-flowing granular materials. The

1 *Manuscript received March 20, 1957.*
Contribution from the Chemical Engineering Laboratories, Royal Military College of Canada, Kingston, Ont.
2 *Present address: Professor of Chemical Engineering, Faculty of Engineering, McMaster University, Hamilton, Ont.*
3 *Present address: Lecturer, Department of Chemical Engineering, McGill University, Montreal, Que.*
4 *Lecturer, Department of Chemical Engineering, Royal Military College.*

technique of measuring mass transfer rates by naphthalene evaporation has also previously been described by Ju Chin Chu and co-workers [3], and by Plewes et al. [4]. Of the various methods available for the presentation of mass transfer data, that used by Ju Chin Chu et al. [3] was chosen, wherein the term

$$j_D = \frac{K_G \cdot p_{BM} (N_{Sc})^{2/3}}{G_M}$$

as proposed by Chilton and Colburn [5] was plotted against

$$N'_{Re} = \frac{D_P v_S \rho}{\mu (1 - \epsilon)}$$

as employed by Carman [6].

Experimental Procedure

(1) Mass transfer from coated glass beads

Figure 1 illustrates the apparatus used in this investigation. Since the compressed air from the laboratory lines was always at a lower temperature than the room, it was brought up to room temperature before its passage through the bed, by passing it through a heat exchanger (B) with room air blown outside the finned tubes. Since the laboratory temperature was automatically regulated, air temperatures were thus held quite steady during the short runs. Quick-opening valves (D) gave instantaneous air flow and pressure relief, with close control of flow provided by a needle valve (A). The packed section of 4-in. glass pipe (E) below the column was used to minimize channelling of the air flow. The bed was supported on a stainless steel screen (F), and the section (G) was removable for weighing. Air pressures above and below the bed of beads were recorded, and temperatures were measured by means of calibrated copper constantan thermo-couples (T_1, T_2). Air left the column through a manifold which took the form of a collar near the top, with the air entering the collar by means of four equally spaced $\frac{3}{4}$-in. holes drilled in the column wall. The sound was passed down the column by means of a 30-watt University transducer (H), which operated from a flat-response amplifier receiving a signal from a quartz oscillator.

Sound intensity at the bed level was measured with a hot-wire microphone developed and calibrated for this specific purpose. This instrument measured the sound as a function of the increased heat transfer from a hot wire due to the agitation of the air. Its construction and calibration will be described in detail in a subsequent paper. Its distinguishing feature was its tiny size, enabling point measurements to be made without altering the physical characteristics of the reactor cavity. By measuring sound intensity over a range of frequencies, the resonant frequency could be established to an accuracy of about 0.3%.

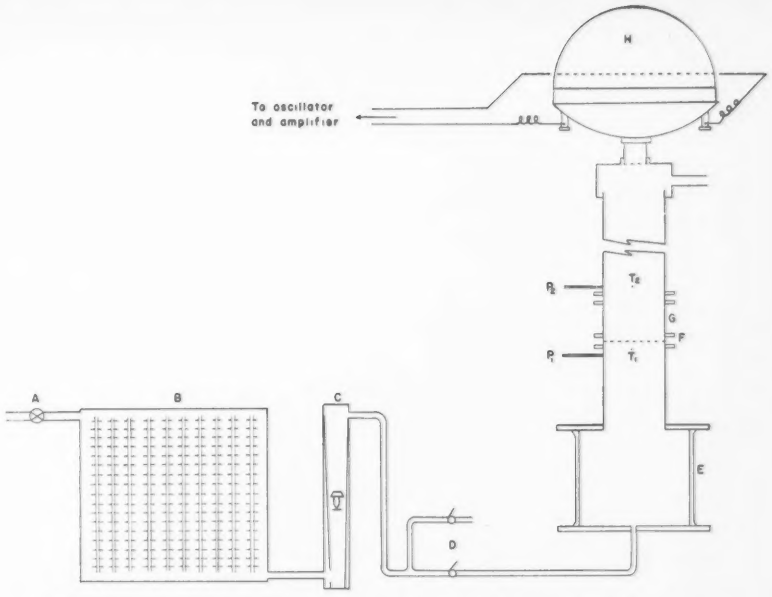

Figure 1—Apparatus for measuring mass transfer in a bed of spheres.

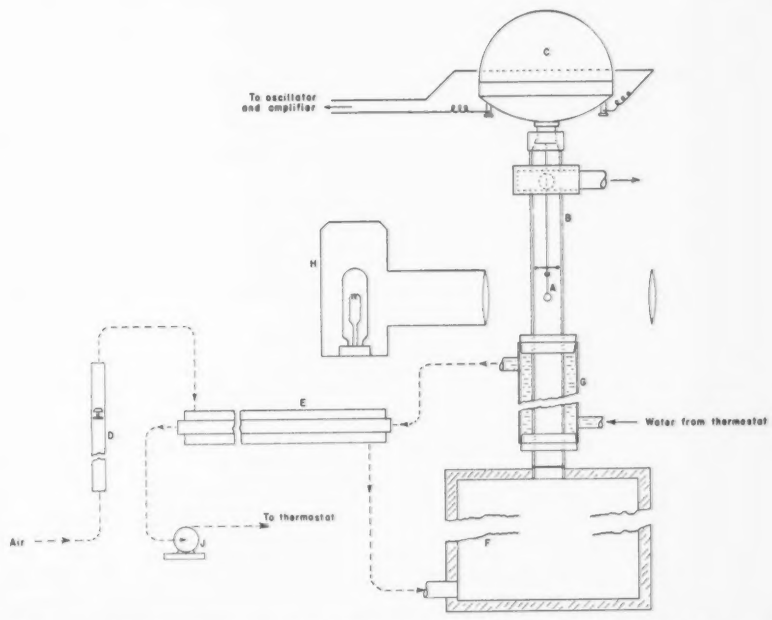

Figure 2—Apparatus for measuring mass transfer at the surface of a single sphere.

The solid bed consisted of coated glass spheres 3-6 mm. in diameter, depending upon the value of N'_{Re} desired. In order to make the naphthalene adhere to their surfaces, they were first etched by fluidizing them in a copper column with an air stream containing HF vapor. Molten naphthalene was then sprayed on the beads as they tossed in a baffled cylinder. The spray was achieved by means of a glass atomizer, and naphthalene, atomizer and incoming air were all kept above the melting point of naphthalene. Spraying was continued until the coating represented about 10% of the total weight of the coated

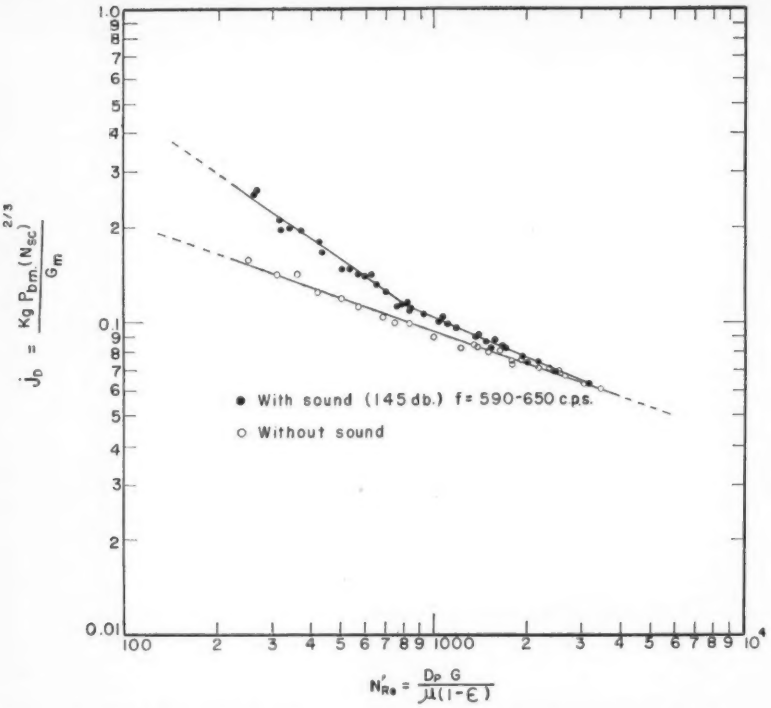

Figure 3—Effect of sound (600 c.p.s.) on mass transfer from a bed of spheres.

beads (determined by Soxhlet extraction with ether).

For an experimental run, 70-100 grams of coated beads were weighed in the removable 4-in. section of the column (G). The section was immediately inserted in the apparatus, and the sound (if applicable) and air turned on simultaneously. The inlet air temperature, flowrate, and pressure were recorded. The outlet air temperature was recorded on a strip chart potentiometer, and the average temperature for the run was subsequently determined by graphical integration of the record. From the weight of naphthalene evaporated from the beads, the mass transfer coefficient could be calculated. These results were obtained for a range of flowrates, in the presence, and in the absence of sound. Measurements were made to determine the effect of frequency and intensity of the added sonic energy on the rate of material transfer from the solid to the gas phase.

Early in the experimental work, it was found that the first run after the beads were coated frequently yielded erratic results, due presumably to the elutriation of naphthalene dust. Accordingly, before any quantitative experiment in which freshly-coated beads were used, the beads were fluidized for a couple of minutes at high air flowrate and high sound intensity, to shake off any loosely-adhering particles. This precaution made for consistency in the results of subsequent duplicate runs.

(2) Mass transfer from a single naphthalene sphere:

A simpler system in which to investigate the mass transfer in a sound beam, was to use a single sphere of naphthalene suspended in an air stream. Because of the small surface area, the experiments had to be carried on over a longer period of time, and this necessitated close control of temperature during the runs. The apparatus is shown in Figure 2.

Naphthalene spheres of the desired diameter were prepared by evaporating pressed naphthalene moth balls in a stream of hot air while contained in a rotating cylinder; this allowed evaporation to proceed uniformly. Final accurate sizing was accomplished by rolling the sphere through a series of steel dies. The sphere (A, Figure 2) was suspended on a very fine steel wire at the axis of a vertical Lucite tube, 1½ in. in diameter, and 32 in. long (B). Surmounting the tube was a University 30-watt transducer (C) which received a signal from an oscillator-amplifier combination. Metered air was passed through the jacket of a heat exchanger (E) into a 6-litre cylindrical damping volume (F), covered with heavy insulation. A water jacket (G) surrounding the bottom section of the Lucite tube provided final control of the air temperature immediately before it reached the naphthalene sphere. The water in the heat exchangers was in continuous circulation from the thermostat, and final air temperature control was ± 0.1°C. Temperature was measured at the sphere by a calibrated copper-constantan thermo-couple and continuously recorded by strip-chart potentiometer. In order to have visual means of following the progress of the evaporation, the image of the sphere was projected on a target at intervals during the run, and thus qualitative observations could be made without interrupting the experiments.

Sound levels were measured by the previously-mentioned hot-wire microphone, which was also used to determine the resonant frequency. The power input to the horn was read on an electronic wattmeter, and kept at a constant value manually.

To perform an experiment, the following steps were followed:

(i) The sphere and its hook were weighed on an analytical balance.

(ii) The sphere was attached to the support rod on the adapter at the top of the tube, and the sphere, adapter and horn fixed in place.

(iii) The air and the signal to the horn were started simultaneously.

(iv) Time, atmospheric pressure, and tube temperature were recorded.

(v) At the end of the run, the loss in weight of the sphere was determined.

Experimental Results

(i) Experiments with beds of coated beads:

Typical data for these experiments are shown in Table 1 (Page 21): (Runs marked with an asterisk were performed using sound at 600 c.p.s. and 145 decibels.)

Results for many experimental runs are summarized in Figure 3 and Figure 4, using the experimental conditions shown. For beds of beads it is seen that maximum enhancement of mass transfer by sound occurs at low values of N'_{Re} when the bed is stationary, and is more pronounced at low frequency.

TABLE 1

Wt. Loss (grams)	Surface area (ft.²)	Duration (hours)	Voidage	Bed Ht. (cm.)	Temp. (°C.)	N'_{Re}	N_{Sc}	K_G	j_D
0.1443	0.692	0.050	0.48	1.9	22.8	250	2.52	1.42	0.157
*0.1090	0.584	0.033	0.49	1 65	23.0	260	2.52	2.28	0.256
0.1351	0.724	0.033	0.48	1.7	23.9	360	2.52	1.83	0.142
*0.1386	0.584	0.033	0.49	1.65	22.9	368	2.52	2.52	0.195
0.1904	0.603	0.033	0.51	1.75	23.6	680	2.52	2.37	0.104
*0.1912	0.605	0.033	0.56	2.00	23.2	685	2.52	2.68	0.127

Table 1—Effect of sonic vibrational energy on mass transfer from a packed bed of spheres.

TABLE 2

Sphere dia. (inches)	Air flowrate c.f.m.	K_G (quiet run) (lb. moles hr.$^{-1}$ ft.$^{-2}$ atm.$^{-1}$)	K_G (using sound)	% Enhancement
0.3125	0.50	0.302	0.97	220
0.3125	0.75	0.318	0.99	211
0.3125	1.0	0.366	1.03	182
0.3125	1.50	0.414	0.98	136
0.3125	2.0	0.504	1.01	100

Table 2—Effect of sonic vibrational energy on mass transfer from a single sphere.

At the 590 c.p.s. resonance point, there are two lines which describe the mass transfer during sound input, with a change of slope at $N'_{Re} = 860$, the point of incipient fluidization. In all cases, no enhancement was observed at $N'_{Re} > 2500$.

For quiet runs, the line relating mass transfer factor to N'_{Re} compares very well with the relationship procured by Ju Chin Chu et al. [3]. The experimental scatter of the above results is considerably less than the previous work, and an altered equation is suggested for the relation between mass transfer and flowrate:

$$j_D = 1.051\,(N'_{Re})^{-0.35} \text{ for } 4000 > N'_{Re} > 200$$

For a fixed arbitrary value of $N'_{Re} = 460$, the relationship between mass transfer factor and sound intensity is shown in Figure 5, (frequency = 590 c.p.s.). It has been a common observation that no effect is observable at intensity lower than 120 decibels.

Prompted by the observation that much larger mass transfer enhancement was obtained with single spheres at low resonant frequencies, an attempt was made to establish a resonance point in the tube at lower frequency, but difficulty was encountered in producing resonance at a frequency near the calculated value. It was soon realized that due to the dimensions of the first experimental apparatus two simultaneous standing waves were present in the tube. Part of the energy was sustaining open-tube resonance, while at the same frequency closed-pipe resonance also occurred, with the bed of solids as the closure. It is also apparent that the use of a transducer having a one-inch throat, attached directly to a three-inch tube is inefficient, and in addition makes prediction of the resonance frequency difficult. Accordingly, a 1½-in.-diameter column was used, with the top of the bed of solids located 3 in. below the transducer opening. This alteration in geometry made for more efficient coupling and made it possible to set up open-tube resonance while eliminating closed-pipe resonance.

Mass transfer measurements at 148 decibels and 340 c.p.s. are illustrated in Figure 6.

It is interesting that, although the enhancement is pronounced at values of N'_{Re} below 900, for higher values the relation between mass transfer factor and flowrate is the same as for the three-inch column.

Figure 7 illustrates the relationship between pressure drop across the bed, and flowrate in the three-inch column for a shallow bed of 3 mm. naphthalene-coated glass spheres.

(ii) Experiments with a single sphere of naphthalene.

The rate of removal of naphthalene proved to be strikingly dependent upon frequency. Although for the tube used, resonant frequencies occurred at 275, 480, 640, 1320, and 1610 cycles per second, significant enhancement of mass transfer rate occurred only at the lowest of these frequencies. The mass transfer coefficient in a sonic beam (frequency = 275 c.p.s.; intensity = 160 db.) varies but little over a fourfold range of flowrate; the mass transfer

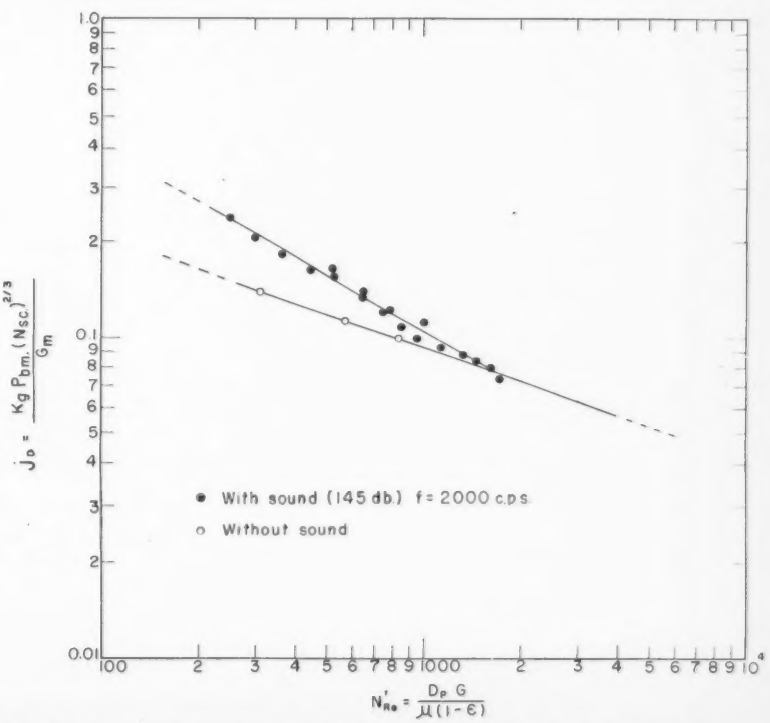

Figure 4—Effect of sound (2000 c.p.s.) on mass transfer from a bed of spheres.

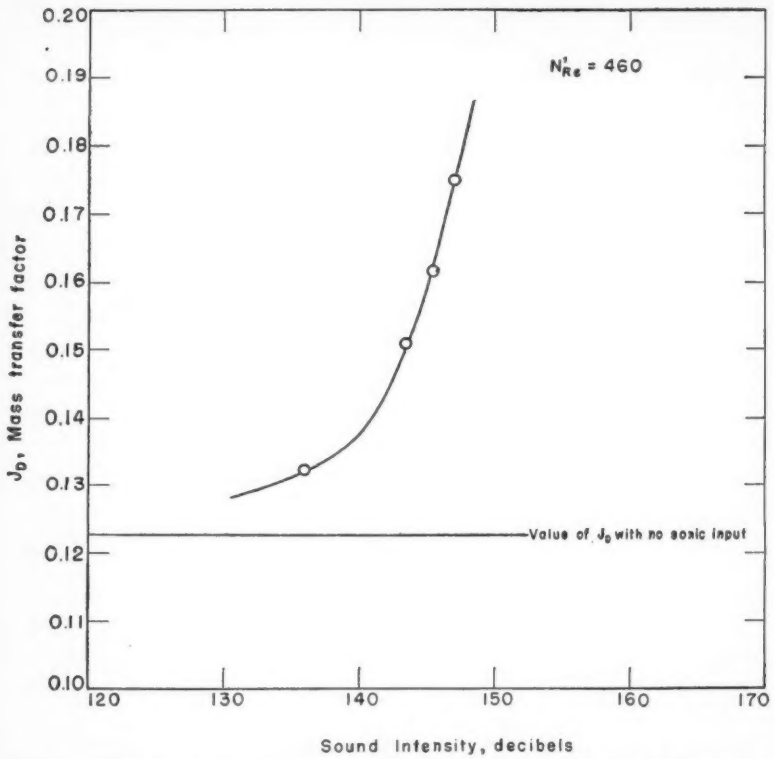

Figure 5—Effect of sound intensity on mass transfer from a bed of spheres.

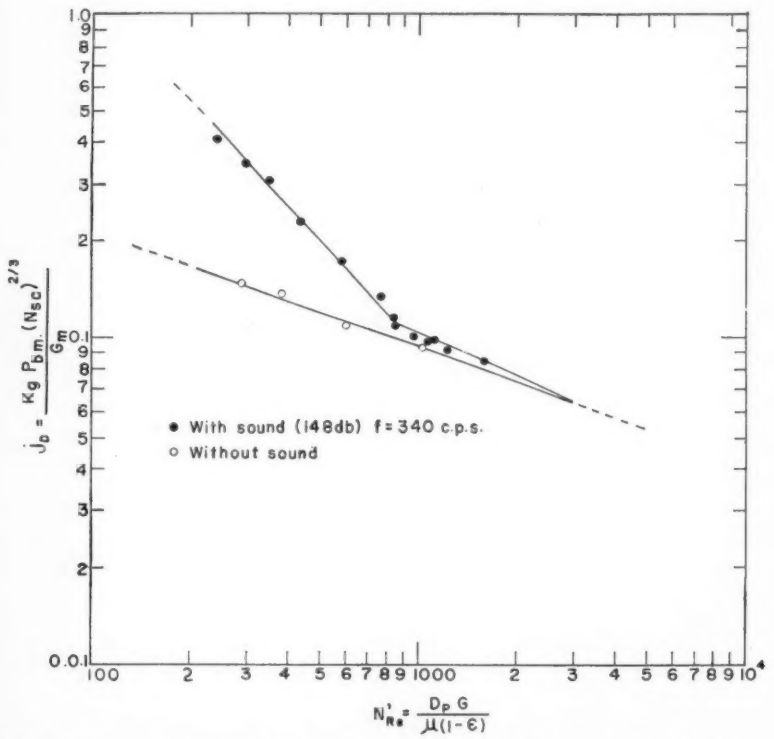

Figure 6—Effect of sound (340 c.p.s.) on mass transfer from a bed of spheres in a tube from which closed-pipe resonance has been eliminated.

for corresponding quiet runs, of course, increases. The values are given in Table 2.

A typical trace of the projected profile of a single naphthalene sphere is shown in Figure 8. The effect of the sonic vibrational energy was invariably that of making the evaporation from the surface of the sphere uniform, rather than having it concentrated on the leading and trailing surfaces. Maximum enhancement occurred when the sphere was located at an antinode in the standing wave, and no improvement was obtained at the position of minimum velocity change—at the node.

The results of an experiment to determine the effect of sphere diameter upon the mass transfer coefficient in the presence of sound, are shown in Table 3.

Discussion

Effects other than increased turbulence at the gas-solid interface could cause an improvement in the mass transfer rate. For example, the values of the diffusivity and of the partial pressure of naphthalene were calculated on the assumption that the temperature of the air effluent from the bed represented the bead surface temperature. In all cases where the sound beam was used, the effluent air did show a temperature rise (0.1 to 0.4°F.), indicating some energy dissipation at the bed. At low flowrate one might suspect that the heat transfer coefficient at the surface of the beads was sufficiently low to allow the bead surface temperature to rise appreciably above that of the effluent air. That this was not the case was demonstrated by measuring surface temperatures during experiments, using fine thermocouples attached directly to beads in the bed.

In every case, the temperature of the effluent air represented the bead surface temperature within 0.1°F. The same was true of the single naphthalene spheres.

The total pressure in the column increases with flowrate. Thus the decrease in enhancement at high flowrate could be caused by the less effective operation of the transducer diaphragm. By repeating some of the low flowrate experiments at elevated pressures, this effect was shown to be negligible over the pressure range involved.

The increased pressure drop across the fixed bed in the presence of sound (Figure 7) is interpreted as a manifestation of increased turbulence in the air passing through the bed, with the maximum pressure change occurring at the low flowrate. Fluidization of course occurs at a lower flowrate in the presence of sound, and once the bed has become

fully fluidized, the pressure drop is not affected by sound input. This behaviour is consistent with the mass transfer measurements. The reason that there appears to be some slight mass transfer enhancement in the fluidized bed is the method of plotting the data; the slightly increased voidage due to the sound has resulted in a higher value for N'_{Re} for a given value of the mass transfer factor. However maximum effect was observed at a flowrate sufficiently low that the voidage was unaffected by the sound. When fluidization develops, increased turbulence manifests itself as kinetic energy used up in expanding the bed. The velocity gradients at the particle surface change but little, thus affecting mass transfer at the boundary layer only slightly.

Maisel and Sherwood [7, 8] discuss the effect of scale and intensity of turbulence on mass transfer in turbulent air streams. In their experiments turbulence was introduced by placing drilled plates in the air duct at various distances upstream of solids from which the rate of evaporation of water was measured. Scale of turbulence was measured by a standard technique involving two separated wire probes, and is a number having the dimensions of length, which is indicative of the size of the eddies in the air stream. Intensity, a measure of the velocity fluctuations at a given point, was measured with an extremely delicate hot wire anemometer providing a signal to an oscilloscope. In all of their experiments (in which the superficial flow was turbulent), the effect of turbulence intensity was marked, but that of scale was of little consequence.

In air in which sonic resonance is being maintained, the amplitude of the movement of the air particles is inversely proportional to the frequency for a given power input, but the displacement velocity is independent of frequency. Since the mass transfer enhancement is so very dependent upon frequency, it is apparent that the amplitude of movement of the air by the sound has a much greater effect than the velocity of the air. Interpretation of these effects in the light of normal turbulence phenomena such as examined by Maisel and Sherwood is questionable, for the velocity imparted to the air particles by the sound is 10-20 times greater than the superficial air velocity through the tube. An increase in the superficial air flowrate in the tube did not cause any change in the

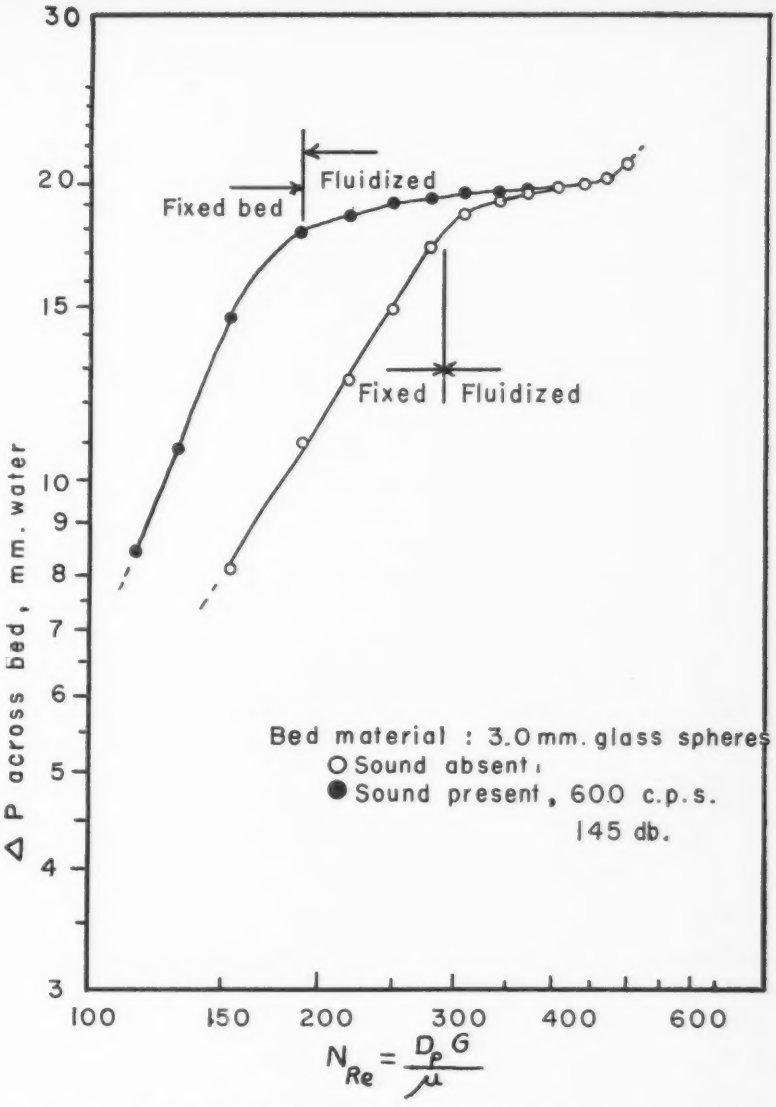

Figure 7—Effect of sound on pressure drop across a bed of 3 mm. diameter glass spheres.

TABLE 3

Air velocity: 1.4 ft. per second
Sound frequency: 268 c.p.s.
" intensity: 163 decibels

Dia. of sphere (inches)	K_G (lb. moles hr.$^{-1}$ ft.$^{-2}$ atm.$^{-1}$)	$N_{Re}\left(\frac{D_p G}{\mu}\right)$
0.297	1.26	203
0.359	1.31	246
0.390	1.24	268
0.453	1.11	314
0.484	1.08	335
0.574	0.895	410

Table 3—Effect of sphere diameter on mass transfer at constant sonic input.

mass transfer rate at constant sonic power.

The mass transfer coefficient decreases with increasing sphere diameter for constant sound input and superficial air flowrate (Figure 3). This is to be expected for turbulent flow past the spherical surface—the mass transfer coefficient should be a function of $(D_p)^{-n}$.

Mass transfer enhancement is not so sharply dependent upon frequency when measurements are made on a packed bed rather than on a single sphere. The reason for this difference in behaviour is not apparent. Further work on these effects should be accompanied by measurements of local turbulence effects.

Conclusion

Addition of sonic vibrational energy at low frequency and at intensity greater than 120 decibels significantly increases the rate at which material is transferred across solid-gas interfaces in a bed of solids. The enhancement is greatest for low flows of gas through fixed beds, and the improvement is negligible when full fluidization has developed. Maximum effect was observed at sonic resonance for low frequency sound (200-600 cycles per second).

The work described is exploratory; attention is now being directed at the attenuation in beds of solids, the suitable design of reactor cavities, the effect on surface reactions, and higher frequency effects. Whether the experimental conditions described have counterparts in practice has not yet been ascertained.

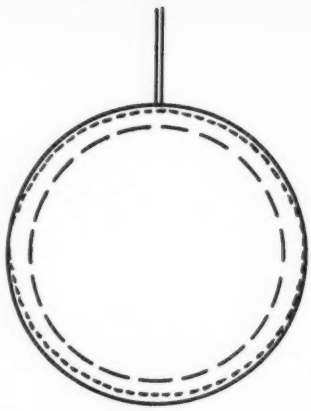

Figure 8—Typical profile of single sphere of naphthalene showing the effect of sound upon evaporation.

Nomenclature

A = sphere surface area, sq. ft.
D_p = sphere diameter, ft.
D_v = diffusivity of naphthalene vapour in air, ft.^{2} hr.$^{-1}$
ϵ = voidage of bed
G = mass velocity, superficial, lb. hr.$^{-1}$ ft.$^{-2}$
G_M = mass velocity, superficial molar, lb. mole hr.$^{-1}$ ft.$^{-2}$
j_D = mass transfer factor
$= \dfrac{K_G \cdot p_{BM} \cdot (N_{Sc})^{2/3}}{G_M} =$
$S/A \cdot \ln (1 - p_G/p_S)^{-1} (N_{Sc})^{2/3}$
K_G = mass transfer coefficient, lb. moles hr.$^{-1}$ ft.$^{-2}$ atm.$^{-1}$
$= \Delta W/M_a \cdot A \cdot t \cdot p_{LM}$
M_a = molecular wt. of naphthalene, lb./lb. mole
μ = air viscosity, lbs. hr.$^{-1}$ ft.$^{-1}$
N_{Re} = particle Reynold's Number, $\dfrac{D_p.G}{\mu}$
N'_{Re} = modified Reynold's Number, $\dfrac{D_p.G}{\mu(1-\epsilon)}$
N_{Sc} = Schmidt number, $\dfrac{\mu}{\rho D_v}$
p_{BM} = mean partial pressure of air in interfacial film, atm.
p_{LM} = log mean partial pressure of naphthalene in air, atm.
ρ = air density, lb. ft.$^{-3}$
S = tube cross section, ft.^{2}
t = duration of transfer period, hrs.
v_s = superficial air velocity, ft. hr.$^{-1}$
ΔW = wt. loss of naphthalene from the column, lbs.

References

(1) Reynst, F. A., Chaleur et Industrie, 30: 304, 1949.
(2) Morse, R. D., Ind. Eng. Chem. 47: 1170, 1955.
(3) Ju Chin Chu, Kalil, J., and Wetterath, W. A., Chem. Eng. Prog. 49: 141, 1953.
(4) Plewes, A. C., Butler, R. M., and Marshall, H. E., Chem. Eng. Prog. 50: 77, 1954.
(5) Chilton, T. H., and Colburn, A. P., Ind. Eng. Chem. 26: 1183, 1934.
(6) Carman, P. C., Trans. Inst. Chem. Eng. (London) 15: 150, 1937.
(7) Maisel, D. S., and Sherwood, T. K., Chem. Eng. Prog. 46: 131, 1950.
(8) Maisel, D. S., and Sherwood, T. K., Chem. Eng. Prog. 46: 172, 1950.

Acknowledgment

The authors are indebted to D. C. Farquharson, who developed the hotwire microphone which was so useful in this investigation. Its description will be included in a forthcoming paper.

We are also glad of this opportunity to express our thanks to the Defence Research Board of Canada for their generous cooperation in financing this project.

★ ★ ★

Studies on Flocculants for Settling, Thickening and Filtration in the Sherritt Gordon Process[1]

D. J. I. EVANS[2], *W. KUNDA*[3], and *P. CHIANG*[3]

Excessively slimy leach residues were encountered during the first few months of operation of the Sherritt Gordon Process. The effect of these slimes on the liquid-solids separation of the leach liquor from the residues is described and the laboratory investigations to find the most suitable flocculant for improving the characteristics of the slurries are detailed. The paper is concluded with a discussion of the effect of the flocculant selected, Separan 2610, on the refinery operation.

Sherritt Gordon Mines Limited employs an ammonia pressure leaching process in their refinery (1) at Fort Saskatchewan, Alberta, for the recovery of nickel, copper and cobalt from the nickel concentrate produced at Lynn Lake, Manitoba.

The process (2, 3, 4, 5) involves leaching the sulphide concentrate under pressure with air and ammonia to dissolve the nickel, copper, cobalt and most of the sulphur, and to leave the iron and siliceous material as a discardable residue. The copper is recovered from the solution as a high-grade sulphide precipitated during a distillation stage for the re-circulation of part of the ammonia. After further solution purification, to remove traces of copper and undesirable sulphur compounds, the nickel is precipitated by hydrogen under pressure. The cobalt, together with unreduced nickel, is precipitated as a mixed sulphide (by hydrogen sulphide) for eventual cobalt recovery and the end solution is evaporated to produce crystalline ammonium sulphate.

The leaching operation (the circuit is shown in Figure 1) is essentially a continuous, two-stage, counter-current system with fresh concentrate being partially leached (60%) in the leach liquor produced in the second stage leaching circuit (adjustment and final leach respectively). Such a system is necessary to produce a solution suitable for treatment in the copper sulphide precipitation step.

Horizontal, water-jacketed autoclaves, fitted with four agitators operating in compartments separated by overflow weirs to give a certain amount of staging during leaching, are used in both leach circuits. The adjustment leach (two autoclaves in parallel operating at 170-180°F and 90-100 psig.) is followed by a thickener-filter, liquid-solids separation circuit. The final leach, two parallel trains of three autoclaves processing (under the same conditions) the repulped partially leached solids, is also followed by a thickener-filter liquid-solids separation circuit. In the latter, three washing stages, consisting of repulping and refiltering, are given to the residues to ensure a maximum recovery of soluble metal values before discarding the leach residues to a pond.

The thickeners are 105 ft. diameter, completely enclosed. Hardinges thickeners; the filters are Dorr-Oliver American Disc filters with seven discs on the adjustment filter and ten discs on the four filters in the final leach circuit.

A typical analysis of the nickel concentrate (produced by differential flotation) is given in Table 1. The mineral species identifiable in the concentrate under the microscope are:

Pentlandite, (Fe,Ni)S,	35-49%
Chalcopyrite, $CuFeS_2$,	3-6%
Pyrite, FeS_2	1-4%
Pyrrhotite, $Fe_{1-x}S$*,	24-42%

*Where x varies between 0 and 0.2.

together with various siliceous materials such as talc and quartz.

During leaching it is assumed (4) that the sulphur in the pentlandite, chalcopyrite and part of the pyrrhotite is successively oxidized through the thiosulphate and polythionate species to sulphate and sulphamate. Simultaneously the nickel, copper and cobalt are converted to soluble ammine complexes and the iron in the pentlandite, chalcopyrite and part of the pyrrhotite is oxidized to a spongy hydrated iron oxide. The latter is readily broken down by the agitation necessary for satisfactory leaching.

During the first few months of operation, difficulties were experienced in the liquid-solids separation circuits due to an excessive slimes load. Briefly the experience was as follows: satisfactory continuous operation would be achieved for a few days although during this period slow settling pulp would be discharged into the final thickener: the slimes level in this thickener would gradually rise and eventually overflow with the solution recycled to the adjustment leach circuit: due to the recycled slimes, extremely slow settling pulp would then be discharged to the adjustment thickener and the slimes level in this thickener would rise to overflowing: the remainder of the

NOTE: This article is based on a paper presented at the Third Western Regional Conference of The Chemical Institute of Canada, Edmonton, September 13-15, 1956.
1Manuscript received February 17, 1957.
Contribution from the Sherritt Gordon Mines Limited, Fort Saskatchewan, Alberta.
2Assistant Head, Research Department, Sherritt Gordon.
3Senior Research Chemist, Research and Development Laboratories, Sherritt Gordon.

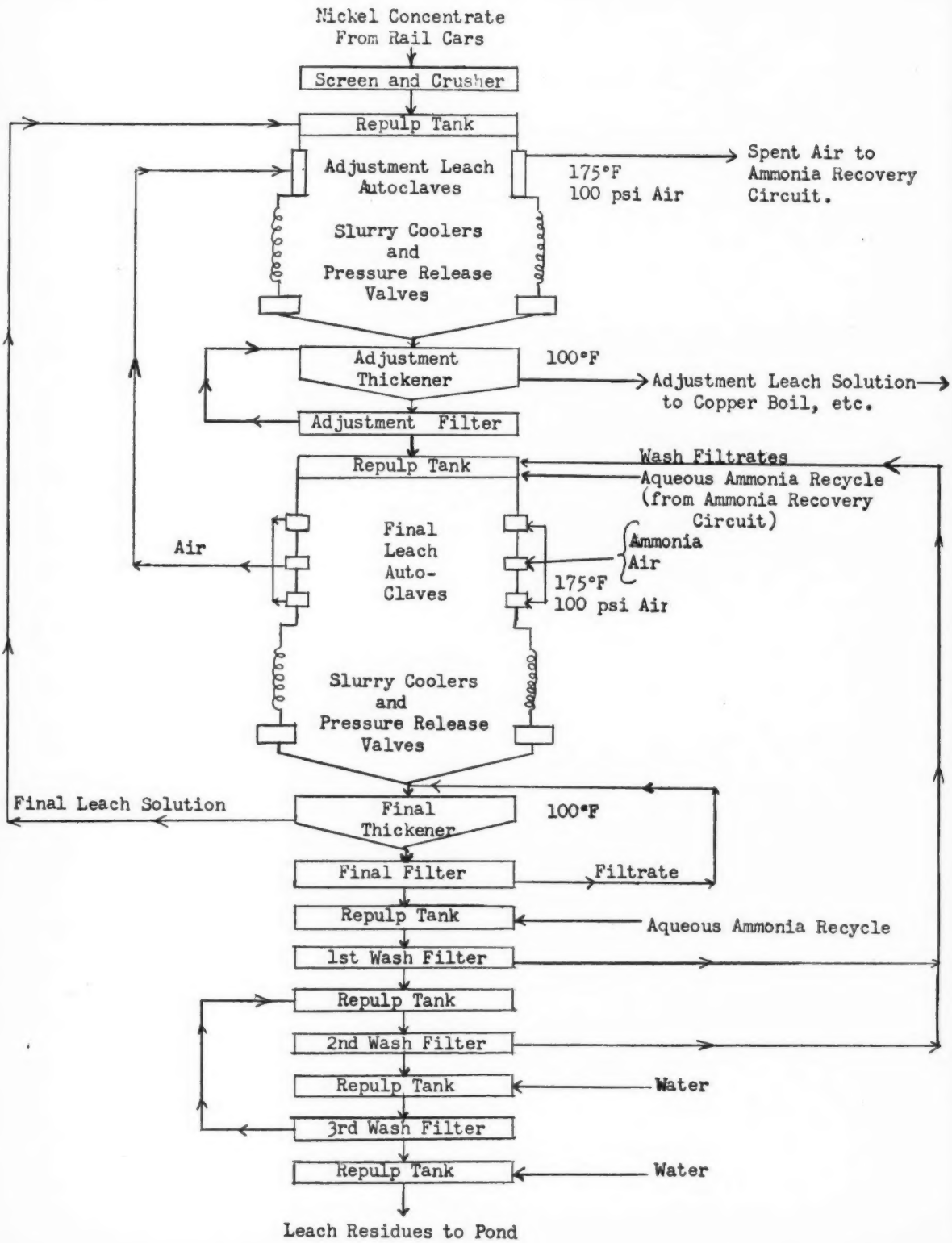

Figure 1—Leach circuit with liquid-solids separation.

circuit, not being designed to cope with large quantities of semi-colloidial hydrated iron oxide, would cease to function satisfactorily and the concentrate feed rate to the circuit would have to be cut to a minimum until the conditions in the thickeners improved.

An intensive study of the plant operation, with a correlation of the settling characteristics of the leach slurries in various parts of the circuit with the operating variables and procedures, was undertaken. This study showed that the pulps were characterised by progressively poorer settling rates as the solids passed through the circuit, indicating that the leach process had an important influence on the settling characteristics. It also showed that extremely slow-settling slurries were produced when the feed to the autoclaves had to be shut off and agitation (to prevent sanding up of the autoclaves) was maintained without leaching or discharge of the solids. Operation at low feed rates was also found to produce slow-settling slurries. Thus the indications from the plant study were that over-agitation was the main factor contributing to the extremely slimy nature of the leach residues; this was proved conclusively later and steps were taken in the plant to provide adequate agitation without excessive degradation of the leach residues.

One aspect of the plant study included the re-determination of the thickener area requirements [6, 7] since the original design data was obtained from the Ottawa pilot plant where no difficulties had been experienced in the liquid-solids separation. It was shown that the thickeners available would have sufficient capacity (without allowing the standard 30% safety factor in design) to handle 200 tons per day of concentrate under normal conditions but with slow-settling pulps (such as those discharged after a temporary shutdown for maintenance and those produced when the slimes were re-cycled to the head of the leaching circuit) the capacity would be reduced to below 100 tons per day of concentrate. The desired throughput, at that time, was 200 tons per day of concentrate.

Thus the necessity of improving the settling and thickening characteristics of the leach slurries was evident if considerable capital expenditure on further thickeners and filters was to be avoided. The use of flocculants sugested itself as an obvious and immediate remedy.

Flocculant behaviour

The chemical, screen and sub-sieve size analyses (as determined by the beaker decantation method [9] of the solids to be separated in the two liquid-solids separation stages are given in Table 1. The slurries are 20-25% solids by weight. The liquors (s.g. 1.1-1.2), in both cases, are highly ammoniacal (pH 8-10) and contain ammonium sulphate, nickel, cobalt and copper ammine complexes and small quantities of sulphamate, polythionate and thiosulphate radicals, giving a total electrolyte concentration of 450-500 g.p.l.

TABLE 1
NICKEL CONCENTRATE, ADJUSTMENT AND FINAL LEACH RESIDUES
CHEMICAL AND SIZE ANALYSES, NOV.-DEC. 1954

	Nickel Concentrates	Adjustment Leach Residues	Final Leach Residues
Chemical Analysis			
Ni	13.53%	8.34%	1.28
Co	0.42	0.42	0.29
Cu	1.49	1.24	0.13
Fe	36.86	40.70	47.80
S	30.86	22.23	14.33
Insol	13.78	15.80	17.30
Ca	0.19	0.18	0.20
Calculated Mineralogical Composition[8]			
Pentlandite, (Fe,Ni)S	42.50%	26.73%	1.95%
Chalcopyrite, $CuFeS_2$	4.31	1.21	0.16
Pyrite, FeS_2	2.02	2.2 (assumed)	2.4 (assumed)
Pyrrhotite, $Fe_{1-x}S$	34.15	30.56	33.70
Ferric Oxide Fe_2O_3	nil (assumed)	16.50	37.60
Adsorbed Ni (on $Fe_2O_3nH_2O$)	–	not determined	0.64
(Assumed, Fe/Ni ratio in Pentlandite = 1.0, Assumed x in Pyrrhotite formula = O, Degree of hydration of Fe_2O_3 not known).			
Screen Analysis (Tyler)			
+ 65 mesh	5.0	0.3	0.5
−65 + 100	7.3	2.3	2.4
−100 + 150	11.0	6.4	6.1
−150 + 200	10.5	8.9	7.3
−200 + 325	12.6	12.9	12.2
−325	53.6	69.2	71.5
Sub-Sieve Size Analysis (on −325 mesh fraction; reported as % weight of total solids).			
−40 + 30 microns	39.6	34.1	32.5
−30 + 15	6.1	9.7	9.2
−15 + 5	5.7	12.8	10.6
−5	2.2	12.6	19.2
Average S.G. of Solids	3.68	3.48	3.41

The problem presented was to find the most economic addition agent that would improve the thickening characteristics of these slurries adequately without affecting the chemistry or operation of the remaining stages in the Sherritt Gordon process.

Although little is known concerning the mechanism of dispersion and flocculation it is possible to formulate a hypothesis based on the fundamental physico-chemical principles governing the behaviour of solid suspensions in aqueous solutions to account for the majority of the observations on the ammonia leach slurries.

All minerals, when suspended in an aqueous solution, are soluble to some extent and it is the tendency of the ions on the surface of the particles and within the liquid boundary layer to establish a condition of equilibrium that results in an electrical charge (zeta-potential) on the particles. The generally accepted concept of the electrical charge is of two diffuse layers of oppositely charged ions (the Helmholtz and Gouy layers). Although it has not been proven (streaming potential studies would be required to verify this point) it is probable that the high electrolyte concentration of the ammonia leach slurries, with the correspondingly marked tendency for ionization, results in a high electrical charge on the suspended particles. The metal ions in the sulphide minerals, the absorbed nickel on the hydrated iron oxides [10] and the metal ions in solution are the ions common to both solid and liquid phases.

It has been shown experimentally [11] that it is the zeta-potential on the suspended particles that primarily controls the slime-coating on mineral particles and it is suggested that the

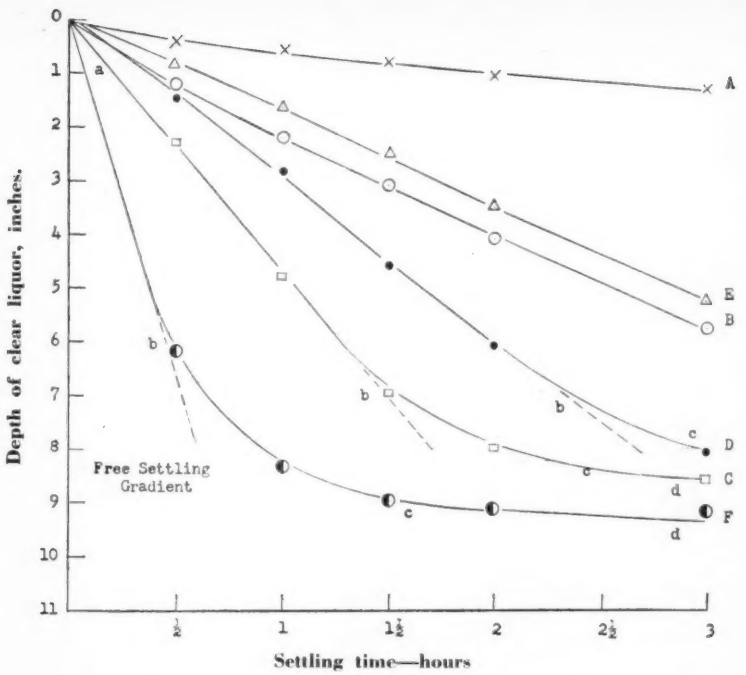

Figure 2—Settling rate curves, with flocculants.

A—Final leach discharge
B—Final leach discharge with 2.0 lbs./ton*, causticized Beetsol starch
C—Final leach discharge with 2.0 lbs./ton*, uncausticized Beetsol starch
D—Final leach discharge with 0.62 lbs./ton*, Aerofloc 552
E—Final leach discharge with 0.06 lbs./ton*, Separan 2610
F—Final leach discharge with 0.31 lbs./ton*, Separan 2610
***Of Solids.**

conclusions drawn from this work can be applied equally to the mechanism of flocculation. Thus flocculation is governed by:

1. The sign and magnitude of the charge on the suspended particles. Thus flocculation is facilitated by the mutual attraction of oppositely charged particles in a multi-solid phase system and is inhibited by the electrostatic repulsion of similarly charged particles.
2. The surface tension between the liquid and solid phases. This is an influencing factor only when the particles have actually made contact with one another.
3. The Van der Waals forces governing the attraction of solid particles. Here again these forces are weak and are only of significance when the interpenetration of the outer ionic layers has been achieved.
4. The average particle size and the particle size range [12]; the form and shape of the particles; and the form, size and shape of the resulting aggregates. These factors are also of less significance than the electrical charge on the particles.
5. The solids concentration in the suspension.

With regard to the electrical charge there is a certain critical zeta-potential above which dispersion is maintained and below which orthokinetic coagulation and flocculation takes place [13]. This critical zeta-potential is dependent upon the physical and chemical nature of the solid particles, the solids concentration and the ionic atmosphere of the liquid phase. Below the critical charge the particles can approach one another sufficiently for the surface tension and Van der Waals forces to become effective and cause flocculation [14]. With only the latter forces binding the particles together in the floccules, the bonds may be readily broken by mechanical forces.

Laboratory testing of flocculants

Confirmation that the solids in the ammonia leach discharge slurries were well dispersed was afforded by the fact that the sands settled rapidly away from the slimes (i.e. free settling conditions were prevailing). With a flocculated pulp the heavier and coarser particles would have been bonded with the slimes and the resulting aggregates, due to the high specific gravity unleached sulphides, would have settled much more rapidly than the slimes alone.

Thus to prevent the inherent dispersion of the slurries (and since it was impossible to reduce either the $(OH)^-$ ion or electrolyte concentrations) it was necessary to find a material that would provide either a coagulating ion (such as Ca^{+++}) or a protective coating on the particles, preventing their ionization tendency and reducing the zeta-potential to below the critical.

No effective coagulating ion could be found; lime, calcium salts, phosphates and polyphosphates were tried without success.

A considerable amount of work has been carried out to improve the sedimentation of the red muds in the Bayer Process (a similar system to the one discussed here) with the conclusion that organic materials such as flour and starch were the most useful for improving the liquid-solids separation of the colloidal iron oxide slimes from the caustic aluminate liquors [15]. Recent work has confirmed that the flocculating effect of these materials is accompanied by an almost complete neutralization of the zeta-potential on the particles [16]. For this reason the initial laboratory tests on the ammonia leach slurries were carried out with a wide range of starches and starch products. A number of commercial organic flocculants, available at the time of the investigations, were included in the testing program; it was assumed that these flocculants would act like the starches.

For the initial evaluation of these materials, sedimentation tests were carried out in one-litre graduated cylinders on final leach discharge slurry samples treated with various quantities of the flocculants. On settling, the slurries gave a distinct demarcation between the clear liquor and the settling solids. The depth of clear liquor was determined at regular intervals; the settling rate (actually of the slowest settling particles) was determined by plotting the depth of clear liquor to a time abscissa and calculating the gradient of the free-settling portion of the curve. Typical settling rate curves are given in Figure 2. Curves C, D and F show both free-settling (a to b), in which the particles fall unhindered by each other or at least where the elimination of water is by a regular subsidence of the slimes level, and compression settling (c to d) in which the particles or flocs rest on, or are partly supported by, each other. Sections b to c on the curves represent

the transition between free and compression settling. Curves A, B, and E are in the free-settling zone only; compression settling conditions would be reached if the data beyond the three hours were included.

The settling rates of the final leach discharge samples taken for the flocculant testing series were far from constant as they were, necessarily, taken over a period of several weeks. For this reason the criterion used for evaluating the effectiveness of a flocculant was the settling rate ratio—the ratio of the settling rates, with and without the flocculant, on the same slurry sample. Good consistency in the results was obtained by using this criterion.

Simultaneously with the sedimentation tests, filtration tests were carried out using a 0.1 sq. ft. Eimco laboratory test filter leaf covered with Duplan 2080 nylon filter cloth. The filter leaf was immersed in the lightly-agitated, conditioned slurries and the volume of filtrate collected in a given time was recorded. Here again the filtration rate ratios (with and without flocculants as before) were preferred to the actual filtration rates for comparative purposes.

The settling rate, and filtration rate, ratios for some of those materials which improved the settling characteristics are given in Table 2. The program included testing all the materials received on the final leach discharge slurries, selecting those which offered improvement and confirming this tendency on the adjustment leach discharge slurries. Those giving the best results in both series were then further investigated.

Of the commercial starches tested, Cellodex and W.W. Dextrine gave the best results when added in the causticised state at 2.0 lbs. per ton of suspended solids. Beetsol and Hercules Regular starches, proved more effective when added in the uncausticized state and also more effective than the causticized Cellodex starch. The behavior of the starches was very specific and few of them brought about any improvement on the settling rate.

Of the 30 commercial flocculants tested, Separan 2610 proved superior to all of the other flocculants, even at concentrations as low as 0.18 lbs. per ton of solids; it also improved the filtration rate more than any other addition agent tested. Reagent S-3000 and Aerofloc 552 followed Separan in efficiency.

The beneficial effect of Aerofloc 552 had been shown early in the investigations by the leach plant operating staff and, being readily available, it was added to the leach discharge slurries in quantities of 0.5 - 1.0 lbs. per ton of concentrate feed, over a period of three months. Its improvement on the settling rate was apparent although sliming conditions in the thickeners still occurred at frequent intervals. With Separan 2610 becoming available in commercial quantities a switch to this material was recommended.

Separan was preferred because smaller quantities were required to give the same improvement in the settling characteristics so resulting in a lower reagent cost, less dilution of the leach liquors and a greater flexibility in application. Separan was also superior to the other flocculants in that the incidence of compacting settling took place at a higher pulp density (advantageous in a thickener employing a raking mechanism). The compacting settling characteristics were also improved by Separan, indicating that the desired high pulp density in the thickener underflows could be obtained in a shorter time.

It was also found that Separan and the starches, in addition to improving the filtration rate, gave an easily detachable filter cake whereas the unconditioned slurry, and the Aerofloc 552 and S-3000 conditioned slurries gave filter cakes which were firmly adherent to the filter cloth.

Prior to recommending Separan for plant use, it was necessary to determine its effect on the other process stages and to determine the most suitable point of application. It was apparent that the quantity to be added and the operational control could best be determined (using the laboratory figures as a guide) from observation of its effect on the plant operation.

In the initial laboratory investigations on the effect of Separan, an excess (5 lbs. per ton) added to leaching charges in the laboratory autoclave, was shown to have no effect on the metals extractions; the settling rates after leaching were also unaffected.

An excess (1.2 lb. per ton) was also

TABLE 2

SEDIMENTATION TESTS ON FINAL LEACH DISCHARGE WITH ADDITION AGENTS

Note: 1. Flocculant Costs, January, 1955.
2. Starches 2–6 added in causticized state (0.2 lbs. Caustic Soda per lb. of starch)
3. Starches 7 and 8 added uncausticized.

No.	Addition	Supplier	Cost $/lb.	Quantity lbs/ton of solids	Ratios	
					Settling Rate	Filtration Rate
1.	Blank				1.00	1.00
2.	Cellodex Starch	Ogilvie Flour	0.115	1.0	3.51	
			0.115	2.0	6.04	
3.	W.W. 20 Dextrine	Ogilvie Flour	–	1.0	2.27	
			–	2.0	5.88	
4.	Cato Starch	National Adhesives	–	1.0	1.45	0.93
			–	2.0	2.09	1.02
5.	Beetsol Starch	Canada Starch	0.115	1.0	3.07	1.40
			0.115	2.0	3.72	2.04
6.	Hercules Regular Starch	Canada Starch	0.115	1.0	3.37	1.25
			0.115	2.0	3.80	1.88
7.	Beetsol Starch	Canada Starch	0.115	1.0	3.65	1.46
			0.115	2.0	8.70	1.78
8.	Hercules Regular Starch	Canada Starch	0.115	1.0	3.75	1.40
			0.115	2.0	7.50	1.92
9.	Aerofloc 548	Cyanamid	0.70	0.31	2.5	0.88
			0.70	0.62	4.8	1.03
10.	Aerofloc 552	Cyanamid	0.75	0.31	2.5	1.08
			0.75	0.62	5.5	1.31
11.	S-3000	Cyanamid	1.00	0.31	5.0	1.44
			1.00	0.62	9.1	1.61
12.	Separan 2610	Dow Chemical	1.00	0.06	3.2	1.29
			1.00	0.18	9.5	2.09
			1.00	0.31	26.0	2.27
			1.00	0.62	80.0	2.78
13.	High Viscosity Cellulose Gum No. 20	Hercules	–	0.31	3.4	1.18
			–	0.62	4.0	1.63
14.	Hallmark, Jaguar MD-C	Stein-Hall	–	0.50	1.0	1.08
			–	1.00	1.0	0.97
15.	Acrysol GS	Rohm and Haas	–	0.50	2.1	1.03
			–	1.00	4.2	1.03
16.	Lytron X886 (also 887 and 889)	Monsanto	–	0.50	3.7	1.80
			–	1.00	4.5	2.34

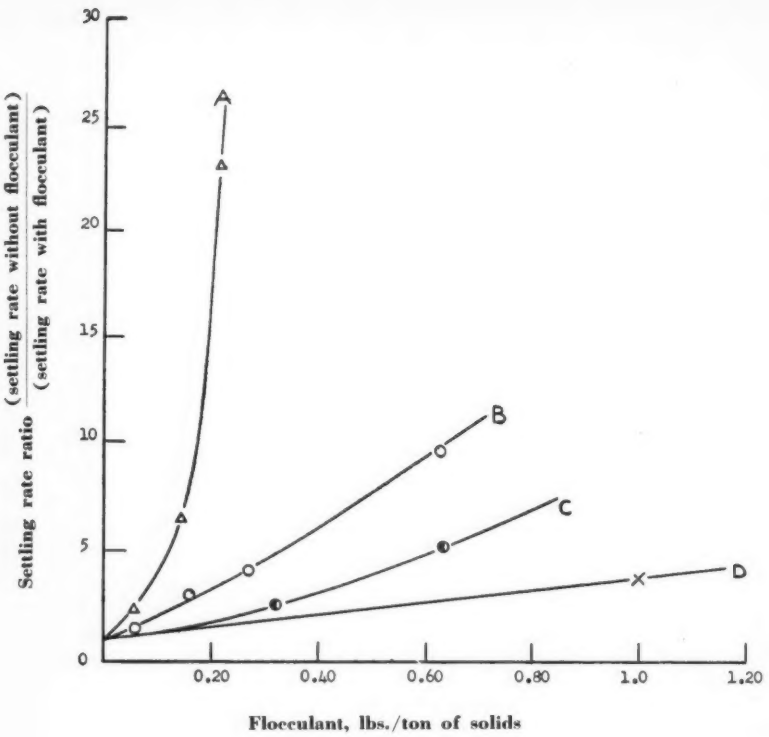

Figure 3—Comparative flocculating efficiencies on final leach discharge (initial settling rate without flocculant—0.49″/hr.)

A. Separan 2160

B. Reagent S-3000

C. Aerofloc 552

D. Beetsol and Hercules regular starches (uncausticized)

TABLE 3

RELATIONSHIP BETWEEN DRY SOLIDS FILTERED PER HOUR AND THE SEPARAN ADDITION TO A FINAL THICKENER UNDERFLOW
(P.D.—1.840)

A. LABORATORY TESTS

Test No.	Separan lbs./ton of solids	% Moisture in Wet Cake	lbs.of dry solids per sq. ft. per hour	% Improvement (based on Filtration Rate ratio)
1.	nil	19.5	14.5	–
2.	0.05	21.5	14.9	2.5
3.	0.10	25.3	16.7	15.0
4.	0.15	23.2	20.6	41.9
5.	0.24	22.0	21.8	50.2
6.	0.32	21.2	28.4	95.5
7.	0.40	20.3	31.0	114.0

B. PILOT PLANT FILTER TESTS:
On Slurry Already Thickened with 0.06 lbs. of Separan per ton of Solids.

1.	nil	19.1	6.54	–
2.	0.05	21.8	8.18	25
3.	0.06	22.2	8.90	36
4.	0.10	22.4	11.00	68
5.	0.12	23.0	11.69	78
6.	0.15	23.1	8.90	36
7.	0.24	22.8	8.45	29
8.	0.25	23.2	8.31	27
9.	0.48	22.6	9.03	38
10.	0.96	31.0	3.00	deteriorated by 54%

added in turn to the adjustment leach discharge slurry and solution, the copper-free solution, and the nickel reduction feed solution. The solutions were then processed through the remaining stages. From this it was concluded that Separan added to the circuit before the oxidation and hydrolysis stage [1, 2] had no detrimental effect on the process. Separan added after that stage (at least in this quantity) caused flocculation of the nickel with consequently poor operation in the reduction densifications [17].

It was also shown by a solution switching procedure and correlation with the settling rates, that 90-100% of the Separan added to a leach slurry would pass out of the circuit with the solids.

These experiments cleared Separan for use in the refinery circuit.

To ascertain the most suitable point of application for the flocculant, series of stability tests were carried out on the six most promising flocculants, (Separan, S-3000, Aerofloc 552, Beetsol starch, Hercules Regular starch and Cellodex starch). It was shown that agitation alone readily caused breakdown of the flocculating bonds of Separan, S-3000 and Aerofloc 552, that agitation at elevated temperatures (175°F) accelerated this breakdown and that neither agitation nor temperature had any effect on the flocculating effect of the starches. From this work it was recommended that if Separan were used it should be added to the cooled discharge slurries at a point where the agitation was sufficient only for mixing prior to thickening. A two-point addition was adopted for each thickener feed.

Effect of Separan on the process

Thickening—Opportunity was taken to confirm the laboratory results and conclusions during the first few months of adding Separan to the liquids-solids separation circuits.

The relationship between the quantity of Separan added and the improvement to the final leach residues settling rate is shown in Figure 3. Comparative relationships for S-3000, Aerofloc 552 and the best of the starches are also included. The advantages of Separan over the other flocculants are obvious.

In earlier investigations it had been shown that settling tests at various pulp densities were necessary to predict the thickener diameter requirements. Thus it was necessary to confirm that the faster initial settling rates with Separan would also mean improved thickening characteristics.

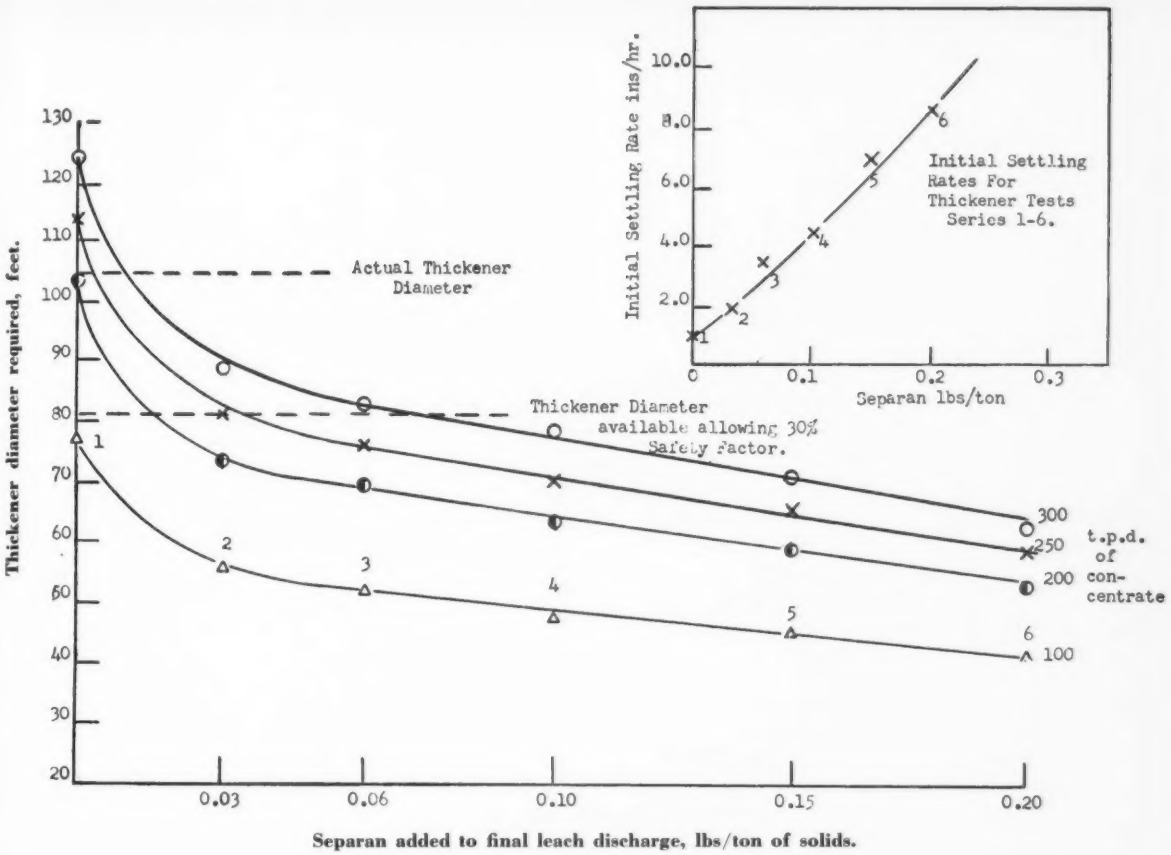

Figure 4—Thickener diameter requirements against Separan addition to the final leach discharge to give a final thickener underflow P.D.—1.850.

Thickening tests [6, 7] with 0.0, 0.03, 0.06, 0.10, 0.15 and 0.20 lb. of Separan per ton of solids were carried out on a sample of final leach discharge of good settling characteristics (1.0 in. per hour).

The thickener diameters required for various feed tonnages are plotted to a Separan addition abscissa in Figure 4. The relationship between the initial settling rate and the Separan addition is included in the inset. The curves show that, without Separan, a concentrate feed rate of 200 tons per day would require a 103 ft. dia. thickener in the final leach circuit; this would leave a safety factor of only 1.9% for abnormal operating conditions. With 0.03 lbs. of Separan per ton of concentrate the diameter required would be reduced to 73 ft. giving a safety factor of 43.7%. This is a more than adequate safety factor. Alternatively, the addition of 0.03 lbs. of Separan per ton would allow the residues from a concentrate feed of 250 t.p.d. to be separated in the 105 ft. thickener available and still leave the 30% safety factor specified normally in design calculations.

Increasing the Separan above 0.03 lb. per ton progressively improves the thickening characteristics of the slurry, although not by as much as does the initial addition. Thus the optimum addition for up to 300 tons per day rate would aparently lie between 0.03 and 0.06 lb. of Separan per ton and the inferences drawn from the settling rate data would appear to be justified.

Filtration—In addition to improving the thickening characteristics Separan also improved the filtration characteristics of the thickener underflows. A laboratory series to illustrate this, using the Eimco Corporation test procedure [18] is given in Table 3. Final thickener underflow was used for the filtration tests and Duplan 2080 (the standard cloth for the plant filters at the time) was used on the laboratory test filter leaf. In Figure 5 a comparison of the effect of Separan on an underflow sample taken under normal operating conditions (A) is made with one taken when an excessively high slimes burden was present in the leaching circuit (B).

The curves show that above 0.05 lb. per ton there is an approximately linear relationship between the Separan addition and the filtration rate (as determined by the weight of dry solids per sq. ft. per hour). The fact that more Separan is required on a slimy pulp to achieve the same filtration rate is also illustrated. From the figures reported, Separan would appear to increase the moisture content of the filter cake at low concentrations. In later studies this trend, although definite, was shown to have little significance.

Pilot plant filter tests, using a two compartment, two-disc Eimco filter, were carried out to confirm the laboratory results. Using this filter, a side-by-side comparison on the same final thickener underflow slurry, with and without a flocculant, was possible. The filter media on both discs was Duplan 2080 (a multifilament nylon cloth).

The results from these series (one series is reported in Table 3) showed a definite optimum Separan addition

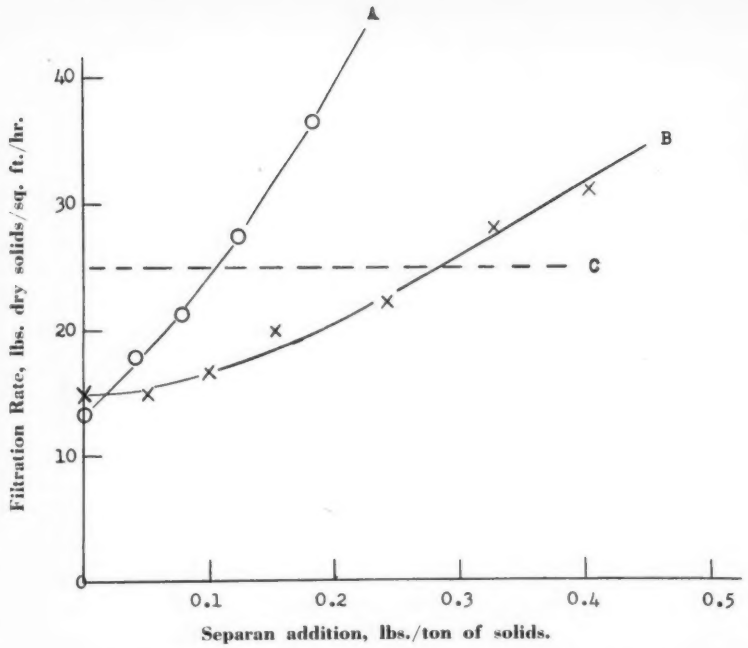

Figure 5—Laboratory tests, effect of separan on filtration rate of final thickener underflow.

A. Normal slurry
B. Slurry from thickener during sliming conditions.
C. Filtration rate needed to process residues from 250 tons of concentrate/day on existing 8'6" x 10 disc filter (assuming 30% safety factor and 100% cake discharge).

for improving the filtration of 0.10-0.12 lb. per ton (in addition to the 0.06 lb. per ton previously added to the thickening stage). At this concentration an improvement of 60-80% was obtained. Thus there would appear to be a contradiction between the laboratory results, giving a linear relationship, and the pilot plant filter tests, giving an optimum, for the filtration efficiency versus Separan addition. This anomaly may be explained by the more efficient agitation in the laboratory tests giving a more uniform cake build-up and the 100% cake discharge in the laboratory tests compared with 30-40% from the disc filters under the conditions of the test. With the higher Separan additions, consolidation settling of the slurries in the filter boots took place and this was a further factor preventing the pick up of a uniform cake.

The pilot plant results were later confirmed in the commercial plant. Since that time a combination of other improvements, to improve the uniformity of the cake build-up and the ease of cake discharge together with the addition of Separan, has improved the capacity of the tailings filter circuit well beyond the design capacity. Thus the need for extra filters, as the production rate of the refinery was gradually increased, was avoided.

Start-up operations for the refinery commenced at the end of May, 1954 with each stage being brought into operation successively [1] and with the first nickel powder being produced on July 21. Between that date and the end of January 1955, when the full capacity of the refinery was attained, difficulties were frequently experienced in the leach plant due to sliming conditions throughout the leaching circuit.

Separan was received in commercial quantities at the refinery on January 19, 1955. At that time operation of the adjustment thickener was satisfactory with 30-40 in. of clear liquor, but sliming conditions existed in the final thickener with solids overflowing back to the adjustment leach. From the laboratory investigations, Separan additions of 0.03 lb. per ton of concentrate to the cooled adjustment leach discharge, 0.06 lb. per ton to the cooled final leach discharge and 0.12 lb. per ton to the final thickener underflow were recommended. Two-point additions of a 0.25% Separan solution in cold water were employed.

By January 24, 70 in. of clear liquor were being maintained in the adjustment thickener and by January 28 the steady improvement in the depth of clear liquor (5 in. per day) had resulted in 45 in. of clear liquor in the final thickener. Apart from an initial over-loading of the rake mechanism when the slimes load was dropped too rapidly due to a considerable excess of Separan, the operation of the thickeners has since been excellent.

Thus from the observation of the plant operation, Separan (the effective constituents of which are high molecular weight acrylamide polymer hydrolytes [19]) has been shown to improve the thickening and filtration characteristics of the ammonia leach residues and to have no harmful effect on the chemistry or operation of the remaining process steps when added to the liquid-solids separation circuit in quantities of approximately 0.2 lb. of Separan per ton of nickel concentrate.

References

(1) Nashner, S., Trans. C.I.M., 58, 212, (1955).
(2) Forward, F. A., Trans. C.I.M., 56, 373 (1953).
(3) Forward, F. A. J. of Metals, 5, 755, (1953).
(4) Forward, F. A. and Mackiw, V. N., J. of Metals, 7, 457, (1955).
(5) Brenthel, C. F., Z. Erzberghau u. Mettallhuttenw, 8, 422, (1955).
(6) Coe, H. S. and Clevenger, G. H., Trans. A.I.M.E., 55, 356, (1916).
(7) Bond, F. C., Trans. C.I.M. 49, 546, (1946).
(8) Lin, W. C., Unpublished data, Sherritt Gordon Mines Limited.
(9) Pryor, E. J. et al., Recent Developments in Mineral Dressing, I.M.M. Symposium, London, 11, (1952).
(10) Herrmann, W. 'The Precipitation of Nickel Compounds in the Presence of Iron Oxide', S.G.M. Research Report, 1953.
(11) Sun, S. C., Trans. A.I.M.E. 153, 479, (1943).
(12) Dallvalle, J. M. 'Micromeritics', Pitman Publishing Co., New York, 1948.
(13) Földvári, A., Kolloid Beihefte, 44, 125, (1936).
(14) Wadsworth, M. E. and Cutler, I. B. Min. Eng. 8, 830, (1956).
(15) Dvornick, O. and Hermann, E. J., Kolloid Z., 128, 75.
(16) Papp, E. et al., Acta Technica Academicae Scientiarum Hungaricae, 13, 33, (1955).
(17) Mackiw, V. N., Lin, W. C. and Kunda, W. Symposium on the Physical Chemistry of Hydrometallurgy. A.I.M.E. General Meeting, N.Y., Feb. 1956. To be published in the Trans. A.I.M.E.
(18) Dahlstrom, D. A. "Filtration of Ammonia Leach Slurries, Sherritt Gordon Mines Limited, Fort Saskatchewan, Alberta". Report of Investigations, The Eimco Corporation, March 1955.
(19) . . . . . Information release, The Dow Chemical Company, February, 1955.

Acknowledgments

The authors wish to emphasize that the solution to the problem was found through the combined efforts of the operating, engineering and research personnel and they wish to acknowledge the assistance given them by their associates at the chemical metallurgical division, Sherritt Gordon Mines Limited, Fort Saskatchewan. In particular they wish to record their appreciation of the suggestions and encouraging interest given them by the late Sydney Nashmer, W. H. Young, C. A. Hames, V. N. Mackiw and R. F. Pearce; also by O. Tangel and J. Shea of the Battelle Memorial Institute. They also wish to acknowledge that part of the experimental work carried out by D. A. Diamond (at present doing post-graduate research at Cornell University) and to thank J. P. Warner for his help in the presentation of this paper.

★ ★ ★

The Decomposition, Oxidation, Ignition and Detonation of Fuel Vapors and Gases[1]

Part 31. The Effect of Flow Configuration in an Annular Reactor of Vycor Glass on the Oxidation of Pentane

R. O. KING[2], *S. SANDLER*[3], *and R. STROM*[4]

The oxidation and ignition of n-pentane-air mixtures in an annulus 1.0 mm. wide between concentric tubes of Vycor glass has been investigated in a flow system at atmospheric pressure and at temperatures rising to 800°C. The mixtures were supplied at rates ranging from 400 to 50 cc./min. and the flow was necessarily laminar. Neither oxidation nor decomposition reactions occurred at surface temperatures lower than 625°C. when a correct mixture was supplied at 400 cc./min. but when time of residence was doubled an oxidation reaction with a negative temperature coefficient occurred over the temperature range 470°C. to 505°C. There was then a temperature range of 145°C. over which no reaction could be detected before the initiation of a high temperature raction. The maximum rate of the initial reaction increased and the temperature range of practically no reaction diminished as the rate of mixture supply was reduced to 100 cc./min. The products of the low temperature reaction were essentially aldehydes, acids and steam but there was no fluorescence, pressure fluctuation or ignition. It is shown that the negative temperature coefficient is a surface phenomenon. Thus it has not been necessary to attribute it in whole or in part to a gas phase reaction dependent upon a chain reaction mechanism.

Introduction

A DISTINCT negative temperature coefficient of the velocity of the low temperature oxidation of propane and the butanes was first described by Pease who attributed it, at the time, to the inhibitory action of excess oxygen or diluent nitrogen at the higher temperatures [1]. Neumann and Aivazov [2] used a bulb method to study the oxidation of n-pentane and attributed the negative temperature coefficient of the primary reaction to autocatalysis by one of the intermediate products of which the maximum concentration was considered to decrease with increase of temperature. This general explanation was elaborated by other investigators in subsequent studies of this phenomenon. Some claimed that the essential intermediate was a peroxide [3] or a peroxide radical [4] while others attributed the results to the accelerating effect on the initial reaction of various aldehydes, an effect which was found to diminish with increasing temperature in the low temperature range [5], [6]. In any case, the general opinion was that the low temperature mechanism of the reaction was that of a degenerate explosion of the branched chain type and the rather sharp suppression of reaction with temperature increase was attributed to suppression of branching by the further reaction of some important intermediate.

A study of the references mentioned and many others indicates a decided lack of agreement in respect of the mechanism of the chain reaction to which the negative temperature coefficient was attributed. The magnitudes of the coefficient as shown by their experiments depended upon whether the flow or bulb method was used. Flow configuration conditions of the experiments differed according to the dimensions and conformation of the reactors but its effect was not considered in discussions of the cause of the negative temperature coefficient.

Flow configuration is however shown by the experiments with pentane-air mixtures described in Part 2 [7], to be a major factor in respect of reaction velocity and the magnitude of the negative temperature coefficient. When, for example, pentane in a mixture with air was oxidized in a 25 mm. diameter pyrex combustion tube, a negative temperature coefficient was obtained when it was in the horizontal position but not when flow configuration was altered by using the tube in a vertical position, as shown by the graphs of Figure 1, reproduced from the reference quoted.

Negative temperature coefficients were also obtained when King reactor No. 10 was used [8, p. 833]. This reactor was designed and used mainly to obtain conditions in which the oxidation of pentane went to final products when doped with iron carbonyl. The design of the reactor was such that oxidation of pentane, either with or without the dope, became a surface effect. Experiments were carried out with various rates of mixture supply and mixture

[1] *Manuscript received March 3, 1957.*
Contribution from Defence Research Board, Ottawa, Ont., in association with the Department of Chemical Engineering, University of Toronto, Toronto, Ont.
[2] *Scientific Officer in Charge Combustion Research Section, Defence Research Board, and Special Lecturer, Department of Chemical Engineering, University of Toronto.*
[3] *Principal Scientific Research Officer, Defence Research Board.*
[4] *Senior Scientific Research Officer, Defence Research Board.*

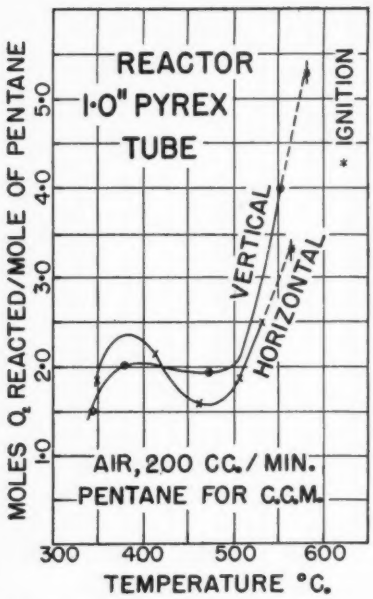

Figure 1—The change in the temperature coefficient of reaction due to changing a tube reactor from the horizontal to the vertical position.

strengths and are described in Parts 1 [8], and 2 [7], and in Part 7 [9] from which results obtained when the dope was not used are shown by the reproduced graphs of Figure 2. They show the increase in percentage of oxygen reacted in the low temperature region that accompanied an increase in the concentration of pentane in the mixture with air. When the concentration was double that required for a chemically correct mixture, the rate of oxygen reacted attained a maximum value of 33% at 415°C. The rate then diminished to 16% over the temperature range 420°C. to 500°C. The low and high temperature reactions were not separated by a temperature range of no reaction. Explosive ignition did not occur although the temperature was raised to 650°C.

It was indicated by experiments with vertical combustion tubes described in Part 23 [10] that aldehydes formed on the tube surface in the low temperature range were carried from the boundary layer into the central stream by circulating convection currents, and there accounted for the occurrence of fluorescence, pressure waves and the consequent mild type of non-explosive ignition. The occurrence of ignition in the low temperature range thus depended upon the existence, apart from the boundary layer, of a central stream in which there were circulating convection currents. Similarly, ignition in the high temperature range was attributed to the effect of the convection currents in removing oxidation products from the boundary layer in order to allow access of less reacted mixture to the surface. By analysis of the effluent from the tube no distinction could be made between the reactions that occurred on the surface and those that might have occurred in the central stream. It was decided, therefore, to eliminate the effect of the central stream by using a reactor in the form of a narrow annulus between two concentric tubes. The mixture flow through it was necessarily laminar thus circulating convection currents were eliminated and boundary layer conditions obtained. The results of experiments made accordingly are given in this Part.

The term "negative temperature coefficient" is used to mean the differential quotient of the reaction velocity with respect to temperature, which can be positive or negative. The phenomenon is also but not commonly, described as the factor by which the reaction velocity changes with an increase of 10°C. in temperature. By this arbitrary method, the factor can be greater or less than unity but is never greater than zero in conditions of experiment generally used. It cannot be applied to conditions used for the experiments described in this Part in which there is a temperature interval of zero reaction which is greater than 10°C. between the low and high temperature reactions.

Experimental

The concentric tubes of the reactor were of Vycor glass. The inside diameter of the outer tube was 19.0 mm. and the wall thickness 3.0 mm. The outside diameter of the inner tube was 17.0 mm. and the wall thickness 2.0 mm. The width of the annulus was thus 1.0 mm. Vycor glass is 96% silica. Tubes of pure silica were not available in the required diameters.

The design of the reactor and its arrangement in a vertical tubular electric furnace 2.0 in. in diameter are shown by Figure 3. Concentricity of the tubes was maintained by small bosses spaced 120° apart at the relatively cool ends of the reactor. The heated length of the furnace was 6.5 in. and temperature as measured on the exterior surface of the outer tube attained a maximum value at approximately the midsection of that length. This temperature is given in subsequent text as related to rates of reaction and to the occurrence of ignition. There were steep temperature gradients from the position of maximum temperature to the relatively cool ends of the reactor. On the other hand, the temperature variation across the reactor at the position of maximum temperature was always very small, being usually about 2 or 3°C.

The methods used for the measurement of temperature, rates of air and pentane supplied, oxygen reacted and oxides of carbon formed, were as described in the appendix to Part 23 [10, pp. 125-126]. Unsaturates were determined, in one set of conditions only, by absorption in a saturated solution of mercuric sulphate in a 25% sulphuric acid solution using the conventional Orsat apparatus. A modification of the methods used by Widmaier and Mauss [11] in the analysis of the products of oxidation of gasolines was adopted for the determination of total aldehydes and peroxides.

Chemically correct mixtures are described as "correct" or by the abbreviation C.C.M. and contain 2.63 cc. of the vapor of pentane in 100 cc. of air. Mixtures are described as percent weak or rich according to the

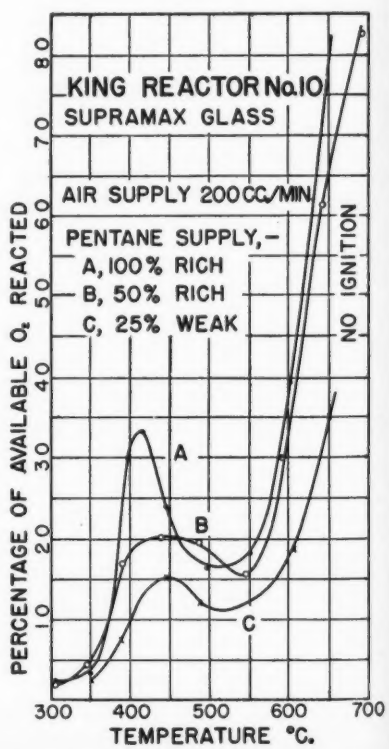

Figure 2—Oxidation of pentane in King reactor No. 10 and the effect of mixture strength on the negative temperature coefficient.

percentage by which the pentane vapor is less or more than that required for a correct mixture. Technical grade n-pentane as supplied by the Phillips Petroleum Company was used for the experiments.

Flow Configuration in the Annular Reactor

The Reynolds number for the flow of air through an annulus is calculated on the basis of the mean hydraulic radius being ¼ of the difference in the diameters of the boundary surfaces. Reynolds numbers thus calculated for the annular reactor, Figure 3, for a rate of air supply of 50 cc./min. were 1.91 at 25°C., 1.19 at 300°C., 1.07 at 400°C. and 0.98 at 500°C.

The Reynolds number increases in direct proportion with increase in the rate of air supply. The maximum rate used for the experiments was 400 cc./min. and they were always carried out at annulus temperatures exceeding 300°C. The Reynolds number was therefore never greater than 9.60. This is so far below the critical value of approximately 2300 required for the initiation of turbulence that the effect of small percentage additions of pentane vapor can be neglected and flow through the annulus 1.0 mm. wide regarded as laminar in all of the experimental conditions. Thus there would always be a stationery layer of gas on the boundary surfaces and the velocity profile of the flow would be parabolic. A difference in the temperature of the boundary surfaces would cause merely a distortion of the parabolic profile, without creation of circulating convection currents.

Results

1. The Effect of Residence Time, Correct Mixtures with Air Supplied at Rates of from 400-50 cc./min. to the Annular Reactor

The continuance of reaction that begins on the heated surface must depend upon diffusion of the products from it in order to permit access of reacting mixture to it. The rate of surface reaction will therefore depend upon the rate at which the products escape from the surface and diffuse into the mixture passing through the annulus. The rate will thus depend upon the time of residence of the mixture in the reactor. This time is basically proportional inversely to the rate of supply of the mixture which always contains an excess of diluent consisting of nitrogen and unreacted oxygen. The range of residence times investigated is from 0.4 to 3.2 sec. as calculated for an average gas temperature of 500°C. and corresponding to rates of air supply varying from 400 cc./min. to 50 cc./min.

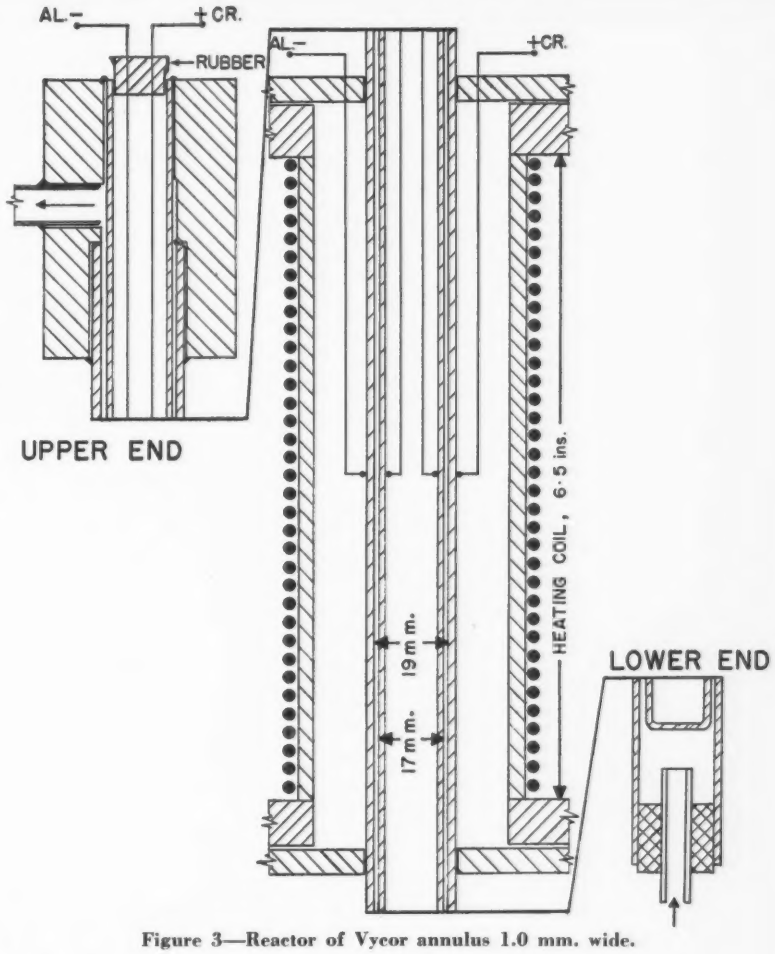

Figure 3—Reactor of Vycor annulus 1.0 mm. wide.

Experimental results obtained to show the influence of temperature on rates of oxygen consumption and formation of oxides of carbon are given by the graphs of Figures 4 to 8 for the several rates of mixture supply.

(a) Air Supplied at 400 cc./min.

At the shortest residence time used, Figure 4, measurable reaction did not occur until the maximum temperature exceeded 625°C. The product of the reaction then contained the oxides of carbon and a small proportion of unsaturates as would be expected if decomposition as well as oxidation of the pentane had occurred. The rate of formation of both carbon oxides increased rapidly with temperature. However, carbon monoxide production began at a lower temperature than that of carbon dioxide and continued at a greater rate as the temperature was raised until the mixture ignited at 745°C. when little more than 50% of the available oxygen was reacted. The yield of unsaturates reached a maximum some 20°C. before ignition occurred and then diminished rapidly.

(b) Air Supplied at 200 cc./min.

When the residence time was thus doubled reaction began at 420°C. as shown by Figure 5, and the rate increased to a maximum of 0.15 moles of oxygen reacted per mole of n-pentane, at 370°C. The temperature coefficient then became negative and reaction ceased to be measurable at 505°C. and so remained at temperatures rising to 650°C. The high temperature reaction then began and proceeded with increasing velocity until ignition occurred at 745°C. when approximately 50% of the available oxygen was reacted. The oxidation products of the low temperature reaction were aldehydes, acids and water; carbon monoxide and dioxide formation being negligible. Those of the high temperature

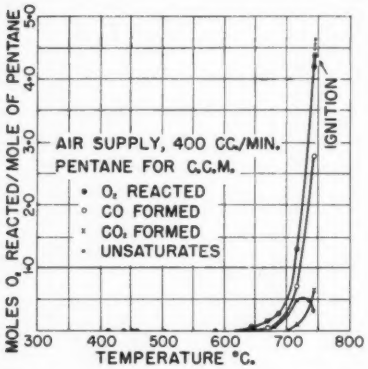

Figure 4—Rate of reaction in the annular reactor with pentane for a correct mixture with air supplied at 400 cc./min.

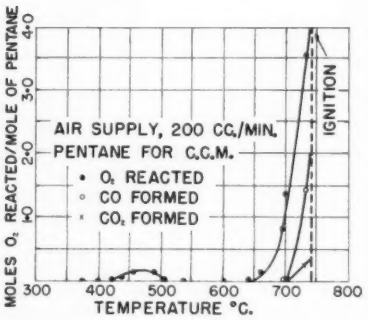

Figure 5—Rate of reaction in the annular reactor with pentane for a correct mixture with air supplied at 200 cc./min.

reaction were the oxides of carbon and water. Unsaturates were also detected. Neither oxidation nor decomposition products could be detected in the intermediate temperature range. A low-temperature fractional distillation (Podbielniak-Semi-Robot) of the effluent obtained at one point in this range indicated that n-pentane was the sole hydrocarbon present.

(c) Air Supplied at 150 and 100 cc./min.

Experimental results obtained when the rate of air supply was 150 cc./min. are given by the graphs of Figure 6. Reaction began at 405°C. and proceeded with increasing velocity to a maximum rate of 0.70 moles of oxygen reacted at a temperature of 435°C. The temperature coefficient then became negative and rate of reaction ceased to be measureable at 585°C. The high temperature reaction began at 620°C. that is, after a temperature interval of 35°C. only of no measurable rate of reaction. Ignition occurred at 745°C., again when approximately 50% of the oxygen was reacted.

The experimental results obtained when the rate of air supply was further reduced to 100 cc./min. are given by the graphs of Figure 7. They differ from those obtained with a rate of supply of 150 cc./min. in that maximum rate of oxygen reacted per mole of pentane in the low temperature range increased from 0.70 moles to 0.80 and remained nearly constant until the temperature coefficient became negative at 500°C. and reaction rate decreased to practically nil at 610°C. The high temperature reaction began 25°C. later, at 635°C. and as before proceeded with increasing velocity until ignition occurred at 747°C.

(d) Air Supplied at 50 cc./min.

The experimental results are given by the graphs of Figure 8. A comparison of the results with those presented for the 100 cc./min. rate of supply is of interest. The following differences should be noted: (1) at the lower flow rate, reaction began at a temperature 50°C. lower, coincident with the formation of some carbon dioxide, and was followed about 15°C. later with the formation of the monoxide in addition to aldehydes, acids and water as found in the products obtained at the lower residence time, (2) maximum rate of reaction in the low temperature range increased from 0.80 moles to 1.30 moles of oxygen reacted, (3) the low and high temperature ranges of reaction were not separated by a temperature range of no reaction thus 0.75 moles of oxygen was reacted per mole of pentane at 625°C. whereas there was no reaction at that temperature when the air was supplied at 100 cc./min.

(e) Ignition Temperatures

The ignition of a correct mixture occurred within the temperature range 745° to 750°C. with rates of supply ranging from 100 cc. to 400 cc./min. Ignition was uncertain at rates less than 100 cc./min. and at 50 cc./min. temperature was raised to 800°C. without the occurrence of ignition, although the mixture strength was varied from 50% weak to 85% rich.

(f) Production of Aldehydes

The influence of temperature on the total aldehyde production is shown by Figure 9. A maximum was obtained at a temperature of 430°C., which corresponds to that at which the low temperature rate of oxygen consumption was a maximum. The rate of aldehyde formation then decreased rapidly with temperature over the next 100°C. As oxygen consumption remained relatively constant over this range, see Figure 6, the formation of oxygen containing products other than those for which analyses were performed is thus indicated.

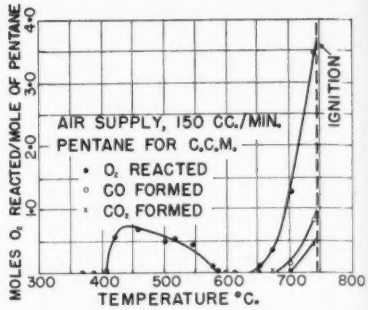

Figure 6—Rate of reaction in the annular reactor with pentane for a correct mixture with air supplied at 150 cc./min.

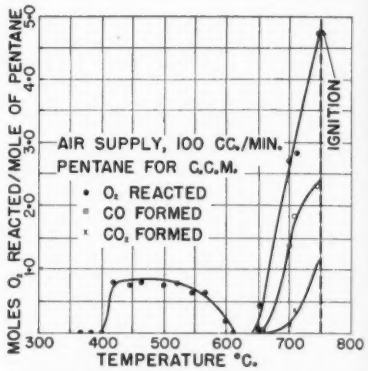

Figure 7—Rate of reaction in the annular reactor with pentane for a correct mixture with air supplied at 100 cc./min.

The graph of Figure 10 shows the effect of increase of residence time on the rate of aldehyde formation when a correct mixture was used and the maximum temperature of the reactor was maintained at 430°C. It will be seen that the volume percentage of aldehyde formation increased slowly as rate of air supply was increased from 50 cc. to 100 cc./min. The maximum percentage formation was then attained. The percentage formation of aldehyde then decreased as rate of air supply was further increased and become nearly zero when a rate of air supply of 200 cc./min. was attained.

2. The Effect of Mixture Strength at a Constant Rate of Air Supply of 50 cc./min. to the Annular Reactor

(a) Rates of Oxygen Reacted and Carbon Oxides formed

Figure 11 shows the effect of enriching or weakening the mixture. A more pronounced negative tempera-

ture coefficient of reaction was obtained with the rich mixture and a more complex low temperature mechanism was in operation for the weak mixture. In the latter, a maximum was obtained during the initial rapid increase in oxygen consumption, after which the rate of oxygen consumption declined slightly, remained steady over a prolonged temperature range, and then dropped again until the high temperature reaction began.

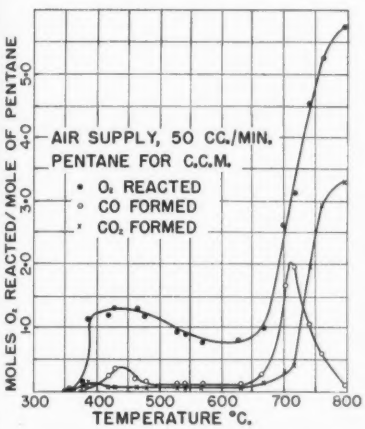

Figure 8—Rate of reaction in the annular reactor with pentane for a correct mixture with air supplied at 50 cc./min.

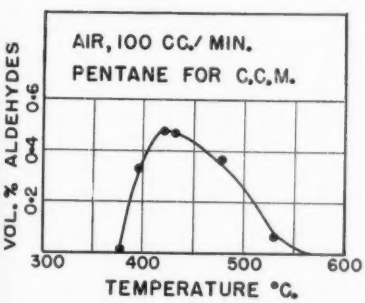

Figure 9—Rate of formation of aldehydes in the annular reactor as affected by temperature.

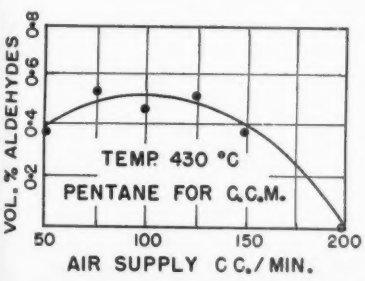

Figure 10.—Rate of formation of aldehydes in the annular reactor as affected by rate of supply of a correct pentane air mixture.

Figures 12, 13, and Figure 8, *ante* show the variations in carbon monoxide and dioxide formation with temperature, for various mixture strengths. In the rich mixture, the monoxide formation exceeded that of the dioxide over the whole range of temperatures as opposed to the effect previously described for the correct mixture. The weak mixture on the other hand, showed no formation of carbon oxides in the low temperature region. However, in the high temperature region the products were similar to those obtained with the correct mixture except that the rate of formation of carbon monoxide was less than that of the dioxide.

(b) Production of Aldehydes and Peroxides

The influence of mixture strength on aldehyde production at 430°C. for a flow of 100 cc./min. is given by Figure 14, which shows that the aldehyde content of the effluent increased steadily with increased mixture strength over the range 25% weak to 100% rich. When calculated on the basis of moles of aldehyde produced per mole of pentane however, a variation of from 0.16 to 0.22 only, was noted over this range of mixture strengths.

The analyses for peroxides indicated that their rate of formation was negligible in the conditions of these and all preceding experiments with the annular reactor.

Discussion

The narrow annulus provided a combustion space in which the flow of mixture was always laminar. Thus reaction in the low temperature range began by the oxidation of the stationary layer of mixture on the surfaces and its continuance and rate depended upon the release of products from the surface, their rate of diffusion into the moving stream and the rate of replacement of the layer by diffusion of unreacted mixture from the stream. Thus, the velocity of the low temperature reaction would be expected to depend largely on the time of residence in the reactor, as has been demonstrated.

The occurrence of a negative temperature coefficient of reaction over a subsequent temperature range can be attributed to the increasing activity of the surface in this range in the further reaction of an active intermediate product of the low temperature reaction. It was shown in Part 23 [10] that the occurrence of ignition in the low temperature range depended on the existence apart from the boundary layer of a central stream in which there were circulating convection currents. It was in-

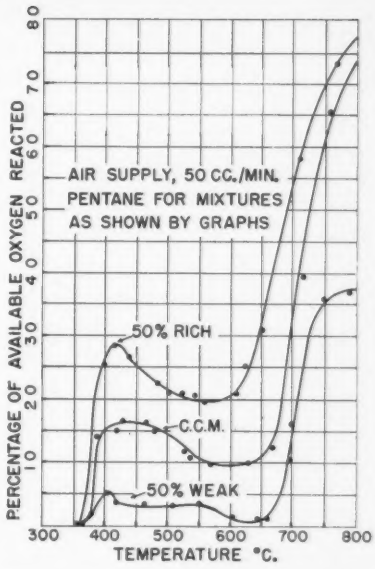

Figure 11—Percentage of available oxygen reacted in the annular reactor as affected by mixture strength and temperature.

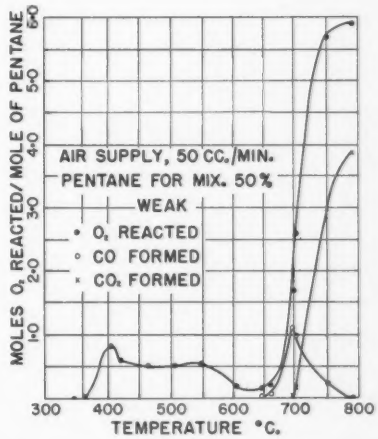

Figure 12—Rate of reaction, 50% weak mixture supplied to the annular reactor at 50 cc./min.

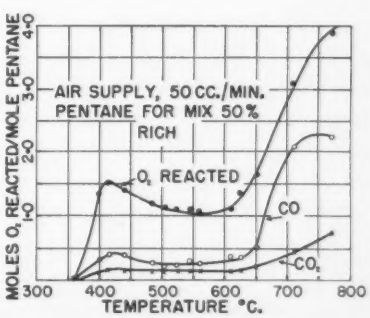

Figure 13—Rate of reaction 50% rich mixture supplied to the annular reactor at 50 cc./min.

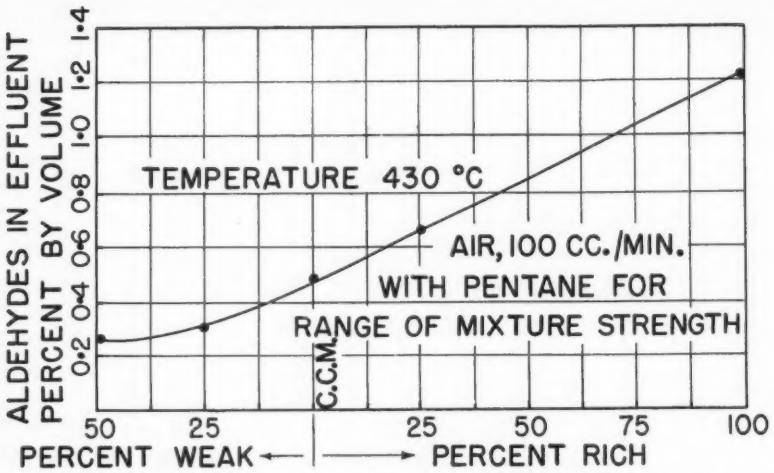

Figure 14—Volume percentage of aldehyde formation as affected by mixture strength with annular reactor temperature maintained at 430°C.

dicated by the experimental results that ignition occurred when aldehydes initially formed on the surface were carried from the boundary layer into the central stream. It has been shown here in Figure 9 that the rate of formation of aldehydes rose to a maximum with temperature in a manner similar to that of the overall rate of oxygen consumption and then decreased rapidly. Since low temperature ignitions did not occur in these conditions it is suggested that further reaction of aldehydes on the surface at an increasing rate with temperature within a certain temperature range accounts for the negative temperature coefficient of the reaction. Although the particular aldehyde responsible for the effect has not been determined, these results appear to confirm experiments previously reported in which the addition of acetaldehyde to hydrocarbon-air mixtures was shown to autocatalyze the first stage reaction [2]. The decomposition of this substance to final products at increasingly higher temperatures under high residence time conditions or its further oxidation under low residence time conditions accounts for the decreased rate of oxygen consumption in this temperature range.

The occurrence of a range of temperatures in which no reaction is apparent can be accounted for, therefore, by the combination of the two factors given above. Thus when the residence time is short enough so that the rate of diffusion of products from the surface and reactants to the surface is inappreciable and the temperature is such that complete reaction of aldehydes on the surface occurs, a condition is attained such that no oxidation or decomposition products appear in the effluent and the overall rate of reaction is so low as to be nonmeasurable. This state of affairs continues until the temperature is raised to a point where a new reaction mechanism is operative and where the rate of diffusion of the products has been raised to a value comparable with the residence time. This is not in accordance with statements by Prettre [12]) and others that chain branching occurs on the wall and that deactivation of the carrier occurs in the gas phase and is accelerated by raising the temperature. Instead, it has been shown that the deactivation is a surface effect and in consequence it is not necessary to devise a gas phase reaction mechanism or to make use of any of those devised by others in order to account for the negative temperature coefficient.

Experiments involving more comprehensive analyses of the oxidation and decomposition products are being carried out to determine the nature of the substances formed in the temperature range over which the coefficient of the reaction velocity is negative. Further experiments to demonstrate the powerful influence of surface on this phase of the reaction are also in progress.

References

(1) Pease, R. N., J. Am. Chem. Soc., *51*: 1839-1856, (1929).
(2) Neumann, M., and Aivazov, B., Nature, *135*: 655-656, (1935).
(3) Egerton, A., and Ubbelohde, A. R., Nature, *135*: 997-998, (1935).
(4) Walsh, A. D., Trans. Faraday Soc., *43*: 297-305, (1947).
(5) Antonovskii, V. L., and Shtern, V. Ya., Doklady Akad. Nauk. S.S.S.R. *78*: 303-306, (1951).
(6) Knox, J. H., and Norrish, R. G. W., Proc. Roy. Soc. (London), *50*: 151-170, (1954).
(7) King, R. O., Can. J. Research, F, *26*: 36-56, (1948).
(8) King, R. O., Can. J. Reesarch, F, *25*: 326-342, (1947).
(9) King, R. O., Can. J. Research, F, *26*: 426-440, (1948).
(10) King, R. O., Sandler, S. and Strom, R., Can. J. Tech. *32*: 102-126, (1954).
(11) Widmaier, O., and Mauss, F., Rev. Inst. Franc. Petrole, *3*: 151-160, 1948 and *3*: 183-191, (1948).
(12) Prettre, M. J., Chim. Phys., *36*: 39, (1939).

Acknowledgments

The experimental work was carried out in the Department of Chemical Engineering, University of Toronto, with the co-operation of Professor R. R. McLaughlin, Head of the Department and Dean of the Faculty of Applied Science, and with the aid of an extra mural grant from the Defence Research Board, Canada. The authors are indebted to the Chairman of the Board for permission to publish.

★ ★ ★

Flooding Phenomena in Packed Gas Absorption Columns[1]

G. W. MINARD[2] and M. D. WINNING[3]

This paper embodies the results of an investigation of pressure drop and flooding in a 6 in. diameter gas absorption column packed with half inch Raschig rings and Fiberglas. Pressure drops and flow rates were measured for eight combinations of gas and liquid phases in a series of 437 runs. The flow rates and fluid properties varied over wide ranges. Data were obtained on visual flooding.

This investigation attempts to show that pressure drops may be predicted by an empirical relationship which appears to depend on gas flow rate, liquid flow rate and fluid properties. The visual flooding data correlate after the method of Sherwood, Shipley and Holloway. A new relationship applicable to pressure drop flooding is presented in the form

$$\frac{\Delta p}{\rho_L \, D \, \epsilon} \left(\frac{D}{a}\right)^{1/3} \mu_L^{0.1} = 0.62$$

Introduction

This paper reports the results of an investigation which dealt with the relationships between flow rates and pressure drop, between flow rates and visual flooding, and between fluid and packing properties and pressure drop flooding.

Flooding in packed absorption columns has been previously defined as: the build-up of liquid on top of the packing; the entrainment of liquid in the gas phase; the spraying of liquid from the top of the column; the rise of "slugs" of foam through the packing. Pressure drop flooding has been defined as the point, on a graph of pressure drop across a packed column versus gas flow rate, at which the pressure drop increases excessively with a slight increase in gas flow rate at a constant liquid flow rate. Both "visual" and "pressure drop" definitions are used as means of studying the data in this investigation. Similarities and differences between the two definitions are reported.

In the design of packed absorption columns, both flooding and the pressure drop due to fluid flow through a packing must be considered. Flow rates usually set the column diameter. Where these flow rates have been established by an economic study, they must be checked to insure that they will not produce flooding with its resultant loss of liquid and build-up of back pressure on the gas stream. When blowers are being sized the pressure drop across the column must be available. Flooding can seldom be observed visually, but the pressure drop across a column may be observed on a differential pressure gauge. Thus the prediction of the pressure drop below which flooding is unlikely to occur is useful to operating personnel.

Both visual flooding and pressure drop are related to flow rates. For visual flooding, liquid and gas velocity relationships have been given by Sherwood, Shipley and Holloway [1]. The relationship between pressure drop and flow rate is usually depicted graphically. Early interpretations [2, 3] of the resulting logarithmic graphs postulated two intersecting straight lines with a definite break point or discontinuity as shown in Figure 1. Attempts were made by various investigators to relate this discontinuity to visual flooding. Zenz [4], on the other hand, suggested that the graph should not show a discontinuity, but rather continuous pressure build-up with increasing flow rate. Data obtained by Ufford [5] bore out this contention, and the authors on examining the data in the literature found that the two straight lines could be replaced by a smooth curve. This paper suggests a form of empirical equation to fit the proposed smooth curves.

In the pressure drop flooding definition the flooding point would be that at which the tangent to the pressure drop-flow rate curve is a vertical line parallel to the pressure drop axis. Since much of the data in the literature does not reach this region, it was found convenient to take the pressure drop at flooding as that pressure drop at which the slope of the tangent to the pressure drop-flow rate curve exceeded 85°.

The authors conclude from the data examined [3, 4, 5] that this particular pressure drop associated with flooding in the pressure drop flooding definition, appears to be independent of flow rates, and is instead a function of packing and fluid properties. The points marked (*) in Figure 1

1 *Manuscript received March 10, 1957.*
Contribution from the Department of Chemical Engineering, University of Toronto, Toronto, Ont.
2 *Present address: Associate Professor of Chemical Engineering, Bucknell University, Lewisburg, Pa.*
3 *Present address: Gas Engineer, Shell Oil Company, New York, N.Y.*

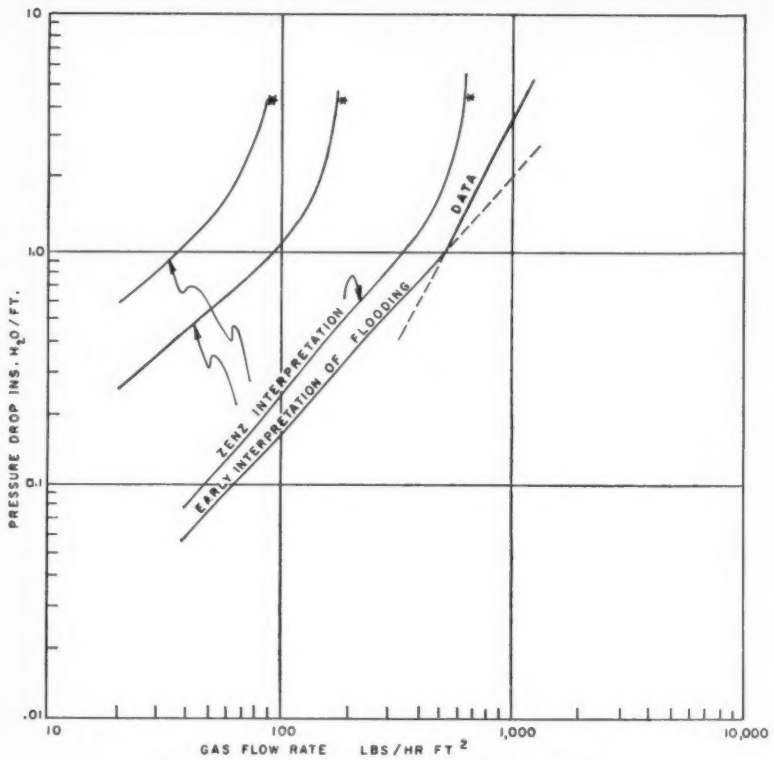

Figure 1—Typical pressure drop-flow rate curve.

are considered to fit the definition of pressure drop flooding. It may be seen that the pressure drop at these points is constant, being independent of the liquid and gas flow rate. The nature of the relationship between pressure drop and packing and fluid properties will be discussed in this paper.

Equipment

Basically, the equipment consisted of a packed column common to two flow circuits. The liquid flow circuit consisted of the column, a centrifugal pump, a supply tank, a constant head tank, a pair of rotameters, and the pipe, fittings, and valves necessary for connecting the parts and for controlling the flow rate. The gas flow circuit consisted of the column, a blower, a gasholder, a pair of rotameters and the necessary pipe, fittings, and valves.

The instrumentation was relatively simple. Two double clean-out manometers were connected to the column via a valve-manifold system to permit measurement of the differential pressure across the packing. Static pressures were also measured on these manometers at the gas meters, gasholder, column base and column top. Copper-constantan thermocouples were used, in conjunction with a potentiometer, to measure temperatures.

Figure 2 is a schematic diagram of the equipment.

The Column and Packings

The column was a standard 6 ft. length of 6 in. I.D. Pyrex glass pipe mounted vertically in a supporting framework. The ends were attached to metal plates by aluminum flanges. Further connections were then made to the metal plates which also served as a means of attaching the pipe to the rigid metal framework. The packing support was attached to the underside of the lower plate. This support consisted of one-quarter in. wire mesh basket 4 in. deep and 8 in. square. This type of support was chosen to prevent any reduction of flow area at the support.

Two column packings were used. One-half in. Raschig rings were employed in the first part of the investigation, and "Fiberglas" was employed in the second part. The rings were dumped into the water-filled column to give a packed height of 5 ft. The fiberous packing was made by cutting 6 in. circles from one inch "Fiberglas Dustop Air Filters". The short cylinders so obtained were then pushed

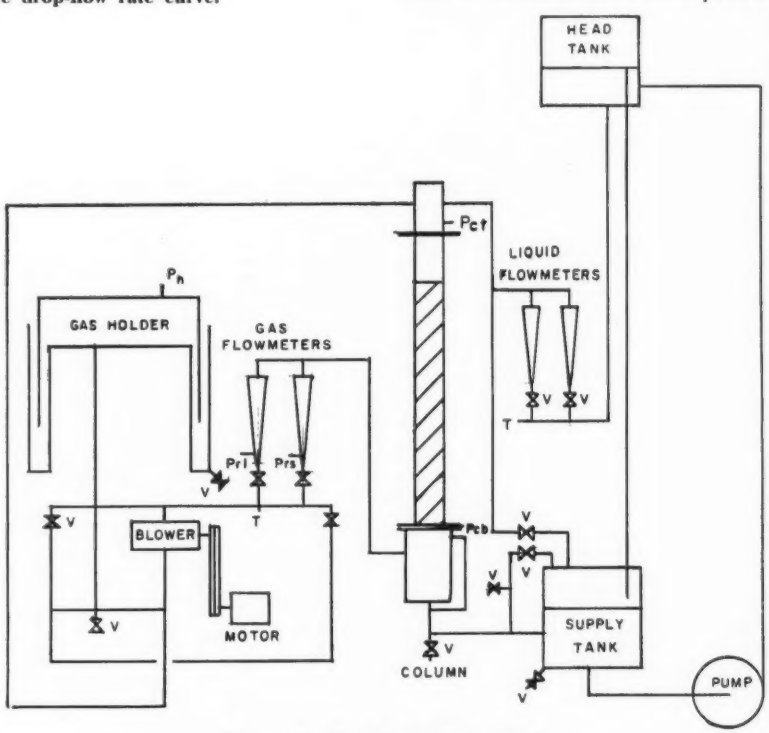

Figure 2—Equipment flow sheet.

Symbols

V—valve T—thermocouple well
Pet—pressure tap at column top
Pcb—pressure tap at column bottom
Prl—pressure tap at large gas rotameter
Prs—pressure tap at small gas rotameter
Ph—pressure tap at gasholder.

up inside the dry column from the bottom. A variation in the fraction of free void was obtained by varying the height of a constant mass of fiberous packing.

A seven-holed liquid distributor at the top of the column provided uniform liquid distribution.

Column Operation for Flooding and Hold-up Measurements

To determine flooding conditions in the packed column, gas and liquid were circulated at constant rates. When stable operation had been obtained at one particular set of flow rates, readings were taken of the pressure drop across the column, of gas and liquid temperatures, of the pressure in the gas rotameter and of room temperature at the panel board. Periodically, during the runs, the barometric pressure was noted.

After recording the flooding data the dynamic liquid hold-up was determined in the following manner. While the column was operating, the height of liquid in the bottom section was noted. Then all flows including the column discharge were simultaneously shut off. After a draining period of ten minutes the liquid level

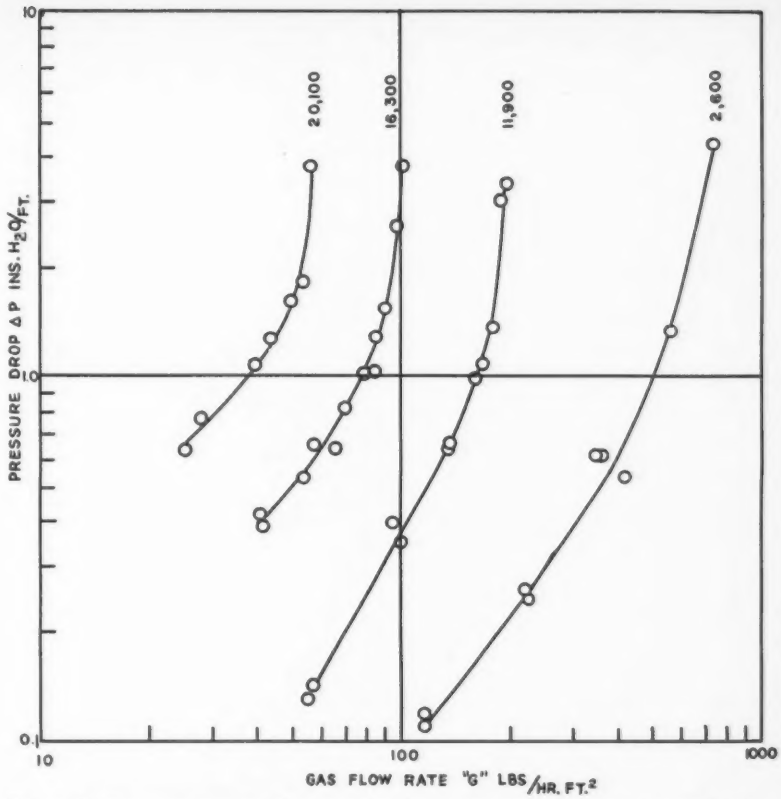

Figure 4—Pressure drop vs. flow rate for the system carbon dioxide-water flowing through Raschig rings. The parameter is the liquid flow rate "L" $\frac{\text{LBS}}{\text{HR. FT}^2}$

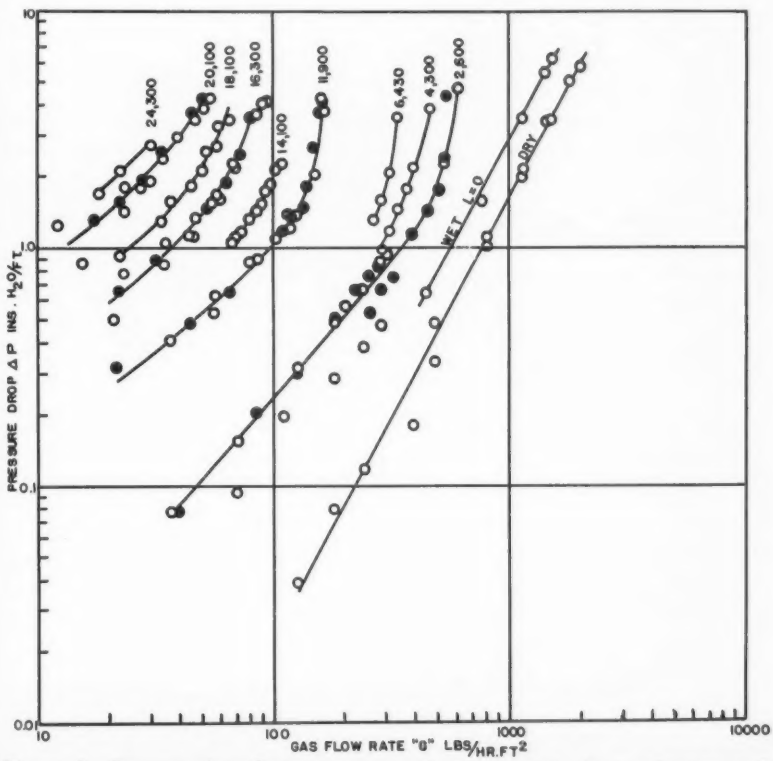

Figure 3—Pressure drop-flow rate curves for the system air or nitrogen and water flowing through Raschig rings. The parameter is liquid flow rate "L" LBS/HR. FT^2; air ○; nitrogen ●.

in the bottom section was again recorded. The difference of the two readings was taken as the dynamic liquid hold-up.

The above procedure was then duplicated for other flow rates.

For those systems other than air-water-Raschig rings no hold-up data were collected. Several runs were made with the packing wet but with no liquid flowing. At the conclusion of those runs with wet packing, the top section of the column was removed, and the packing was dried by blowing air through it. Then pressure drop-flow rate data for the dry packing were secured.

Experimental Results

Visual Observations

1. *Column Operation with Raschig Ring Packing*

The flow characteristics observed for Raschig ring packing agreed closely with those of White [3].

At low liquid rates the flow of liquid through the packed column appeared to vary with gas flow rate. At low gas rates the liquid formed drops on the packing, and as these became larger they flowed down from one unit of packing to the next below. For a higher gas rate, the liquid hold-up in the column had

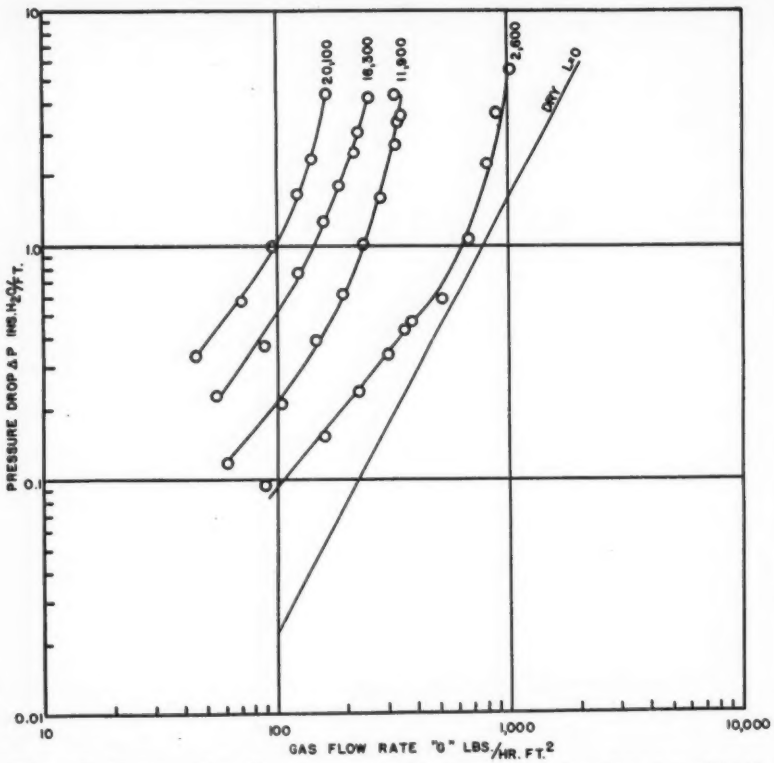

Figure 5—Pressure drop-flow rate curves for the system air-carbon tetrachloride flowing through Raschig rings $\rho L = 99.5$ LBS/FT^3. The parameter is liquid flow rate "L" LBS/HR.FT^2

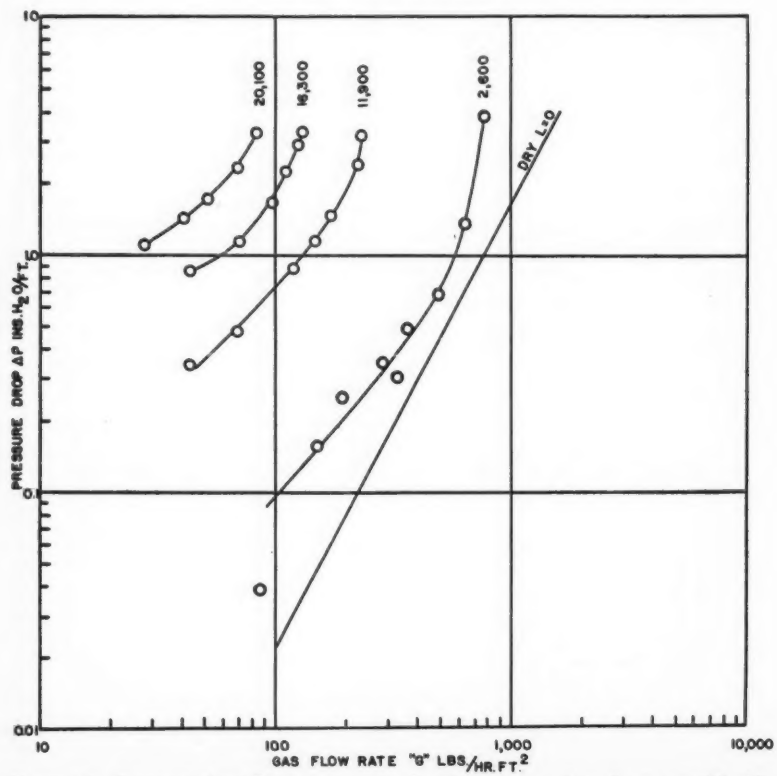

Figure 6—Pressure drop-flow rate curves for the system air-carbon tetrachloride and ethanol flowing through Raschig rings $\rho L = 74.6$ LBS/FT^3. The parameter is liquid flow rate "L" LBS/HR.FT^2

accumulated enough to form continuous streams instead of drops. Further increase in gas flow rate increased the size of the streams until the liquid appeared to become the continuous phase with the gas bubbling through it. Generally at this set of conditions a layer of liquid or foam formed on the top of the packing.

At high liquid rates (say L ~ 10,000 lbs./hr./ft.^{2}) the first liquid flow was not in the form of drops but rather in continuous streams; i.e., the first flow stage mentioned in the paragraph above was not present. Increasing the gas flow rate had the same effect as previously noted. At the higher liquid rates the layer of foam noted at flooding became a layer of liquid with only a few gas bubbles in it.

The behaviour of the column followed the same general pattern for variations in gas and liquid rate. When the flow rates are high enough to cause visual flooding, a slight difference is noted in the layer of liquid on top of the packing.

2. *Column Operation with Fiberglas Packing*

The effect of gas and liquid flow rates on the appearance of the Fiberglas packed column did not differ greatly from that for ring packing provided the flow rates were below those which would cause flooding. A few major differences in appearance were noted between the ring packed and Fiberglas packed columns when visual flooding had been achieved.

As flooding conditions were approached the packing appeared to fill completely with liquid. However, a slight increase in gas velocity beyond flooding caused the packing to loosen or expand, and to move about in the column. The expansion opened up a number of large voids in the packing. A further slight increase in gas velocity caused a build-up of liquid on the top of the packing as well as an increase in the size of the void.

A greater increase in gas velocity over that for flooding caused such a loosening effect that channelling developed, and the liquid head on top of the packing disappeared. An additional increase in gas velocity only aggravated this condition. When the gas and liquid flows were stopped, after a period of flooding, it was found that the top layer of fiber had been broken into short lengths by the agitation of the liquid. Under further operation some of these fibers

could be noted being blown up to the top of the column.

The loosening and breaking of the Fiberglas packing resulted in a change in the fraction of free void. This change could not be measured.

The operation of the column was stable for all flow rates below, at and above those required for visual flooding in both packings used. For operation at flooding a period of time was necessary for the conditions in the column to become steady. However, a stable operation was always achieved.

Correlation of Results

1. *Pressure-Drop and Flow Rate Relationships*

a. *Raschig Ring Packing*: The first data collected were obtained for the purpose of finding the variation in pressure drop-flow rate relationships due to variations in gas properties.

Water was used as the liquid and air, nitrogen, and carbon dioxide were used respectively as the gas. The data for air and nitrogen fell so closely together that the same graph could be used to represent both. The data for carbon dioxide did show significant differences. Changes in gas viscosity are rather small so that the effects shown were generally due to gas density.

Figure 3 presents the relationship between pressure drop (ΔP) and gas flow rate (G) with liquid flow rate (L) as the parameter, for the systems air-water-Raschig rings, and nitrogen-water-Raschig rings. Also included are the base lines for air flowing through dry packing and moistened packing. Figure 4 presents the corresponding data for the system carbon dioxide-water-Raschig rings.

The data from which the Figures 3 to 11 have been prepared are tabulated in the Ph.D. thesis [6], by M. D. Winning entitled, "Flooding Phenomena in Gas Absorption Columns". 1952, University of Toronto, which is available from the University library.

Several important features are immediately evident from Figures 3 and 4. First it will be noted that the data fall on smooth curves. This bears out the contention of Zenz [3]. It is true that for the lowest liquid flow rate, a portion of the curve appears straight, but the curvature is very evident at the higher liquid rates. It will also be noted that the curves straighten out at the higher liquid rates.

Although it is difficult to distinguish between the data for air and

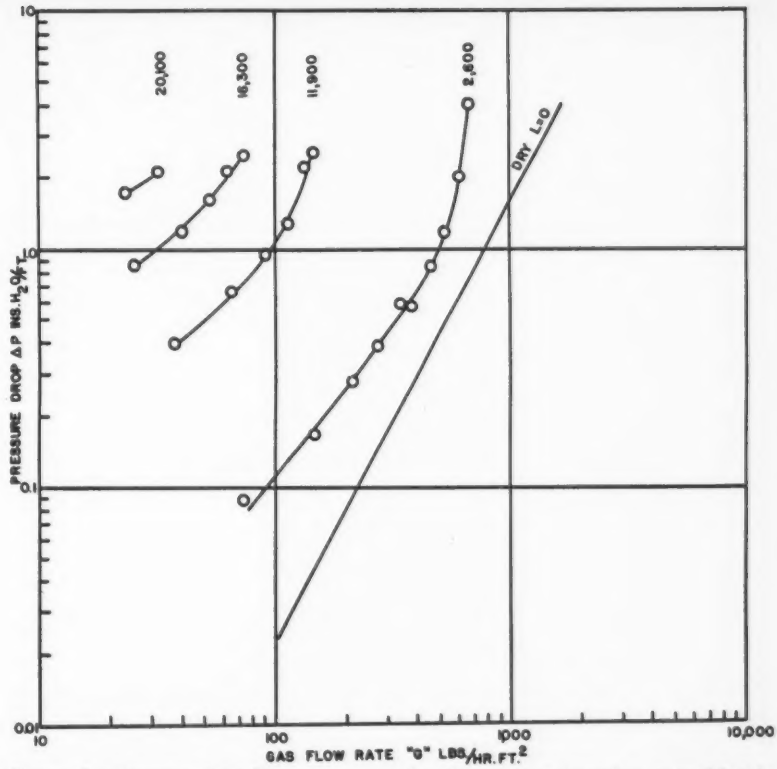

Figure 7—Pressure drop-flow rate curves for the system air-carbon tetrachloride and ethanol flowing through Raschig rings $\rho L = 61.5$ LBS/FT^3. The parameter is liquid flow rate "L" LBS/HR.FT^2

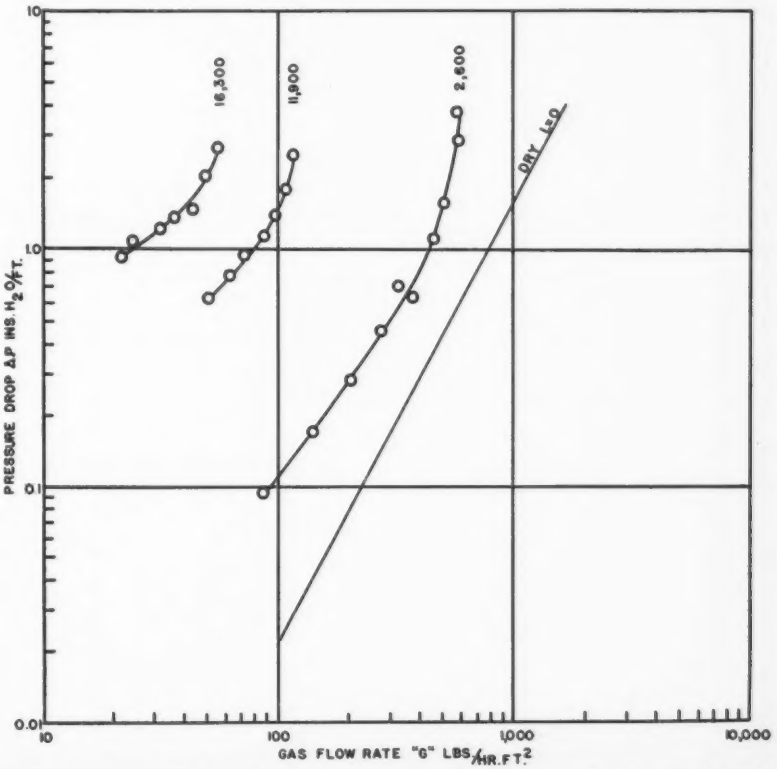

Figure 8—Pressure drop-flow rate curves for the system air-carbon tetrachloride and ethanol flowing through Raschig rings $\rho L = 56.8$ LBS/FT^3. The parameter is liquid flow rate "L" LBS/HR.FT^2

nitrogen, comparison of these with the lines for carbon dioxide show that increasing the gas density increases the amount of the gas passed at the same pressure drop.

As a result of the fact that the curves appear to be continuous, attempts were made to find empirical equations to fit the curves. Equations for gas flow through dry or wet packings were easily obtainable in the form $\Delta\mathcal{P} = q\,G^r$ where $\Delta\mathcal{P}$ is the pressure drop in inches of water per foot of packing height, "G" is the gas flow rate in pounds per hour square feet of column area, and "q" and "r" are constants. When gas and liquid are present in the column in counterflow the pressure drop appeared to increase more rapidly than would be indicated by a simple power function of the gas flow rate.

Of a number of equations tested against the data the relationship

$$\Delta\mathcal{P} = qG^r + s\tan\left(\frac{\pi}{2}\frac{G}{t}\right)$$

was found to fit the data reasonably well. The terms q, r, s, and t were found to vary with liquid flow rate and gas density, but because of insufficient data in the literature, it has not been possible to obtain a generalized correlation between them.

A second set of data was obtained for mixtures of ethanol and carbon tetrachloride as liquid, air as gas and for Raschig ring packing. Mixtures of these two liquids allow a wide variation in liquid density with but slight change in viscosity. Figures 5 to 9 show the effect of variation of liquid density on the pressure drop-flow rate relation.

It may be noted that changes in liquid density have two effects. First at one liquid velocity, the gas capacity of the column increases, with increasing liquid density, as shown by a shift of the curves to the right. Second, the liquid capacity of the column is increased as shown by the great variation in the positions of the curves at high liquid flow rates. Just what fraction of the gas capacity increase is due to liquid density changes and what part is due to gas density changes cannot be determined.

As with the first set of data, attempts were made to obtain empirical equations. In all cases it was found possible to relate the pressure drop and the gas flow rate by the equation

$$\Delta\mathcal{P} = qG^r + s\tan\left(\frac{\pi}{2}\frac{G}{t}\right)$$

The influence of free void fraction was not investigated nor was the influence of packing orientation.

b. *Fiberglas Packing*: Fiberglas has been suggested as a possible packing material for columns on the basis of the large surface area obtainable per cubic foot of packed volume. In order to improve on the other packings already in use, an arrangement of packing to give an area greater than 250 sq. ft per cu. ft. is suggested. Tests were made on two packings of Fiberglas having a calculated area of 270 and 412 sq. ft. per cu. ft. respectively. The fractions of free void for these packings when wet were 0.95 and 0.91 respectively.

The tests on the packing having a free void fraction of 0.91 indicated that the packing would pass gas without difficulty, but flooding occurred even at the lowest gas rates when there was any liquid flow. The runs made with the packing having a free void fraction of 0.95 indicated allowable flow rates high enough to warrant using the packing industrially. The data obtained are shown in Figure 10.

The data for Fiberglas packing show that much smaller pressure drops occur than for other packings with equivalent flow rates. Thus, a tower packed with Fiberglas would have a greater capacity, both for liquid and gas, than a tower filled with the more common industrial packings. However, when the increase in pressure drop which characterizes flooding, occurs, it is extremely abrupt. The lifting or opening of the packing mentioned under visual observations creates some doubt as to whether the pressure drop recorded is the result of flooding or due to lifting of the packing.

The doubt as to the reliability of the fraction of free void at flooding, together with the knowledge that the Fiberglas disintegrates under the agitation of flooding, restricts the range of data for which empirical equations may be determined. However, for the flow of air and water through Fiberglas having a fraction of free void of 0.495, where the gas rate does not exceed 700 lbs./hr./ft.^{2} and the liquid rate does not exceed 10,000 lbs./hr./ft.^{2}, pressure drop ($\Delta\mathcal{P}$) may be evaluated as

$$\Delta\mathcal{P} = (39{,}500 + 2.42\,L) \times 10^{-9}\,G^{1.44}$$

L = Liquid flow rate in pounds per hour square feet of column area.

TABLE 1

CALCULATED VALUES OF $\dfrac{\Delta p}{\rho_L D\epsilon}\left(\dfrac{D}{a}\right)^{1/3}\mu_L{}^{0.1}$

1. Schoenborn	0.630	8. Elgin and Weiss[7]	0.542
2.	0.582	9. Elgin and Weiss	0.578
3.	0.581	10. Elgin and Weiss	0.648
4. and	0.690	11. White[3]	0.648
5.	0.695	12. Zenz[4]	0.605
6.	0.602	13. Authors	0.667
7. Dougherty[8]	0.645	14. Authors	0.622

TABLE 2

PACKING & GAS/LIQUID SYSTEMS USED IN PRESSURE DROP FLOODING CORRELATION

Investigator	Packing Type & Size		Gas	Liquid
Schoenborn and Dougherty[8]	Carbon Rings	1″	Air	Water
	Ceramic Rings	1″		
	Porcelain Rings	½″		and
	Berl Saddles	½″		
	Carbon Rings	¼″		Oil
Elgin and Weiss[7]	Berl Saddles	½″	Air	Water
	Berl Saddles	¼″		
	Clay Rings	⅝″		
	Clay Balls	½″		
White[3]	Rings	1¼″	Air	Water
	Rings	1″		
	Rings	¾″		
	Rings	⅜″		
	Rings	½″		
	Rings	⅜″		
Zenz[4]	Reviewed all the above plus			
	Ceramic Rings	1″	Air	Water

The restrictions applied here still allow a range of operating variables which should be of use industrially. However, no attempts should be made to use Fiberglas near flooding conditions without introducing some means of restricting its movement.

2. *Flooding Correlations*

Visual Flooding: The correlation method of Sherwood, Shipley and Holloway [1] for visual flooding flow rates, was applied to the data of this investigation as a means of comparing them with those of other investigators. The runs which fit the definition of visual flooding were plotted as

$$\frac{L}{G}\sqrt{\frac{\rho g}{\rho_L}} \text{ vs. } \frac{Ug^2\,a}{g\,\epsilon^3}\frac{\rho g}{\rho_L}\mu_L^{0.2}$$

and are shown in Figure 11. The solid line represents the correlation proposed by Sherwood et al., as the best locus for all previous data. The two dashed lines indicate the width of the band covered by previous data. It can be seen that most of the runs of the present investigation fit the proposed correlation remarkably well, and all fall within the indicated band except one of the doubtful runs using Fiberglas.

This shows that the construction of equipment, collection of data and methods of calculation are comparable to those of previous investigations and that the comparison of data with those previously reported is justifiable.

Pressure Drop Flooding: On examining the data of the flow region where the pressure drop appears to increase without limit, certain factors seemed to be related.

These factors were:

Pressure drop – Δp pounds/square foot

Packing size (diameter)–D feet, outside diameter for spheres, fibers, and rings (usually equal ring length), face to face distance for saddles

Packing void fraction–ϵ cu. ft. of free space/cu. ft. of packed volume

Packed surface area–a sq. ft. of area/cu. ft. of packing

Liquid viscosity–μ_L pounds/foot sec.

Liquid density–$\mathcal{P}_L$ pounds/cu. ft.

Dimensional analysis was applied to these factors, and the following equation resulted:

$$\frac{\Delta p}{D\rho_L} = \left[\left(\frac{a}{D}\right)^x, \left(\frac{D^3\rho_L{}^2 g}{\mu_L{}^2}\right)^y, \epsilon^z\right]$$

Various arrangements of these dimensionless ratios were tried as a means of correlating the pressure drop at flooding. Values of the pack-

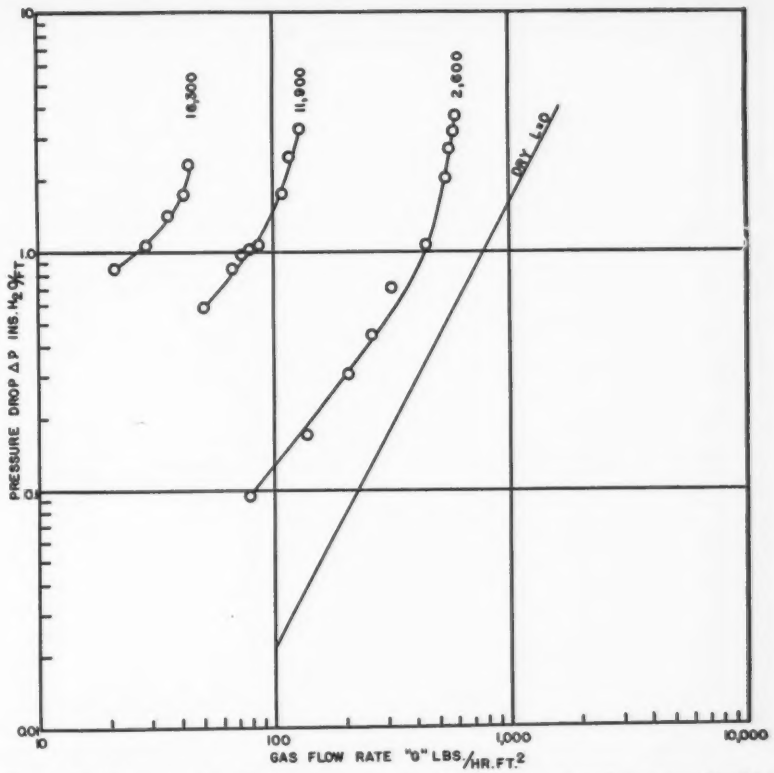

Figure 9—Pressure drop-flow rate curves for the system air-carbon tetrachloride and ethanol flowing through Raschig rings $_\rho L = 53.4$ LBS/FT^3. The parameter is liquid flow rate "L" LBS/HR.FT^2

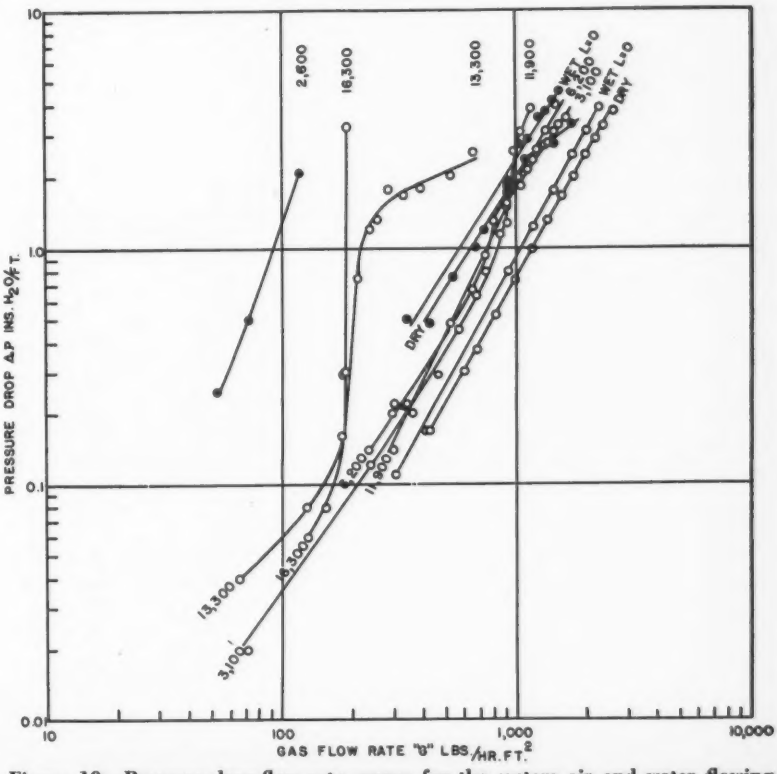

Figure 10—Pressure drop-flow rate curves for the system air and water flowing through Fiberglas. The parameter is liquid flow rate "L" LBS/HR.FT^2; $\varepsilon = 0.95$ ○; $\varepsilon = 0.91$ ●.

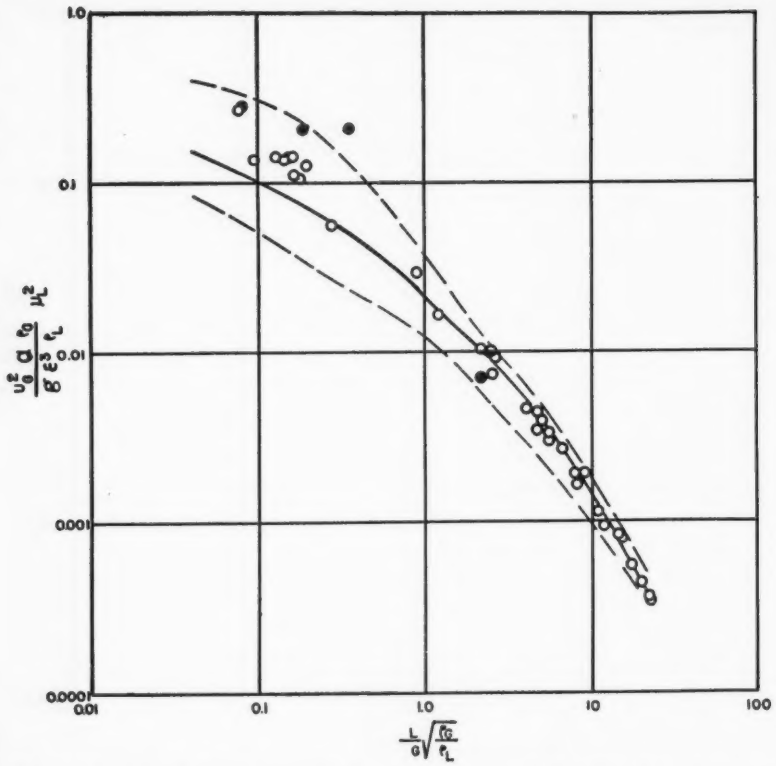

Figure 11—Visual flooding correlation after Sherwood. Raschig rings ○ Fiberglas ●. Solid line represents Sherwood's correlation. Dashed lines indicate range of data used in Sherwood's correlation.

ing and liquid properties, together with the pressure drop were secured from the literature for 14 different sets of conditions. In four of these, the liquid properties were not reported, and it was necessary to assume values. The assumed values were taken as the appropriate liquid property at 70°F. and one atmosphere pressure. As a result, the possible error in the calculated dimensionless ratios is quite large.

When values of

$$\frac{\Delta p}{\rho_L D \epsilon}\left(\frac{D}{a}\right)^{1/3}$$

were calculated, they were found to be almost constant. However, a variation with liquid viscosity was noticed. Finally, multiplying by $\mu_L^{0.1}$ where μ_L is in centipoise instead of pounds per foot second, gave

$$\frac{\Delta p}{\rho_L D \epsilon}\left(\frac{D}{a}\right)^{1/3}\mu_L^{0.1} = 0.62$$

Table 1 gives values

$$\frac{\Delta p}{\rho_L D \epsilon}\left(\frac{D}{a}\right)^{1/3}\mu_L^{0.1}$$

obtained from the published data of other workers along with values from the data obtained in this investigation. Table 2 lists the packings and packing size used by the other workers.

The fact that

$$\frac{\Delta p}{\rho_L D \epsilon}\left(\frac{D}{a}\right)^{1/3}\mu_L^{0.1} \doteq 0.62$$

means that it is possible to predict the pressure drop which will occur at the onset of pressure-drop flooding for any packing and fluid combination. Thus, for design purposes, it is possible to calculate the pressure drop which might occur in a packed column operating at any percentage of flooding capacity.

Conclusions

In this investigation an attempt has been made to study the relationship between pressure drop, gas and liquid flow rates and flooding in a gas absorption column. It has been found possible to fit an empirical equation to flooding data, and it is suggested that additional data be secured in an attempt to relate the terms of this equation to packing and fluid properties. A method of predicting pressure drop at the onset of flooding is suggested.

Nomenclature

a	packing surface area (ft.²/ft.³)
D	packing diameter (ft.)
G	gas flow rate (lbs./hr. ft.²)
g	gravitational constant (ft./sec.²)
L	liquid flow rate (lbs./hr. ft.²)
Δp	pressure drop (lbs./ft.² or lbs./in.²)
q, r, s, t	arbitrary constants
U_g	gas velocity (ft./sec.)
ϵ	packing void
ρ_L	liquid density (lbs./ft.³)
μ_L	liquid viscosity (lbs./ft. sec.)
$\Delta\mathcal{P}$	pressure drop (ins. H_2O/ft. of packing)

References

(1) Sherwood, T. K., Shipley, G. H. and Holloway, F. A. Ind. Eng. Chem., *30*, 765, (1938).

(2) Sarchet, B. R. Trans. Am. Inst. Chem. Engrs., *38*, 283, (1942).

(3) White, A. M. Trans. Am. Inst. Chem. Engrs., *31*, 390, (1935).

(4) Zenz, F. A. Trans. Am. Inst. Chem. Engrs., *43*, 415, (1947).

(5) Ufford, J. R. A Study of Flooding in Column Packings—M.A. Sc. Thesis, University of Toronto (1949).

(6) Winning, M. D. Flooding Phenomena in Gas Absorption Columns—Ph.D. Thesis, University of Toronto (1952).

(7) Elgin, J. C. and Weiss, F. B. Ind. Eng. Chem. *31*, 435, (1939).

(8) Schoenborn, E. M. and Dougherty, W. J. Trans. Am. Inst. Chem. Engrs., *40*, 51, (1944).

Acknowledgment

The authors wish to acknowledge their great indebtedness to:

The National Research Council for financial assistance through a Studentship and Summer Session Scholarship.

The Advisory Committee on Scientific Research at the University of Toronto for financial assistance through a grant.

The Shell Oil Company for financial assistance through a Scholarship.

The Department of Chemical Engineering at the University of Toronto for the equipment and supplies necessary for the investigation.

★ ★ ★